

FACILITY FORM 602

N 66-12248
(ACCESSION NUMBER)
233
(PAGES)
CR 68106
(NASA CR OR TMX OR AD NUMBER)

(THRU) **7**
(CODE) **13**
(CATEGORY)

GPO PRICE \$ _____

POSTI PRICE(S) \$ _____

Hard copy (HC) **4.00**

Microfiche (MF) **1.00**

653 July 65

EXPERIMENTAL AND THEORETICAL STUDIES IN PLANETARY AERONOMY

F. F. MARMO — PRINCIPAL INVESTIGATOR



Bedford, Massachusetts

FINAL REPORT

CONTRACT NO. NASw-840

PREPARED FOR
NATIONAL AERONAUTICS AND SPACE ADMINISTRATION
HEADQUARTERS
WASHINGTON, D. C.

APRIL 1965

GCA Technical Report No. 65-16-N

EXPERIMENTAL AND THEORETICAL STUDIES IN PLANETARY AERONOMY

Principal Investigator

F. F. Marmo

April 1965

Final Report

Contract No. NASw-840

GCA CORPORATION
GCA TECHNOLOGY DIVISION
Bedford, Massachusetts

Prepared for
NATIONAL AERONAUTICS AND SPACE ADMINISTRATION
Headquarters
Washington, D. C.

TABLE OF CONTENTS

<u>Section</u>	<u>Title</u>	<u>Page</u>
I	INTRODUCTION	1
II	TECHNICAL SUMMARIES OF PUBLISHED REPORTS GENERATED UNDER THE CURRENT CONTRACT	7
	A. Photochemistry of Planetary Atmospheres: Technical Summaries of Published Reports	7
	B. Theoretical Studies: Technical Summaries of Published Reports	25
	C. Experimental Studies in the VUV and EUV Spectral Regions: Technical Summaries of Published Reports	49
	D. Theoretical Aeronomy: Technical Summaries of Published Reports	76
III	TECHNICAL SUMMARIES OF INCOMPLETE AND/OR UNPUBLISHED WORK GENERATED UNDER THE CURRENT CONTRACT	85
	A. Photochemistry of Planetary Atmospheres: Brief Technical Summaries of Unpublished Work	85
	B. Theoretical Studies: Brief Technical Summaries of Unpublished Work	89
	C. Experimental Studies in the VUV and EUV Spectral Regions: Brief Technical Summaries of Unpublished Work	93
	D. Theoretical Aeronomy: Brief Technical Summaries of Unpublished Work	113
	REFERENCES	125

I. INTRODUCTION

This Final Report summarizes the work performed under Contract No. NASw-840 for the period 15 October 1963 through 15 March 1965. The diverse investigations reported herein have resulted in the publication of a number of reports in accredited journals and/or as GCA Technical Reports. These are listed below:

<u>Title</u>	<u>Publication</u>
Laboratory Studies of the Chemiluminescence from the Atomic Oxygen-Nitric Oxide Reaction Under Upper Atmospheric Conditions (N. Jonathan and G. Doherty)	Disc. of Faraday Soc. [37, 73-81, 1964]; GCA Technical Report No. 64-2-N
Reactions of ^1D Oxygen Atoms in the Photolysis of Carbon Dioxide. I (P. Warneck)	Disc. of Faraday Soc. [37, 57-65, 1964]; GCA Technical Report No. 64-7-N
Reactions of ^1D Oxygen Atoms in the Photolysis of Carbon Dioxide. II (P. Warneck)	J. Chem. Phys. [41, 3435, 1964]; GCA Technical Report No. 64-15-N
Excited Oxygen Atoms in the Photolyses of CO_2 and N_2O (P. Warneck)	J. Chem. Phys. [to be published]
LiF Color Center Formation and UV Transmission Losses from Argon and Hydrogen Discharges (P. Warneck)	J. Opt. Soc. Am. [to be published]
Microanalysis of $\text{SO}_4^=$ and SO_3 (J. O. Sullivan and P. Warneck)	Microchem. J. [8, 241-244, 1964]
The Photoionization of Atomic Oxygen (A. Dalgarno, R. J. W. Henry and A. Stewart)	Planetary & Space Sci. [12, 235, 1964]; GCA Technical Report No. 64-1-N

<u>Title</u>	<u>Publication</u>
An Expansion Method for Calculating Atomic Properties - I. The 2S and $^2P^o$ States of the Lithium Sequence (M. Cohen and A. Dalgarno)	Proc. Roy. Soc. [A275, 492, 1963]; GCA Technical Report No. 64-5-N
An Expansion Method for Calculating Atomic Properties - II. Transition Probabilities (M. Cohen and A. Dalgarno)	Proc. Roy. Soc. [A280, 258, 1964]; GCA Technical Report No. 64-6-N
Ambipolar Diffusion in the F-Region (A. Dalgarno)	J. Atmos. Terrest. Phys. [26, 939, 1964]
Ionospheric Electron Temperatures Near Dawn (A. Dalgarno and M. B. McElroy)	Planetary & Space Sci. [13, 143, 1965]
Electron Temperatures in the D Region (A. Dalgarno and R. J. W. Henry)	Proc. Roy. Soc. (in press)
New Energy Levels in Xenon and Krypton (J. A. R. Samson)	Phys. Letters [8, No. 2, 107, Jan. 1964]; GCA Technical Report No. 64-3-N
Experimental Photoionization Cross Sections in Argon from Threshold to 280\AA (J. A. R. Samson)	J. Opt. Soc. Am. [54, No. 3, 420, Mar. 1964]; GCA Technical Report No. 64-3-N
Photoionization Cross Sections of Xenon from the $^2P_{1/2}$ Edge to 280\AA (J. A. R. Samson)	J. Opt. Soc. Am. [54, No. 6, 842, June 1964] GCA Technical Report No. 64-3-N
Photoionization Cross Sections of Helium (J. A. R. Samson)	J. Opt. Soc. Am. [54, No. 7, 876, July 1964]; GCA Technical Report No. 64-3-N
Absorption and Photoionization Cross Sections of O_2 and N_2 at Intense Solar Emission Lines (J. A. R. Samson and R. B. Cairns)	J. Geophys. Res. [69, No. 1, 4583, Nov. 1964]; GCA Technical Report No. 64-13-N

<u>Title</u>	<u>Publication</u>
Absorption and Photoionization Cross Sections of CO ₂ , CO, A and He at Intense Solar Emission Lines (R. B. Cairns and J. A. R. Samson)	J. Geophys. Res. [70, No. 1, 99, Jan. 1965]; GCA Technical Report No. 64-13-N
Photoionization Cross Sections of Neon from Threshold to 200Å (J. A. R. Samson)	J. Opt. Soc. Am. [to be published]
A Carbon Film-Scintillator Combination Suitable for the Selective Detection of Radiation in the Extreme Ultraviolet (J. A. R. Samson and R. B. Cairns)	Applied Optics [to be published]
Total Absorption Cross Section of Atomic Oxygen Below 910Å (R. B. Cairns and J. A. R. Samson)	Phys. Rev. [to be published] GCA Technical Report No. 65-6-N
A Congeries of Absorption Cross Sections for Wavelengths Less Than 3000Å. II (J. O. Sullivan and A. C. Holland)	GCA Technical Report No. 64-20-N
Ozone Distribution in the Atmospheres of Mars (F. F. Marmo, Shardanand and P. Warneck)	J. Geophys. Res. [70, No. 9, 2270, 1965]
On the Presence of Ozone and Oxides of Nitrogen in the Martian Atmosphere (F. F. Marmo, Shardanand and P. Warneck)	J. Geophys. Res. [to be published]

In a continuing program of this nature, there always exists some material which is in the publication cycle but has not attained final form. A list of the areas of investigation in this above category follows:

CO₂ Photolyses at 1066Å

The Fluorescence of Solar Ionizing Radiation

Laboratory Measurements of Cross Sections of Atomic Nitrogen and Atomic Hydrogen

Laboratory Measurements of the Kinetic Energies of Photoelectrons from N₂ and O₂

Photoionization Threshold for O₂

EUV and VUV Fluorescence Radiation from Planetary Gases

The Mass Analysis of the Products of Photoionizing O_2 , N_2 and CO_2 Below 1000\AA

Absorption Coefficients of Acetaldehyde from 1800 to 3000\AA

The Scattering of Lyman-Alpha Radiation by Helium, Neon, Argon, Nitrogen and Hydrogen

Reflectance of Beryllium from 584 to 4030\AA

The Role of Interplanetary Debris in Planetary Atmospheres

Spectral Reflectivity and Luminosity of the Earth's Atmosphere for 50\AA Bandwidths for the Region Below 2000\AA

CO_2 Photolyses and Photoionization Rates for Constituents of the Atmospheres of Mars and Venus

In addition to the above-accepted methods of reporting, a significant portion of research results developed under the subject contract have been presented at various scientific technical meetings as follows:

Interplanetary Debris in the Martian Atmosphere (F. F. Marmo and A. C. Holland) - Presented by F. F. Marmo at Conference on Remote Investigations of Martian Biology, Cambridge, Mass., January 10-13, 1964.

Absorption Coefficients of Acetaldehyde from 2000 to 3500\AA (F. F. Marmo and J. O. Sullivan) - Presented by F. F. Marmo at Conference on Remote Investigations of Martian Biology, Cambridge, Mass., January 10-13, 1964.

Photoionization of the Rare Gases (J. A. R. Samson) - Presented by J. A. R. Samson at APS Meeting, New York, New York, January 22-25, 1964.

Photoionization Cross Sections of O_2 and N_2 at Intense Solar Lines (J. A. R. Samson) - Presented by J. A. R. Samson at Optical Society of America Meeting, Washington, D. C., April 1-3, 1964.

Laboratory Studies of the Chemiluminescence from the Atomic Oxygen-Nitric Oxide Reaction Under Upper Atmospheric Conditions (N. Jonathan and G. Doherty) - Presented by N. Jonathan at the Faraday Society Discussions on Chemical Reactions in the Upper Atmosphere, Edinburgh, Scotland, April 2-3, 1964.

The Reactions of 1D Atoms in the Photolysis of Carbon Dioxide (P. Warneck) - Presented by P. Warneck at the Faraday Society Discussions on Chemical Reactions in the Upper Atmosphere, Edinburgh, Scotland, April 2-3, 1964.

The Solar Photodecomposition of NO_2 in the Martian Atmosphere (F. F. Marmo, P. Warneck and Shardanand) - Presented by F. F. Marmo at AGU Meeting, Washington, D. C., April 21-24, 1964.

Photoionization Threshold Potential of O_2 (J. A. R. Samson and R. B. Cairns) - Presented by J. A. R. Samson at the Seventeenth Annual Gaseous Electronics Conference, Atlantic City, New Jersey, October 14-15, 1964 (Paper A-2).

The Scattering of Lyman-Alpha Radiation (1215.6\AA) by He, Ne, A, H_2 and N_2 (F. F. Marmo and Y. Mikawa) - Presented by Y. Mikawa at the APS Meeting, Chicago, Illinois, October 23-24, 1964,

The Measured Photoionization Cross Section of Atomic Oxygen (R. B. Cairns and J. A. R. Samson) - Presented by R. B. Cairns at the APS Meeting, New York, New York, January 28, 1965.

The following sections of this report closely follow the format of the preceding listings. Specifically, in Section II, detailed technical summaries of published reports generated under the contract are presented, whereas Section III contains detailed technical discussions of incomplete and/or unpublished work. In both of the following sections, owing to the nature and scope of the program, the detailed discussions have been subdivided into the following four categories:

- A. Photochemistry of planetary gases
- B. Theoretical studies
- C. Experimental investigations in the VUV and EUV spectral regions
- D. Theoretical aeronomy.

II. TECHNICAL SUMMARIES OF PUBLISHED REPORTS GENERATED UNDER THE CURRENT CONTRACT

Under the current contract effort a number of reports have been generated which have been published in the open literature and/or as GCA Technical Reports. It is appropriate to give rather comprehensive summaries of these previously-published reports including a technical discussion of the approach employed and the pertinent tables, figures and data analyses. The summaries will be complete enough to stand on their own but at the same time will not include unnecessary details which are available to the interested reader in the original published form. In keeping with the format described in the Introduction, four categories are discussed here in turn:

- A. Photochemistry of Planetary Atmospheres
- B. Theoretical Studies
- C. Experimental Studies in the VUV and EUV Spectral Regions
- D. Theoretical Aeronomy.

A. PHOTOCHEMISTRY OF PLANETARY ATMOSPHERES: TECHNICAL SUMMARIES OF PUBLISHED REPORTS

The investigations of the photochemistry of planetary atmospheres has resulted in the generation of six technical papers, each of which has been accepted for publication in the open literature and/or has appeared as a GCA Technical Report. Comprehensive summaries of these reports are given below.

1. Laboratory Studies of the Chemiluminescence from the Reaction of Atomic Oxygen with Nitric Oxide under Upper Atmospheric Conditions

- (a) GCA Technical Report No. 64-2-N.
- (b) Presented at the Discussion Meeting of the Faraday Society at Edinburgh, Scotland, April 1964.
- (c) Published: Disc. Faraday Soc. 37, 73 (1964).

This study was undertaken in an effort to demonstrate that the chemiluminescence associated with the atomic oxygen-nitric oxide reaction is a prime contributor to the observed continuum in the earth upper atmosphere (maximum emission around 90 to 110 km). It has been shown that the essential mechanism for the atomic oxygen-nitric oxide light emission is



followed by the much faster dark reaction



whereby NO is regenerated. Due to its importance, extensive laboratory studies have been performed on this reaction in other research laboratories.

However, in all cases, experimental data were obtained only for pressures greater than 1 mm Hg. However, the pressures encountered in the altitude region where the night glow continuum is emitted is only about 1 micron. Straightforward extrapolation of previous (higher pressure) data was not valid since significant disagreement prevailed regarding the mechanism at low pressures. Accordingly, the need for new laboratory measurements in the appropriate pressure region were made evident. The present experiments represent the first successful measurements in the appropriate pressure domain (of the order of 1 micron). Experimental details are given in the original report and are not repeated here. However, it is significant to note that actual light emissions were observed and measured for pressures even less than 1 micron.

The first experimental requirement was to measure the chemiluminescent intensity as a function of the atomic oxygen and nitric oxide partial pressures; this was performed for the pressure range of from 3 to 200 microns. The data are shown in Table 1. In addition, to establish the order dependence of both nitric oxide and atomic oxygen, the data shown in Tables 2 and 3 were obtained. On the basis of these data, a mechanism was suggested which was both appropriate and compatible to experimental observations which established the first order dependencies for atomic oxygen and nitric oxide. The data also suggested that third-body efficiencies varied with the nature of the gas used but not with the concentration. An appropriate rate constant was established and employed to evaluate the photon flux from the earth night airglow continuum assumed to be due to the chemiluminescent reaction between O and NO. On this basis the data summarized in Table 4 were employed to demonstrate that the chemiluminescent reaction of atomic oxygen with nitric oxide could indeed be responsible for the observed night airglow continuum provided that the nitric oxide concentration is of the order of 10^8 molecules cm^{-3} over the altitude range 90 to 110 km. In this regard, it is interesting to note that since this study was completed, recent direct measurements of the NO content in the earth atmosphere by Barth [1]* established a count of 1.7×10^{14} molecules cm^{-2} above the 85 km level so that it appears that the required 10^8 number density for the present scheme has been established.

In brief, then, the following main concentrations have been derived from this study:

(1) The atomic oxygen-nitric oxide reaction is a three-body process down to pressures of at least 1 micron.

(2) The light-emitting reaction is not pressure dependent and hence the existing rate constant for light emission of 1.7×10^{-17} cc molecule $^{-1}$ sec $^{-1}$ may be applied at total pressures as low as 1 micron.

(3) The atomic oxygen-nitric oxide chemiluminescent reaction in the earth atmosphere is a prime contributor to the observed nighttime airglow continuum.

*The numbers in [] throughout the text represent reference numbers.

TABLE 1 (II-A-1)

CHEMILUMINESCENT INTENSITY AS A FUNCTION OF THE ATOMIC OXYGEN AND NITRIC
OXIDE PARTIAL PRESSURES OVER A TOTAL PRESSURE RANGE OF 3 TO 200 MICRONS

Run No.	Total Pressure (microns Hg)	Atomic Oxygen Pressure (microns Hg)	Nitric Oxide Concentration (microns Hg)	Intensity ($\times 10^6$ amps)	Intensity per micron Nitric Oxide ($\times 10^6$ amps)	I_o ($\times 10^5$ amps)
1	3.0	0.13	0.36	.297	0.825	0.63
2	9.5	0.44	0.90	2.07	2.3	0.52
3	19.5	0.90	2.1	10.8	5.14	0.57
4	30.0	1.35	3.3	25.8	7.82	0.58
5	43.5	1.93	2.0	21.0	10.5	0.54
	43.5	1.79	2.0			0.59
6	80.0	3.01	1.0	14.7	14.7	0.49
	80.0	2.70	2.0	28.7	14.35	0.53
	80.0	2.43	3.0	39.0	13.0	0.53
7	80.0	1.40	1.69	14.0	8.28	0.59
8	200.0	0.94	4.33	26.0	6.0	0.64

TABLE 2 (II-A-1)

INTENSITY AS A FUNCTION OF NITRIC OXIDE PARTIAL PRESSURE AT A TOTAL INITIAL PRESSURE OF 9.5 MICRONS AND ATOMIC OXYGEN PARTIAL PRESSURE OF 0.44 MICRONS

Total Pressure Before NO Addition (microns Hg)	Pressure Atomic Oxygen (microns Hg)	Pressure Nitric Oxide (microns Hg)	Intensity ($\times 10^6$ amps)	I_o ($\times 10^5$ amps)
9.5	0.44	1.11	2.58	0.53
9.5	0.44	0.89	2.04	0.52
9.5	0.44	0.66	1.50	0.52
9.5	0.44	0.48	1.11	0.53
9.5	0.44	0.39	0.81	0.47
9.5	0.44	0.24	0.48	0.45
9.5	0.44	0.13	0.29	0.51

TABLE 3 (II-A-1)

INTENSITY AS A FUNCTION OF ATOMIC OXYGEN PARTIAL PRESSURE AT A TOTAL PRESSURE OF
9.5 MICRONS AND NITRIC OXIDE PARTIAL PRESSURE OF 0.8 MICRONS

Run No.	Total Pressure before NO Addition (microns Hg)	Pressure Atomic Oxygen (microns Hg)	Pressure Nitric Oxide (microns Hg)	Intensity ($\times 10^6$ amps)	I_o ($\times 10^5$ amps)
1	9.5	0.10	0.80	0.388	0.49
2	9.5	0.24	0.80	1.08	0.56
3	9.5	0.28	0.80	1.28	0.57
4	9.5	0.38	0.80	1.64	0.54
5	9.5	0.42	0.80	2.12	0.63

TABLE 4 (II-A-1)

POSSIBLE PHOTON FLUX FROM THE NIGHT AIRGLOW CONTINUUM ASSUMING
THE CAUSE TO BE THE O + NO REACTION

Altitude (km)	Total Particle Concentration (molecules/cc)	Atomic Oxygen Concentration (atoms/cc)	Nitric Oxide Concentration (molecules/cc)	Flux $\text{photons/cm}^2/\text{sec}$
70	2.1×10^{15}	1×10^{10}	10^8 }	26×10^6
80	4.0×10^{14}	2×10^{10}	10^8 }	1×10^8
90	5.9×10^{13}	1×10^{11}	10^8 }	1×10^9
100	7.8×10^{12}	1×10^{12}	10^8 }	1.7×10^9
110	1.2×10^{12}	1×10^{12}	10^8 }	

2. Reactions of ^1D Oxygen Atoms in the Photolysis of Carbon Dioxide. I

- (a) GCA Technical Report No. 64-7-N.
- (b) Presented at the Discussion Meeting of the Faraday Society at Edinburgh, Scotland, April 1964.
- (c) Published: Disc. Faraday Soc. 37, 57 (1964).

Photochemical processes occurring in planetary atmospheres under the influence of solar radiation depend greatly upon the relative abundance of atmospheric constituents. While oxygen is the major dissociable component in the earth's atmosphere, this role is assumed by carbon dioxide in the atmospheres of Mars and Venus. In spite of this fact, too little data exist in the photochemical decomposition of CO_2 . Thus, the vacuum ultraviolet photolysis of CO_2 was investigated in the pressure region 150 to 760 mm Hg using xenon, krypton and hydrogen light sources to cover the spectral region 1236 to 1700Å. Integrated light source intensities ranged from 2×10^{15} to 2×10^{16} quanta/sec for krypton and xenon discharges, and up to 1×10^{16} quanta/sec for the hydrogen lamp. Experiments were performed with a cylindrical flow reactor consisting of two concentric Pyrex tubings, the outer one serving as the gas inlet. Quantum yields for carbon monoxide and oxygen were determined in a closed system in which the gas was circulated by a rotating stirrer whereas the required ozone quantum yields were determined in an open flow system. The experimental details are not given in this summary since they appear in the original publication (see 2(a) and 2(c) above).

The data obtained by mass spectrometric analysis of samples drawn from the closed system are summarized in Figure 1. CO quantum yields of unity were found throughout the investigated pressure region when CO_2 was irradiated with light from krypton or hydrogen discharges, but the xenon light source resulted in an increase of the CO quantum yield from unity at lower pressures to an average of $Q(\text{CO}) = 1.17$ at 740 mm Hg. Similarly, a comparatively higher oxygen quantum yield was observed in the latter case. This indicates a difference in the photolytic mechanism which must be active at the wavelengths of the lines emitted from a xenon discharge on one hand, and a krypton or hydrogen discharge on the other. The results obtained with the krypton lamp can be used to demonstrate that at 1236Å the CO quantum yield is insensitive to pressure variations in the region 10 to 760 mm Hg, thus giving additional support to the conclusion that carbon monoxide is formed directly in the primary process. The observed oxygen quantum yields [$Q(\text{O}_2) = 0.3$ for krypton and hydrogen and $Q(\text{O}_2) = 0.4$ for xenon] were less than $Q(\text{O}_2) = 0.5$ which would be expected if all oxygen atoms produced in the primary process recombined to yield molecular oxygen. A detailed study of this "oxygen deficiency" is given in Summary No. 3 of this series.

The time dependence of carbon monoxide and oxygen formation is plotted in Figure 2 for experiments in which a xenon discharge and pressures close to an atmosphere were employed. The observed linearity substantiates the results presented in Figure 1, indicating that for the irradiation intervals and intensities applied, the quantum yields are time independent. In any case, it was shown that at 1236Å and around 1600Å the quantum yields for carbon monoxide,

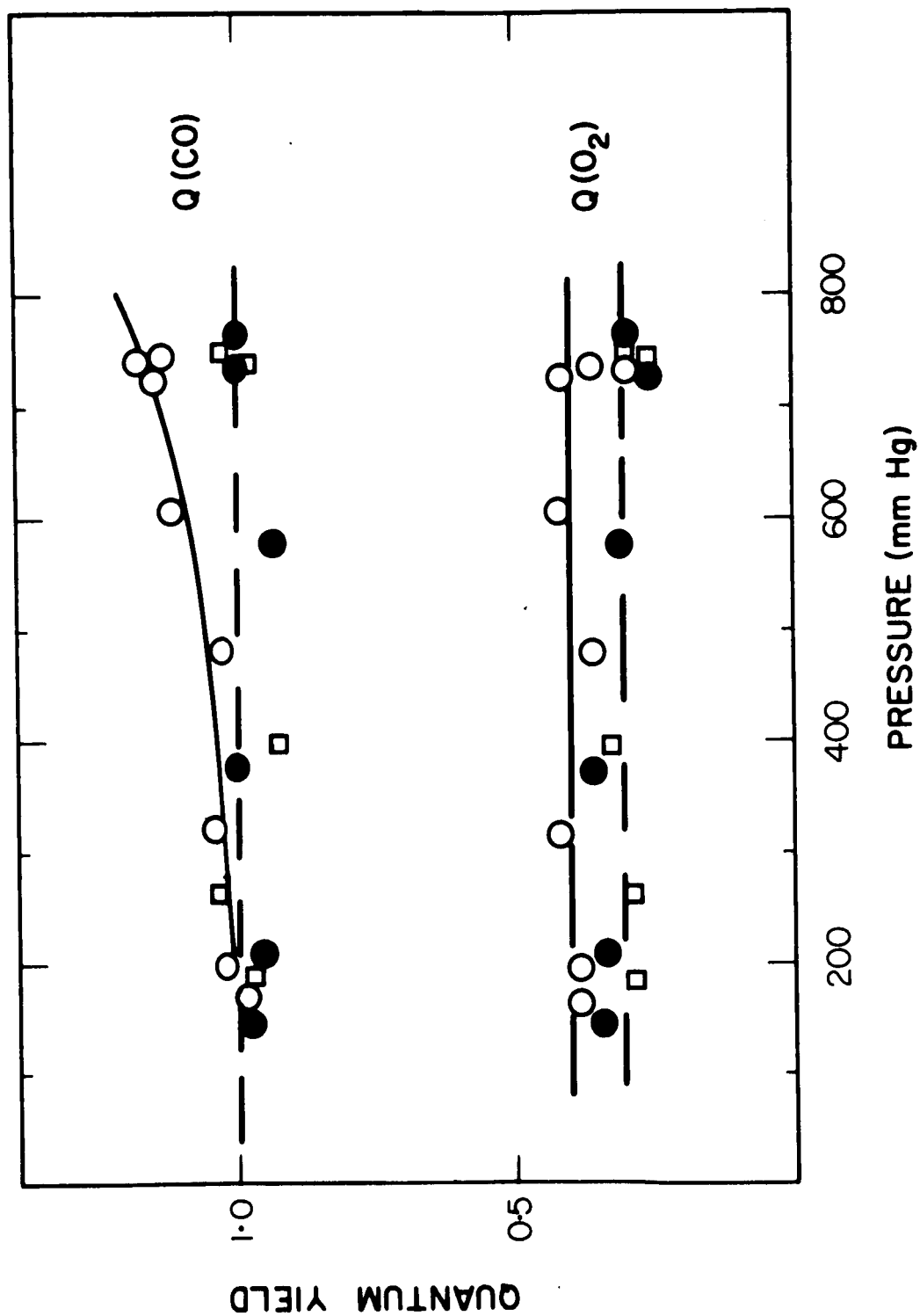


Figure 1 (II-A-2). Quantum yields of carbon monoxide and oxygen; 10-min irradiation with intensities of about 10×10^{15} quanta/sec. Filled circles: at 1236Å; open circles: at 1470Å; squares: at about 1600Å.

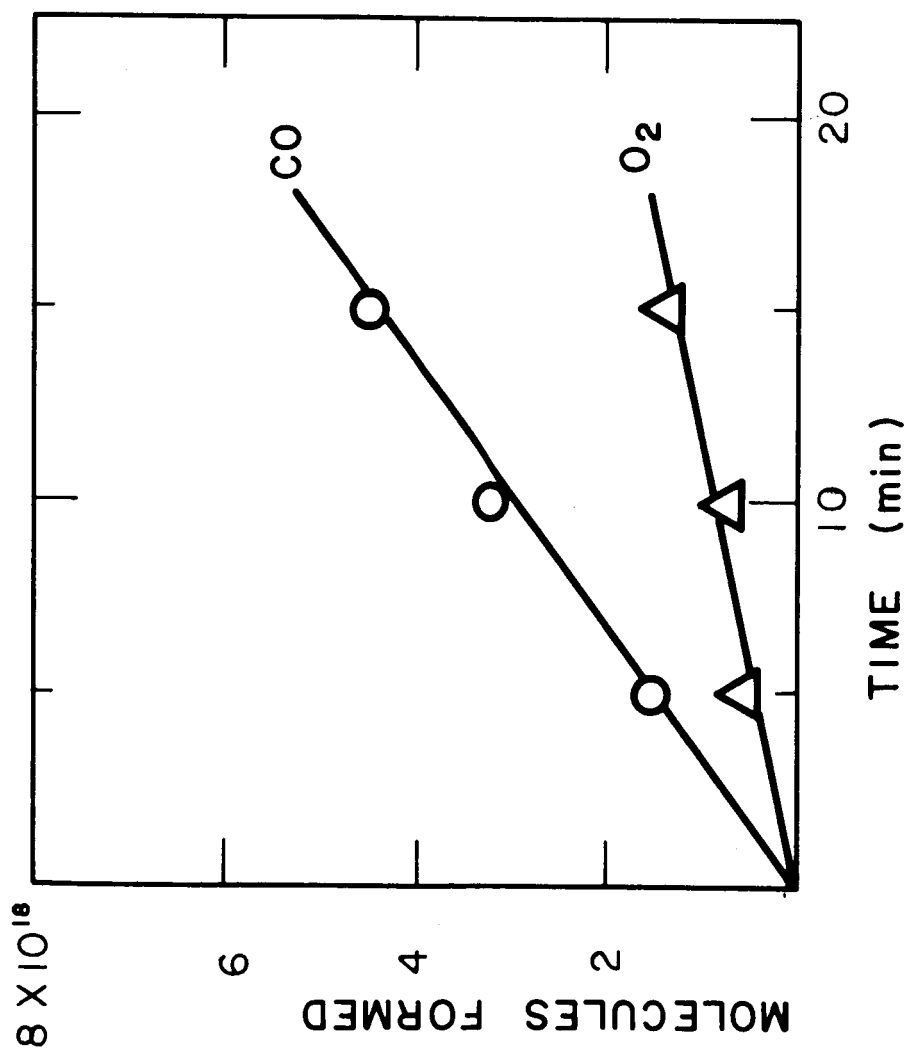
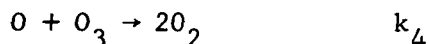
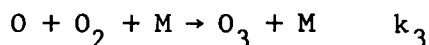


Figure 2 (II-A-2). Time dependence of carbon monoxide and oxygen formation at 1470 Å; irradiation intensity 5×10^{15} quanta/sec.

oxygen and ozone are consistent with the photodissociation mechanism, while an increase in the quantum yields at 1470Å indicates that at this wavelength excited CO₂ molecules are also involved. Also, no pressure dependence was observed for CO and O₂ quantum yields at 1236Å and around 1600Å.

Concerning ozone quantum yield measurements, most of these experiments were performed at atmospheric pressures. However, even at this relatively high pressure, no ozone could be detected when a flow of extensively purified CO₂ was irradiated with the krypton or the hydrogen discharge, even if high light intensities and low flow rates were employed. As a consequence, only an upper limit quantum yield of $Q(O_3) \leq 0.01$ was established. These very low rates of ozone formation were observed in all cases, and from these data it was concluded that the photolysis of CO₂ involves oxygen atoms in the metastable ¹D state. Further measurements employing carbon dioxide containing 2.6 percent oxygen enabled the determination of the ratio of the rate constants associated with the important atmospheric reactions:



It was possible from the present data to derive an average value of $k_4/k_3(M) = 41$ which is about a factor of ten higher than the known ratio involving ground state ³P oxygen atoms. Accordingly, these data add additional support to the conclusion that the photodissociation of CO₂ produces carbon monoxide and metastable ¹D oxygen atoms. The remaining question of accounting for the observed "oxygen deficiency" is discussed in the following summary

3. Reactions of ¹D Oxygen Atoms in the Photolysis of Carbon Dioxide. II

- (a) GCA Technical Report No. 64-15-N
- (b) Published: J. Chem. Phys. 41, 3435 (1964).

In the previous paper (I), it was established that carbon monoxide and oxygen are the major products arising from the photodecomposition of CO₂ in the 1200 to 1700Å wavelength region. Also, it was shown that carbon monoxide formation proceeds with a quantum yield of unity in accordance with the view that photodissociation constitutes the major primary process. However, an important result was that the O₂ quantum yield appears to be a variable depending on the imposed experimental conditions. It is significant that the reported (O₂)/(CO) ratios are much smaller than the theoretical value $R = 0.5$ which should be expected if oxygen and carbon monoxide were the sole products. The existing lack of material balance obviously points to the evolution of one or more additional products and two suggestions have been made in this respect: (1) that ozone is a product, and (2) that the formation of CO₃ should be considered. The flow experiments described in I showed ozone production to be negligible when pure CO₂ was employed, although appreciable quantities of ozone were observed when oxygen was present in small amounts so that the importance of CO₃ formation could not be precluded.

In view of this situation, then, there arose the need to re-investigate the extent of ozone formation in the vacuum ultraviolet photolysis of CO_2 and to study the $(\text{O}_2)/(\text{CO})$ ratio as a function of various experimental parameters. In the present work, the amount of ozone formation was found insufficient to account for the oxygen deficiency reflected in the O_2 quantum yields. The $(\text{O}_2)/(\text{CO})$ ratio was noted to depend on the light intensity; on the time interval after which an irradiated sample was subjected to analysis; and on the ratio of carbon dioxide to admixed rare gas concentration. These results can be shown to be consistent with the assumption that an unstable addition compound, namely CO_3 , is formed by attachment of ^1D oxygen atoms to carbon dioxide.

No detailed description of the experimental factors are given here. However, in brief, the present experiments were carried out employing the closed system in conjunction with the hydrogen light source, the radiation being passed through a BaF_2 window. The amount of CO formation was utilized as an internal actinometer and the gas was circulated by means of a rotating stirrer in order to avoid product accumulation in the vicinity of the window. Samples were analyzed mass spectrometrically.

Again, as in I, low ozone quantum yields were established. For example, when the gas was irradiated with an intensity of about 3×10^{15} quanta/sec over a period of 15 minutes no indication for iodine formation could be obtained, even though the sensitive starch test was used as the indicator. On this basis an upper limit to the ozone quantum yield was set at $Q(\text{O}_3) < 0.03$ and on the basis of comparison experiments in which a flow of oxygen was irradiated with known light intensity. These results made evident that ozone formation cannot account for the observed oxygen deficiency, so that the formation of CO_3 appears to provide an alternative explanation.

Although it has not been possible in the present work to detect CO_3 analytically, it was shown subsequently that the behavior of the $(\text{O}_2)/(\text{CO})$ ratio is consistent with the hypothesis of CO_3 formation. As one example the discrepancy among the $(\text{O}_2)/(\text{CO})$ ratios found in several separate runs led to the belief that R is a function of the light intensity; this was substantiated in experiments carried out at atmospheric pressure. Figure 1 shows the results for a series of runs in which the irradiation period was ten minutes. The general behavior exhibited by R in Figure 1 is characteristic of photochemical systems in which a radical recombination reaction occurs in competition with another reaction, its rate involving the radical concentration in a linear fashion. Accordingly, since oxygen atoms are the known intermediates in the photolysis of CO_2 , the observed intensity dependence of R can be taken as solid evidence that a significant portion of the evolved O_2 is formed by way of atom recombination.

The time dependence of R is shown in Figure 2 which shows that the $(\text{O}_2)/(\text{CO})$ ratio steadily increases with time until a value of $R = 0.42$ is reached after 60 minutes. This is already close to the theoretical value of $R = 0.5$, indicating that an unstable product (presumably CO_3) is formed, releasing oxygen in the process of decomposition.

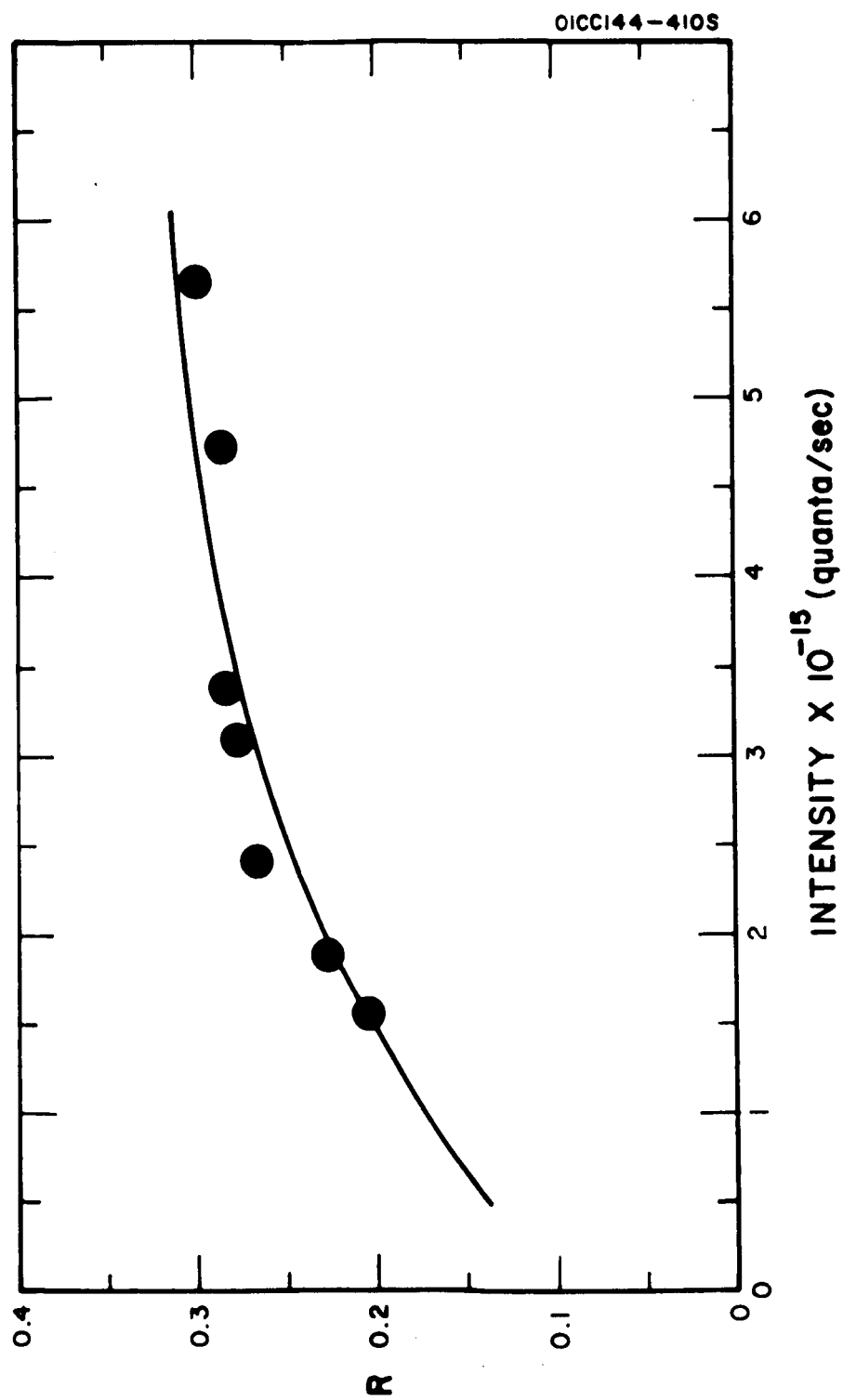


Figure 1 (II-A-3). Variation of $R = \frac{O_2}{CO}$ with light intensity at atmospheric pressure.

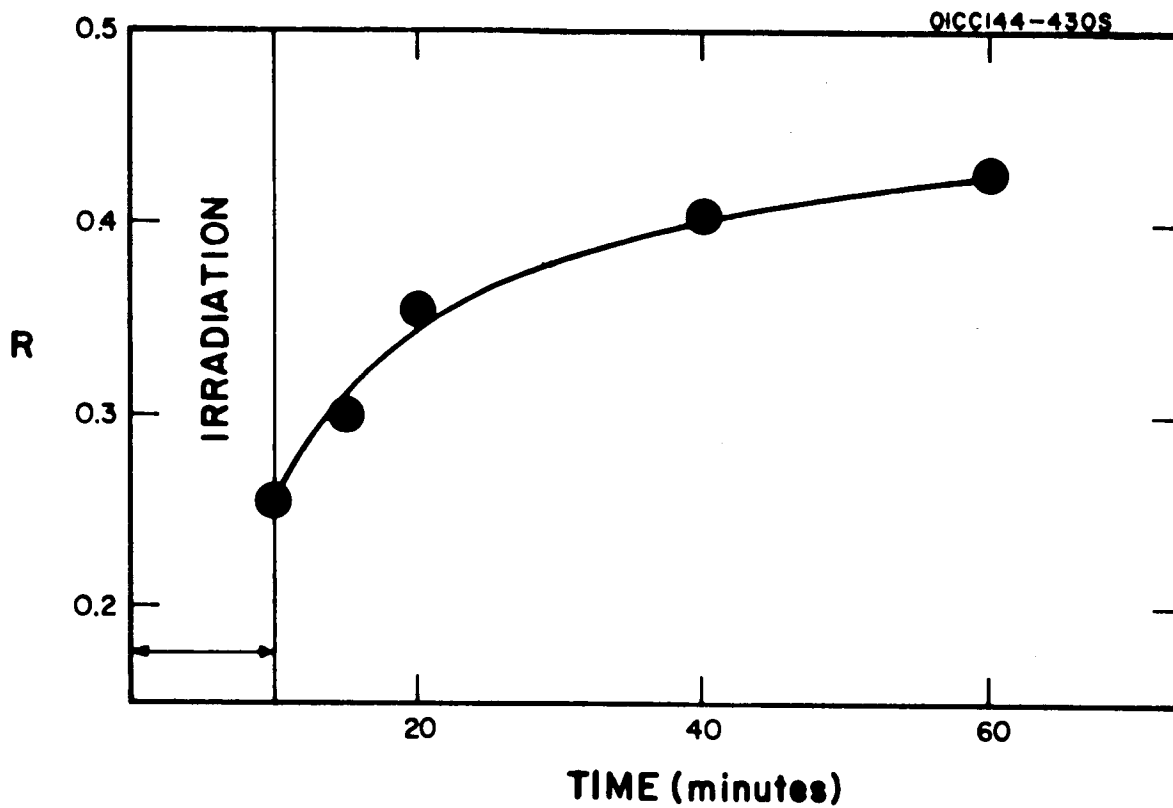
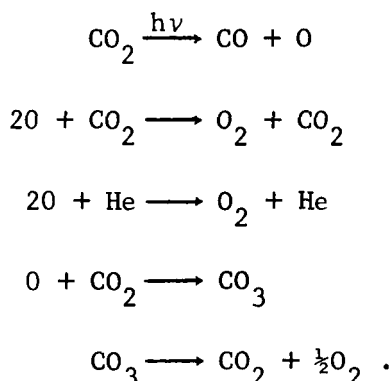


Figure 2 (II-A-3). Time dependence of $R = (O_2)/(CO)$ after irradiation; atmospheric pressure of CO_2 ; light intensity about 3×10^{15} quanta/sec.

Additional support for the occurrence of a reaction between oxygen atoms (in the 1D state) and CO_2 has come from a series of irradiation experiments in which helium was added as an inert constituent. The measured $(O_2)/(CO)$ ratios are shown in Figure 3 in a plot versus $(He)/(CO_2)$. The data reveal indeed an increase of R with increasing helium concentration, thus strengthening the arguments advocating CO_3 formation. It is interesting to note that previously, no pressure effect was observed in experiments employing pure CO_2 . This is again in accord with the suggested mechanism of two competing reactions, since in this case CO_2 is also functioning as the acting third body in the recombination reaction. Accordingly, it appears that the assumption of CO_3 being a product besides O_2 and CO can account for all the experimental facts associated with CO_2 photolysis.

The present results can be interpreted in terms of the following simple mechanism involving oxygen atoms in the metastable 1D state:



Further detailed analysis, not repeated here, has shown that the third-body efficiency of helium for oxygen atoms recombination was found to be only 0.24 of that for CO_2 .

In view of the overall results presented in this paper, it can be concluded that the oxygen deficiency observed in the photolysis of CO_2 can indeed be explained by the formation of CO_3 - owing to the attachment of 1D oxygen atoms to CO_2 - but not by the assumption of ozone formation. Unfortunately, however, specific direct measurement of the CO_3 was not accomplished.

4. Excited Oxygen Atoms in the Photolyses of CO_2 and N_2O

(a) To be published: J. Chem. Phys.

In a series of recent papers, Yamazaki and Cvetanovic [2-4] reported on the chemical behavior of oxygen atoms arising from the 1849 \AA photolysis of N_2O . These oxygen atoms are formed in an excited metastable state as evidenced by their ability to react fairly rapidly with N_2O , H_2 and CO_2 [2,3]. The corresponding reactions of ground-state oxygen atoms, by contrast, are at best very slow. Energetically, N_2O photolysis at wavelengths around 1849 \AA can

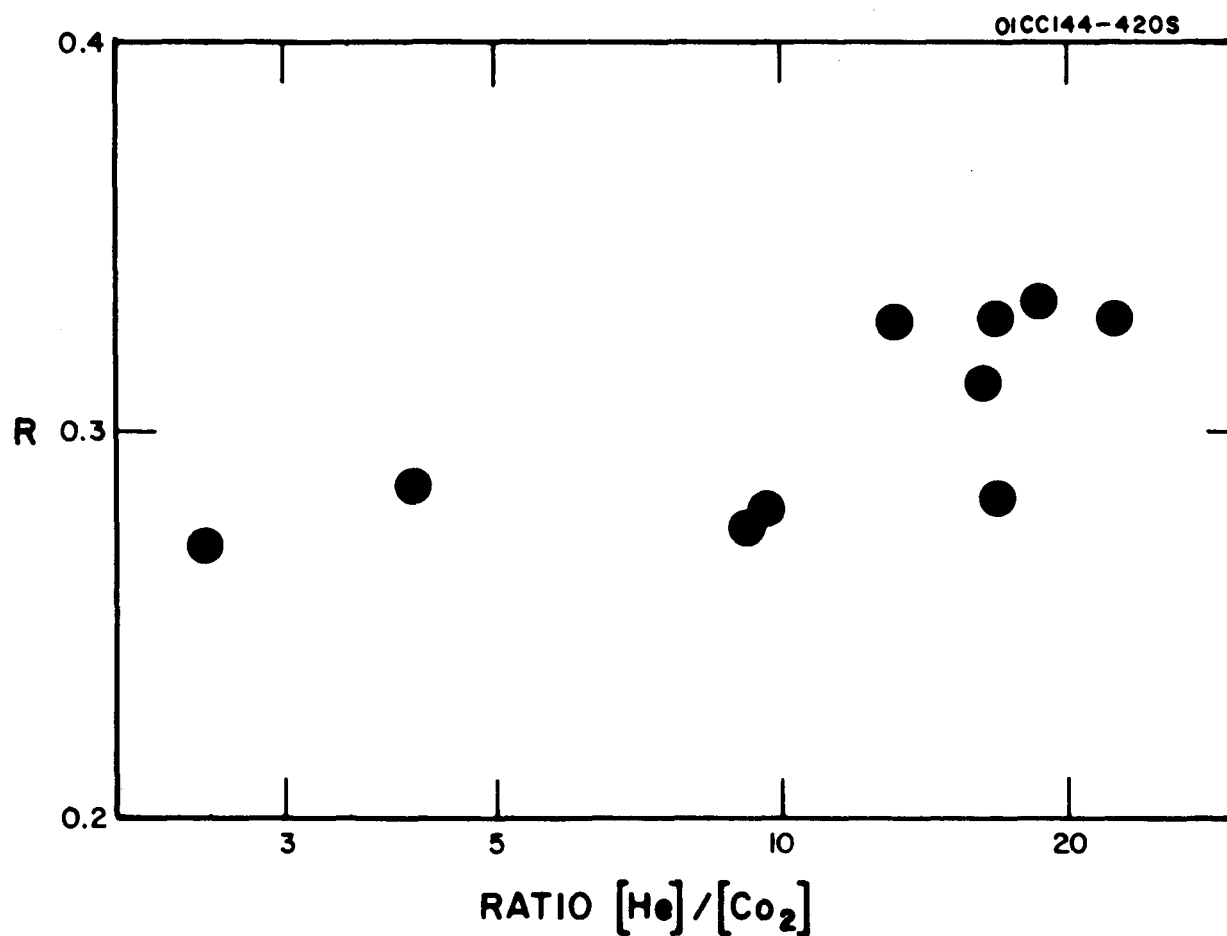
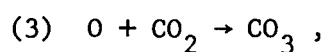
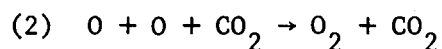
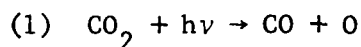
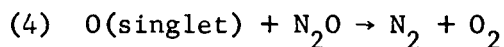


Figure 3 (II-A-3). Dependence of $R = (O_2)/(CO)$ on the ratio of admixed helium to carbon dioxide concentration: Carbon dioxide pressure 22 mm Hg. Effective light intensity about 1×10^{15} quanta/sec.

yield either ^1D or ^1S oxygen atoms, but a stringent test to decide which of the two metastables is involved has not yet been devised. On the basis of photolysis experiments performed at 2139\AA , near the onset of the pertinent N_2O continuum, Yamazaki and Cvetanovic are inclined to believe that ^1D oxygen atoms are produced, but they also point out that more concrete evidence for this assignment should be obtained by generating ^1D oxygen atoms in a different system. It has recently been shown [5-7] that the photolysis of CO_2 at wavelengths around 1600\AA provides a convenient source for ^1D oxygen atoms. The reaction mechanism is relatively simple and consists of:



with the CO_3 slowly decomposing. No collisional deactivation of the metastable ^1D species was observed in the CO_2 system even at CO_2 pressures close to one atmosphere. This appears to be in conflict with Yamazaki and Cvetanovic [2] who found that the excited oxygen atoms generated in the photolysis of N_2O are readily deactivated in the presence of CO_2 . Using the inherent reaction



as an indicator for excited oxygen atoms, Yamazaki and Cvetanovic measured the diminution of nitrogen evolution during N_2O photolysis as a function of the added CO_2 pressure. For example, when they added 80 mm Hg CO_2 , representing a seven-fold excess over N_2O , reaction (4) was almost entirely suppressed. This provides clear indication for the high reactivity between CO_2 and the O-atoms present in their system.

For a more direct experimental comparison of excited oxygen atom behavior in the two photolytic systems, we photolysed CO_2 at atmospheric pressure in the presence of small amounts of N_2O . As in previous experiments [6], a hydrogen light source with a BaF_2 filter was employed. With about 1 mm Hg of N_2O admixed, the fraction of oxygen atoms which reacted with N_2O according to reaction (4) was appreciable. The following quantum yields were observed: $\phi(\text{O}) = 1.0$, $\phi(\text{N}_2) \approx \phi(\text{O}_2) = 0.74$. This result shows that under our experimental conditions, reaction (2) is negligible and reaction (4) is in competition with reaction (3). About 75 percent of the oxygen atoms generated reacted with N_2O , even though a 700-fold excess of CO_2 was present. When only 0.2 mm Hg N_2O were added, an N_2 quantum yield of $\phi(\text{N}_2) = 0.09$ was obtained showing that with this low N_2O pressure, reaction (4) is no longer important with reactions (2) and (3).

These results strengthen the conclusion that ^1D oxygen atoms are not deactivated by CO_2 , whereas the singlet species formed in the photolysis of N_2O does undergo deactivation. The oxygen atoms generated in the two photolysis

systems are evidently not in the same state so that N_2O photolysis cannot involve ^{18}O oxygen atoms. Accordingly, it may be concluded that the photolysis of N_2O involves ^{16}O oxygen atoms. A previous suggestion [8] is in accord with this conclusion.

5. LiF Color Center Formation and UV Transmission Losses from Argon and Hydrogen Discharges

(a) To be published: J. Opt. Soc. Am.

It has been shown that lithium fluoride crystals develop color centers when they are exposed to the vacuum ultraviolet radiation emitted by argon or hydrogen discharges, and that the direct cause of color center formation is the absorption of radiation in the LiF fundamental band. The absorption features associated with color centers produced in this manner include a VUV continuum extending to wavelengths greater than 2500\AA and bands with maxima near 1120\AA , 2500\AA , 4500\AA , and 6200\AA . By a comparison with the F-center formation previously reported for other alkali halides similarly subjected to irradiation with light absorbed in the respective fundamental bands, it is shown that the 2500\AA band is the lithium fluoride F-band. This finding is of significance in view of the uncertainties which had existed concerning identification of lithium fluoride F-band and which were recently discussed by Kaufman and Clarke [9].

The present work also established that under the employed experimental conditions, the 4500\AA and the 6200\AA bands are secondary features. With respect to the 1120\AA band, it was found that its quantum yield is the same as that for the F-band, giving support to the notion that the 1120\AA band constitutes the LiF β -band. The vacuum ultraviolet continuous absorption, finally, is a unique feature associated only with lithium fluoride. While the nature of the associated color center has yet to be determined, it is here shown to be a primary feature arising directly from absorption of radiation in the LiF fundamental band.

6. Microanalysis of $SO_4^{=}$ and SO_3

(a) Published: Microchem. J. 8, 241 (1964).

In the search for a procedure which would allow the determination of microquantities of soluble sulfate it was found that the reverse titration of barium using its rhodizonate complex as an indicator gave good results if a modified method of end-point determination was applied. Normally, the end point is taken to coincide with the color change of the solution from red to yellow or colorless on the assumption that the change is due to the consumption of barium ions, but the instability of rhodizonic acid acting through the equilibrium with the barium complex can give rise to a premature fading of the color, thus introducing considerable uncertainties in the determination of the true end point. As a consequence, the method is generally not considered accurate for sulfate concentrations below 0.1 mole per liter. In the present procedure, however, drops of indicator solution are periodically added to the

solution while titrating, and the end point is established from the color change which the indicator droplet undergoes as it merges with the solution. Accordingly, the above-described difficulty is circumvented. This new method of end-point determination enables one to measure sulfate quantities as low as 2 μ moles with reasonable precision. The details are the topic of this report.

This technique of sulfate determination has also been employed in conjunction with the analysis of SO_3 in sulfur dioxide, SO_3 being generated photochemically by irradiation with a calibrated mercury light source, the deposited amounts of BaSO_4 corresponded to a quantum yield of approximately unity. A quantum yield of unity is in agreement with what is known about the photodecomposition of SO_2 , so that in the micromole range, the employed method of SO_3 analysis appears to give substantially correct results.

B. THEORETICAL STUDIES: TECHNICAL SUMMARIES OF PUBLISHED REPORTS

The investigations of theoretical studies has resulted in the generation of six technical papers, each of which has been accepted for publication in the open literature and/or has appeared as a GCA Technical Report. Comprehensive summaries of these reports are given below.

1. The Photoionization of Atomic Oxygen

- (a) GCA Technical Report No. 64-1-N.
- (b) Published: Planetary & Space Sci. 12, 235 (1964).

The photoionization cross sections of atomic oxygen are basic atomic parameters of fundamental importance in the quantitative understanding of the ionosphere. An accurate calculation at the spectral head has been carried out by Bates and Seaton [10] but the only values at shorter wavelengths, where ejection of the inner shell electrons is energetically possible, are the approximate estimates of Dalgarno and Parkinson [11] and the unpublished results of J. Cooper.

In the present work the problem is formulated with a Hartree-Fock approximation for the final states of a transition involving the ejection of an outer or an inner shell electron from all ground state configurations $1s^2 2s^2 2p^4$ and the cross sections for the photoionization of atomic oxygen by radiation at wavelengths longer than 25\AA are calculated.

The mathematical details of the formulation and method of numerical solution are given in the original reports and are not reported in this brief summary. However, the results can be summarized in the Figures 1-7 and briefly discussed in the light of some current aeronomy problems.

The cross sections for the individual transitions

$$O(1s^2 2s^2 2p^4) {}^3P + h\nu \rightarrow O^+(1s^2 2s^2 2p^3) {}^4S, {}^2D, {}^2P + e^- \quad (1)$$

and

$$O(1s^2 2s^2 2p^4) {}^3P + h\nu \rightarrow O^+(1s^2 2s 2p^4) {}^4P, {}^2P + e^- \quad (2)$$

are important in predicting the electron temperature in the ionosphere [12] and in predicting the intensities of ionic emission lines arising from fluorescence [13]. The results corresponding to both the dipole length (A-curves) and dipole velocity (B-curves) formulations are shown in Figures 1 to 5 and the cross sections for the sum of processes (1) and (2) are shown in Figures 6 and 7.

At the spectral head at 910\AA , we obtain cross sections of respectively $2.7 \times 10^{-18} \text{ cm}^2$ and $3.4 \times 10^{-18} \text{ cm}^2$ in the length and velocity formulations,

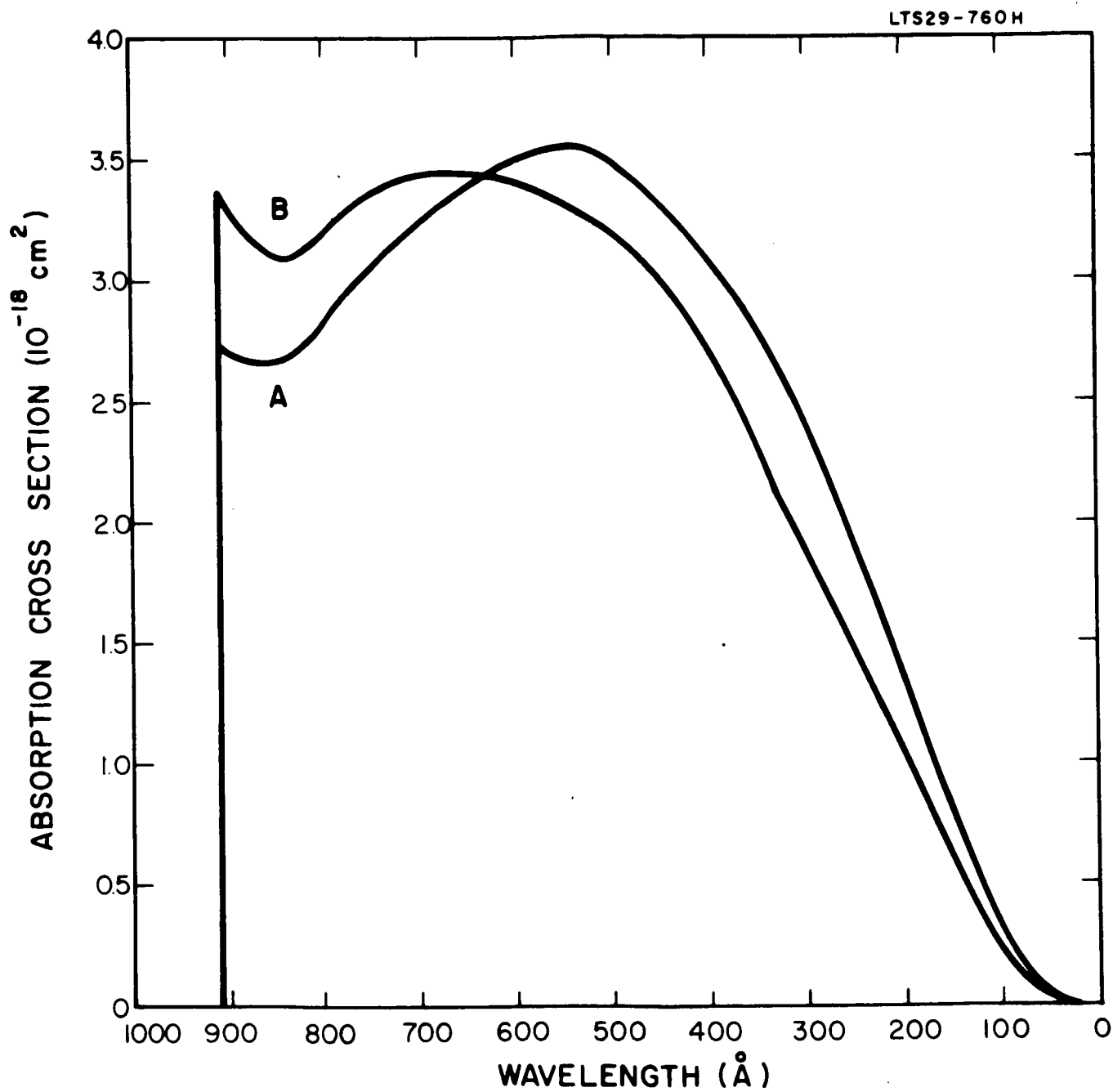


Figure 1 (II-B-1). $\text{O}(^3\text{P}) + h\nu \rightarrow \text{O}^+(^4\text{S}) + e^-$.

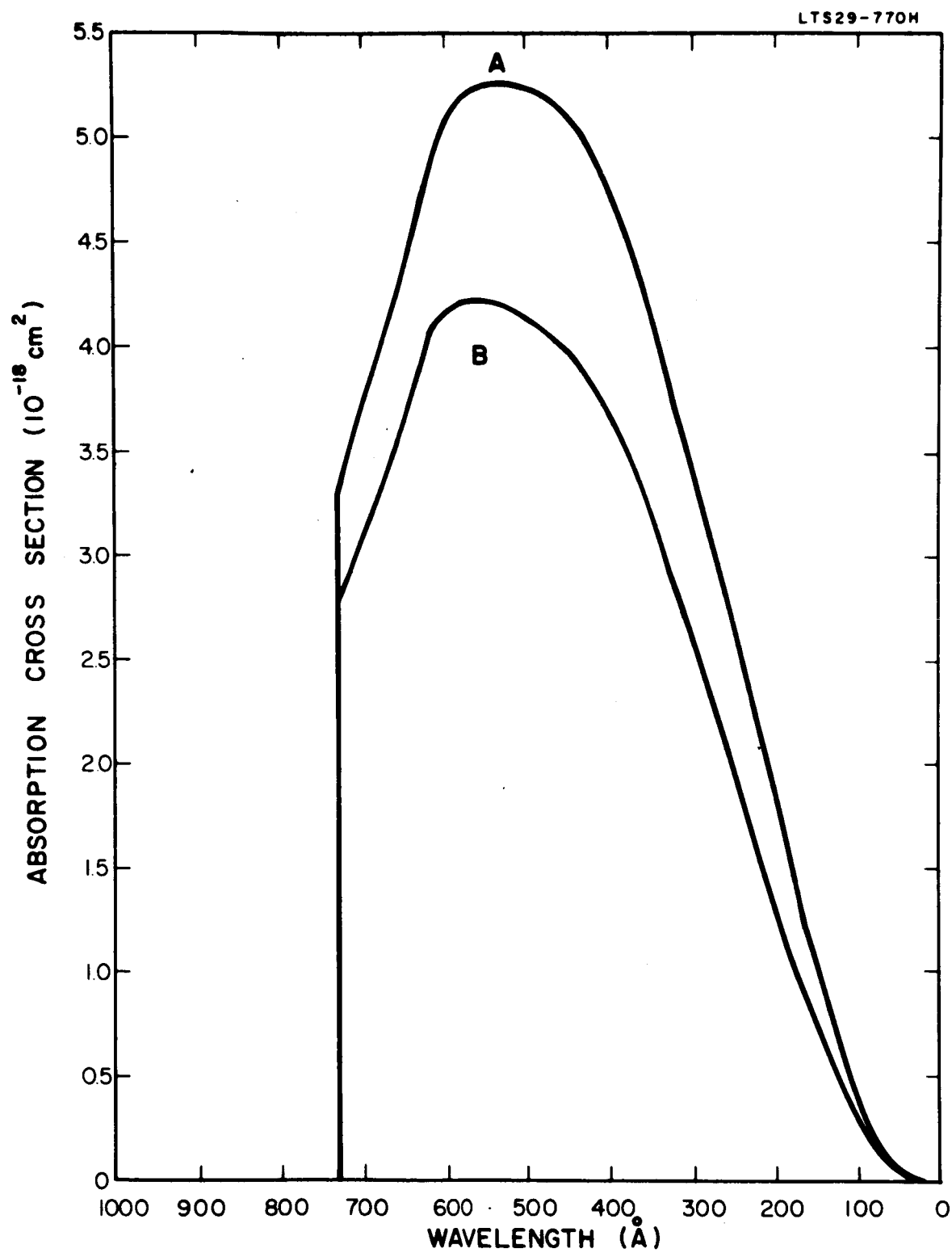


Figure 2 (II-B-1). $O(^3P) + h\nu \rightarrow O^+(^2D) + e^-$.

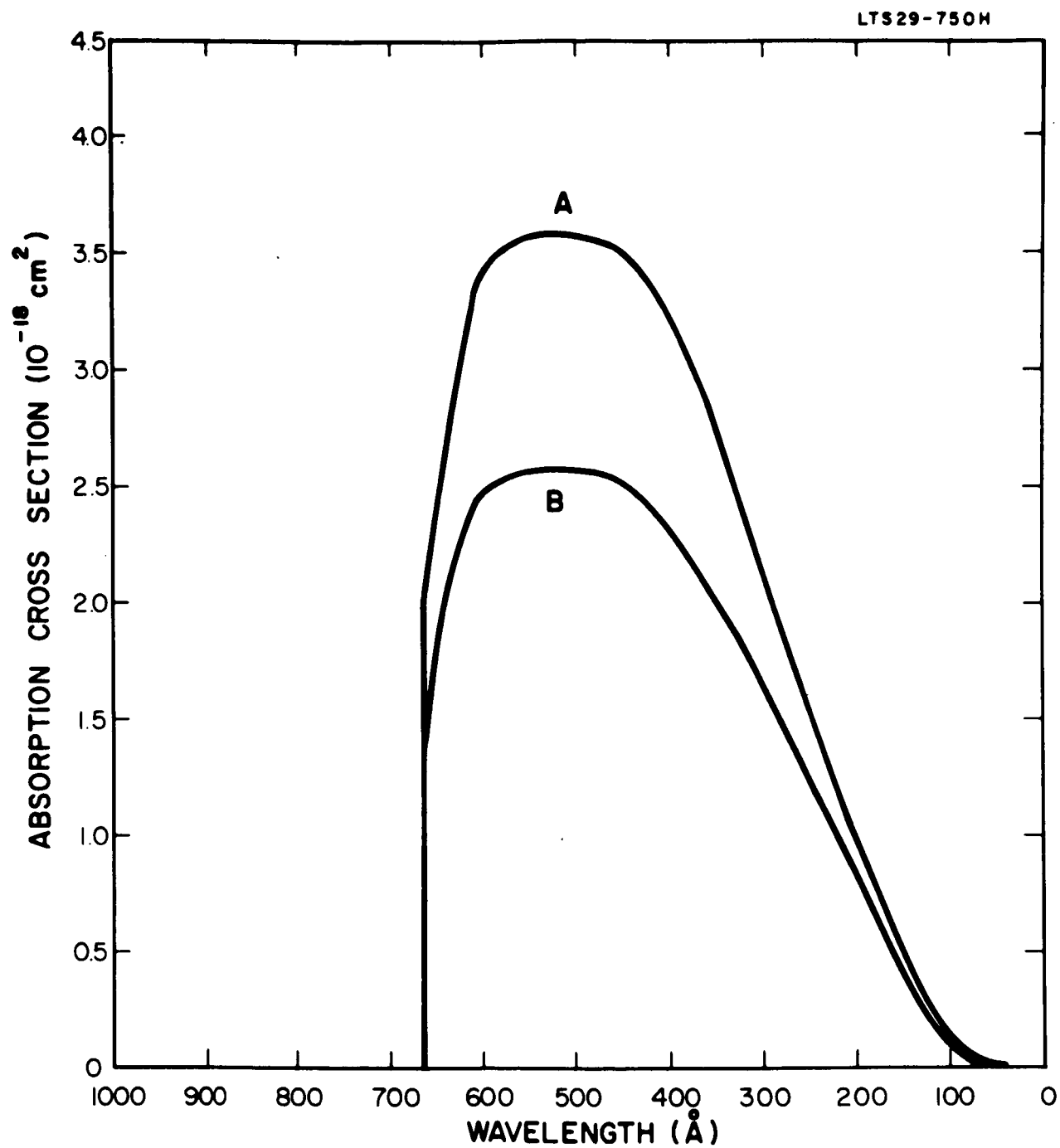


Figure 3 (II-B-1). $O(^3P) + h\nu \rightarrow O^+(^2P) + e^-$.

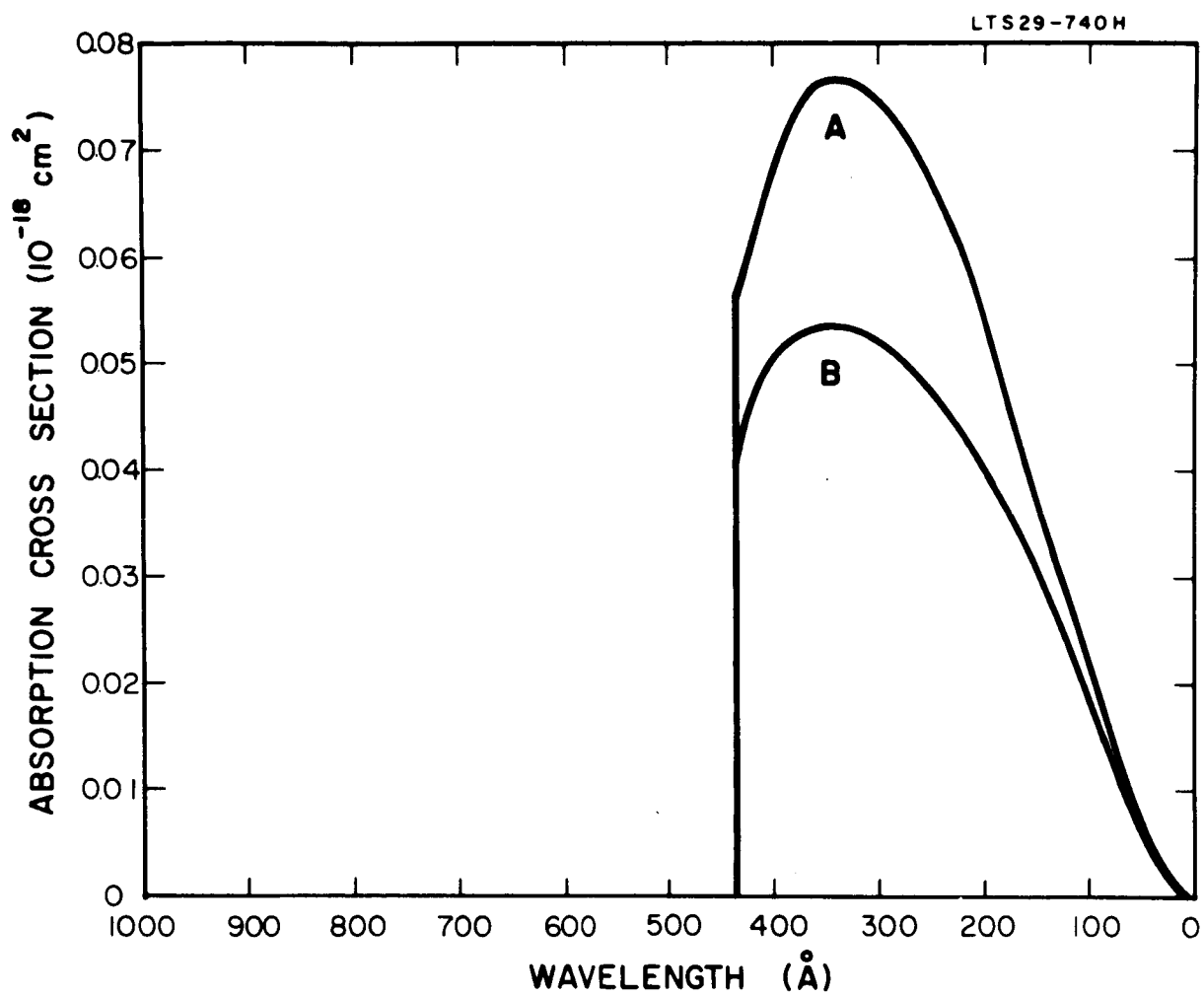


Figure 4 (II-B-1). $\text{O}(^3\text{P}) + h\nu \rightarrow \text{O}^+(^4\text{P}) + \text{e}^-$.

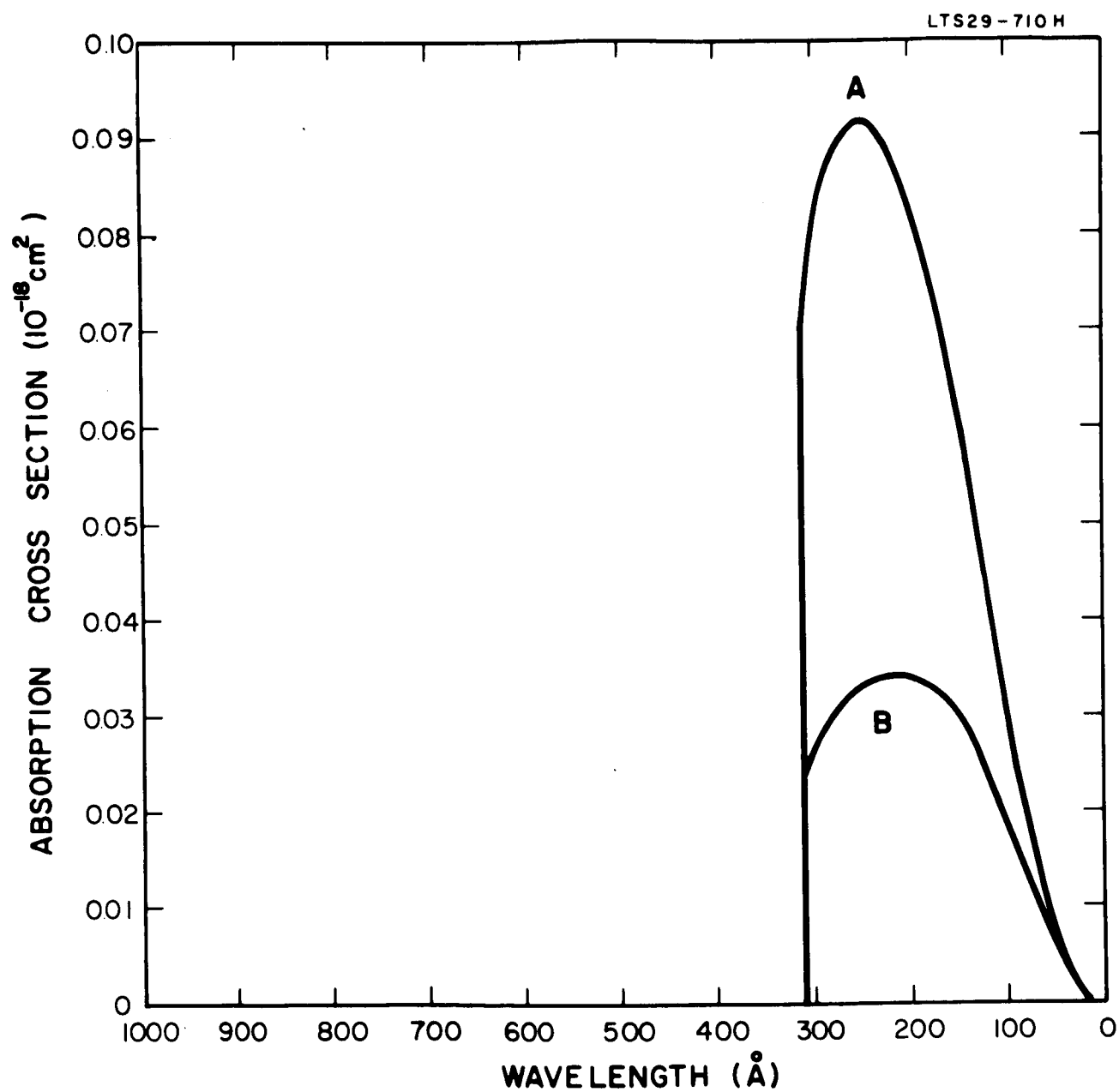


Figure 5 (II-B-1). $\text{O}(^3\text{P}) + h\nu \rightarrow \text{O}^+(^2\text{P}) + e^-$.

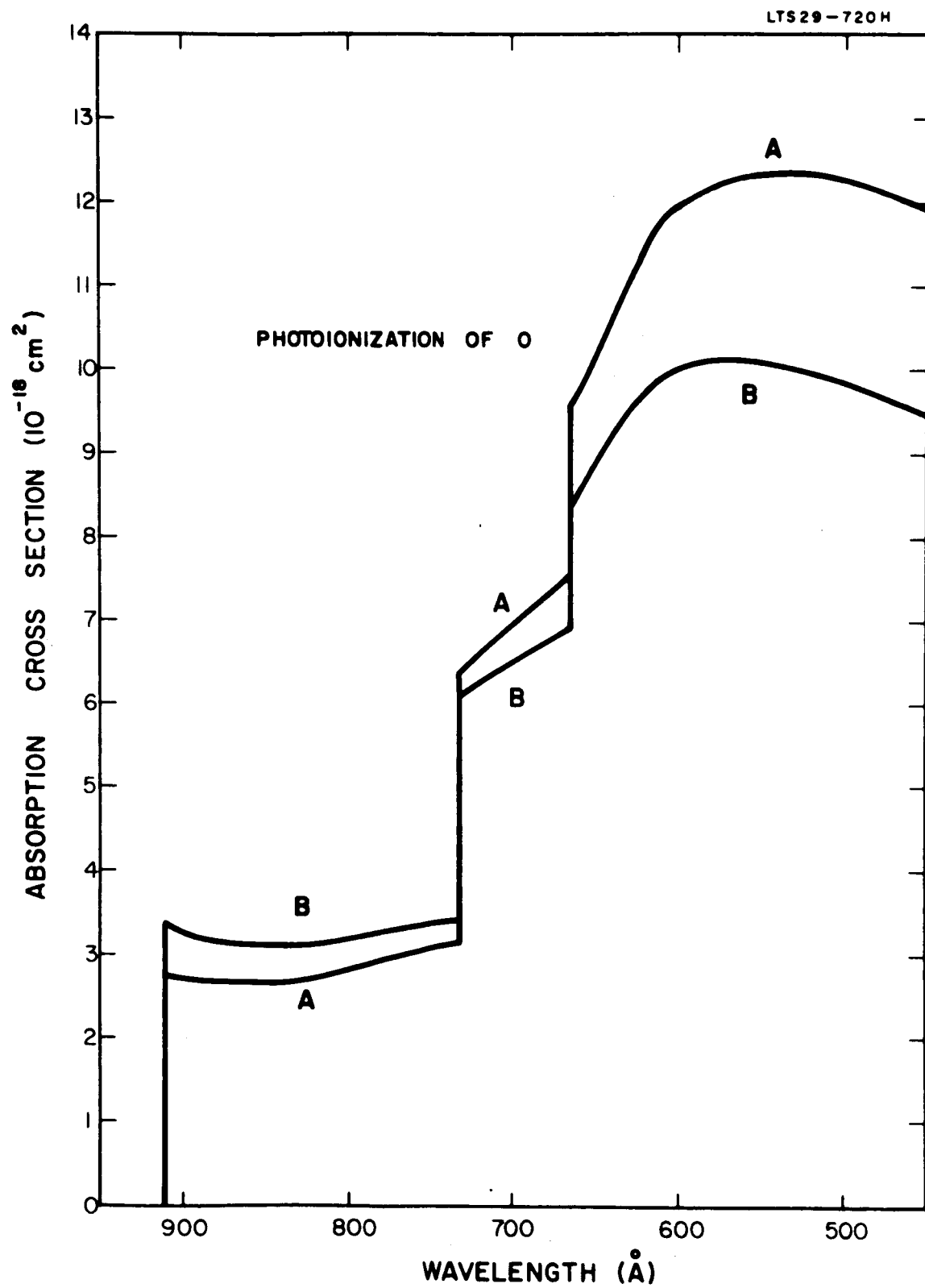


Figure 6 (II-B-1). Absorption cross sections, λ 1000 - λ 500.

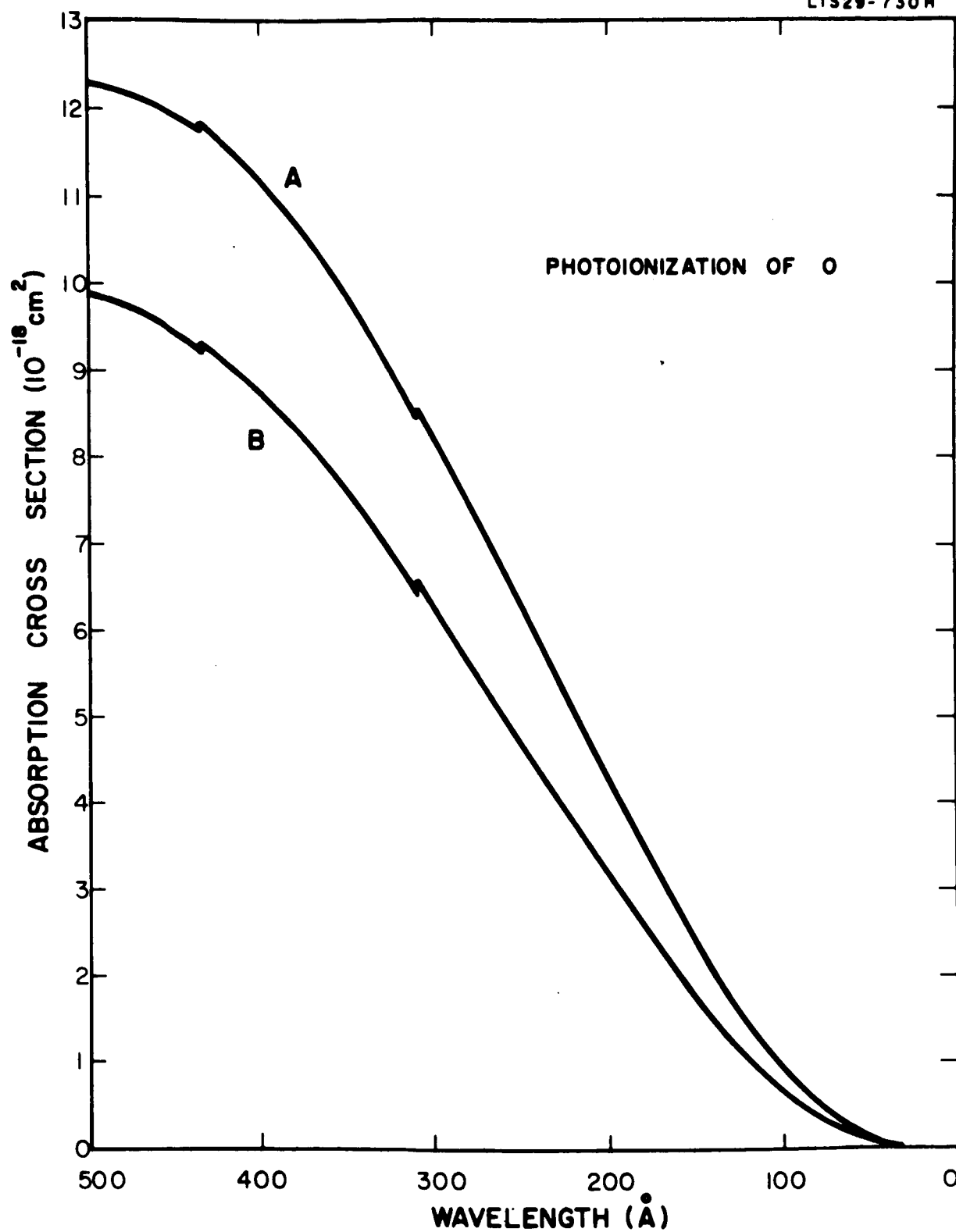


Figure 7 (II-B-1). Absorption cross sections, λ 500 - λ 0.

TABLE 1 (II-B-1)
CROSS SECTIONS APPROPRIATE TO SOME IMPORTANT SOLAR LINES

$\lambda(\text{\AA})$	a_{λ}	$\lambda(\text{\AA})$	a_{λ}
283	5.72(-18)*	584.3	1.01(-17)
303.8	6.34(-18)	610	9.96(-18)
335	7.18(-18)	625	9.60(-18)
368.1	8.11(-18)	629.7	9.45(-18)
465.2	9.64(-18)	770.4	3.30(-18)
500	9.87(-18)	789	3.22(-18)
520	9.98(-18)	834	3.09(-18)
554	1.01(-17)	875	3.19(-18)

* $5.72 \times 10^{-18} \text{ cm}^2$

each of which is about 25 percent larger than that computed by Bates and Seaton [10]. The discrepancies probably arise from the different forms employed for the discrete orbitals.

It is not possible to decide which of the length and velocity cross sections is the more accurate. For the photoionization of neon, a comparison of the theoretical [15] and measured values [15] shows that the velocity values are more accurate at the spectral head and at short wavelengths and the length values are more accurate at intermediate wavelengths, but there seems little reason to expect a similar behavior for oxygen. Because the velocity formulation should be the more accurate at short wavelengths [16] and because it has been found that it converged much more rapidly in the iterative process, we shall regard the velocity cross sections as the more reliable. Except short wavelengths, the differences between the length and velocity cross sections are never greater than 25 percent and this percentage may be accepted as a measure of the accuracy of the dipole velocity results.

Included is a table of cross sections appropriate to the most important of the solar lines observed by Hall, Damon and Hinteregger [17].

Recent discussions of the formations of the ionosphere have been based upon the cross sections given by Dalgarno and Parkinson [11] whose values are generally about 40 percent larger than those in the table.

2. An Expansion Method for Calculating Atomic Properties - I. The 2S and $^2P^o$ States of the Lithium Sequence

- (a) GCA Technigal Report No. 64-5-N.
- (b) Published: Proc. Roy. Soc. A275, 492 (1963).

3. An Expansion Method for Calculating Atomic Properties - II. Transition Probabilities

- (a) GCA Technical Report No. 64-6-N.
- (b) Published: Proc. Roy. Soc. A280, 258 (1964).

Papers I and II of this series will be summarized as one, since the latter simply represents a logical extension of I. The brief summary follows.

A knowledge of the probabilities of absorption and emission of electromagnetic radiation by atmospheric constituents is necessary for a detailed interpretation of the effects of solar radiation on planetary atmospheres. There is available for calculating transition probabilities a general approximation scheme — the Hartree-Fock approximation — but it is extremely laborious to apply and its accuracy is often very uncertain. A new mathematical approach would be desirable. In the present attempt for a new technique, the resulting analysis is essentially purely mathematical. Thus it is not compatible to meaningful summary except that a rather descriptive approach may be employed in which the mathematical details are omitted since the interested reader can refer to the original report.

In this series of papers a new, more accurate simplified method is developed which is generally applicable and which leads to results of definite accuracy. It is shown that the method involves functions that enter the formal theory which are written as series comparisons in inverse powers of the nuclear charge. The calculations can be carried through to any given order, though they become complicated after the second order. Results are automatically obtained for all members of any given isoelectronic sequence in contrast to other schemes which necessitate individual calculations. The one difficulty that the procedure presents arises from the convergence of the series expansions; the material in the two papers prepared under this contract were designed to explore the role of this difficulty for light elements. It turns out that this material also provides the most accurate available transition probabilities for 2s-2p electron jumps in neutral and ionified atomic oxygen and nitrogen; it is also demonstrated that the Hartree-Fock approximation may be seriously inadequate for appropriate solutions of these problems.

4. Ambipolar Diffusion in the F-Region

(a) Published: J. Atmos. Terrest. Phys. 26, 939 (1964).

In an earlier communication with the above title [18], Dalgarno presented values of the diffusion coefficient of O^+ ions in atomic oxygen which were based upon theoretical estimates of the resonance charge transfer cross sections [19]. Recent measurements [20] show that his estimates of the charge transfer cross sections, though giving the correct variation with energy, are too large by a factor of three. It follows that the collision frequency [21] of O^+ in O should be decreased by a factor of three and the diffusion coefficients should be increased by a factor of three. The corrected values are given in the table below.

COLLISION FREQUENCIES ν AND DIFFUSION
COEFFICIENTS D OF O^+ IN O^*

Temperature $^{\circ}K$	300	400	500	700	1000	2000
$(D_n \times 10^{18}) \text{ cm}^{-1} \text{ sec}^{-1}$	3.3	3.9	4.5	5.7	6.9	9.6
$(\nu \times 10^{10}/n) \text{ cm}^3 \text{ sec}^{-1}$	4.7	5.0	5.7	6.3	7.3	10.0

* $n \text{ cm}^{-3}$ is the number density of atomic oxygen.

5. Ionospheric Electron Temperatures Near Dawn

(a) Published: Planetary & Space Sci. 13, 143 (1965).

Solar ultraviolet radiation leads to a source of energy which preferentially heats the ionospheric electrons and maintains the electron temperature T_e above the neutral particle temperature T_g . It has been suggested that near dawn, when the ambient electron densities n_e are small, the electron temperature may be anomalously large; calculations of the location and extent of the anomaly have been performed and are discussed below.

The local heat source Q may be computed following standard procedures and values of Q at altitudes of 200, 250, 300, 350 and 400 km in an atmosphere with an ionospheric temperature of $750^{\circ}K$ are listed in Table 1 for a number of solar zenith angles θ .

TABLE 1 [II-B-5]
VALUES OF Q (keV cm⁻³ sec⁻¹)

h	$\theta=90^\circ$	$\theta=89^\circ$	$\theta=87^\circ$	$\theta=80^\circ$	$\theta=60^\circ$
200	0.1	0.1	0.2	1.0	3.5
250	0.3	1.0	1.5	2.6	3.7
300	0.7	1.0	1.1	1.3	1.4
350	0.4	0.5	0.5	0.5	0.5
400	0.2	0.2	0.2	0.2	0.2

The heated electron gas cools in collisions with the neutral particles and positive ions, the most important processes being elastic scattering by positive ions, rotational and vibrational excitation of molecular nitrogen and excitation of atomic oxygen to the ¹D level. The calculated variation of the cooling efficiency with electron temperature shows that at low altitudes, collisions with molecular nitrogen control the cooling for all electron temperatures; whereas at high altitudes, cooling by collisions is due to (a) elastic scattering by positive ions where T_e is small and to (b) excitations of atomic oxygen where T_e is large.

The equilibrium electron temperature is obtained by equating the rate of heating to the rate of cooling. The value so derived is very sensitive to the assumed ambient electron density n_e , the controlling parameter being Q/n_e at low altitudes and Q/n_e^2 at high altitudes, and the variation of T_e after sunrise will be governed more by changes in n_e than by the changes in Q .

We shall assume arbitrarily that the electron density in the ionosphere changes linearly from the nocturnal profile measured by Sagalyn and Smiddy to the daytime profile derived by Hanson as θ changes from 90° to 80° . The actual situation is much more complicated and our results, presented in Figure 1, serve merely to illustrate the possible behavior of T_e . They suggest that very high values of T_e may occur at 250 km for a short interval following sunrise. Essentially, this behavior has been found by Sagalyn and Smiddy in the Discoverer satellite data.

Cooling by excitation of atomic oxygen is important and the high values of T_e will be accompanied by a glow in the oxygen red lines at 6300Å. The predicted intensity corresponding to the model of T_e shown in Figure 1 varies from 500 Rayleighs at 90° to 1 Rayleigh at 80° . There are other processes which populate the ¹D level of atomic oxygen but a red dawn flash due to the high electron temperatures might be observable. Excitation of the vibrational levels of molecular nitrogen also contributes to the cooling of the hot electron gas and this should be reflected in an enhanced vibrational development of the first negative band system.

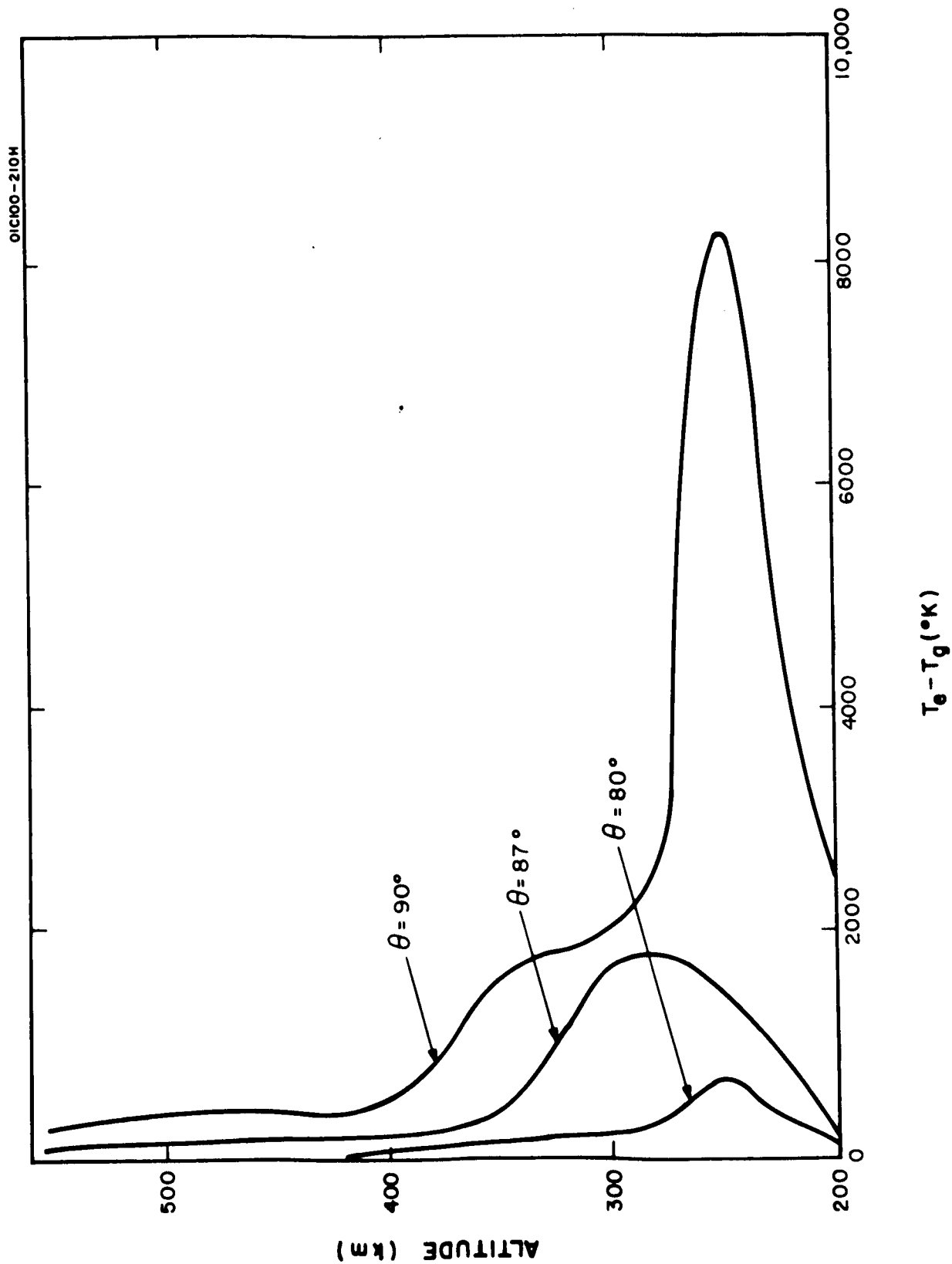


Figure 1 (II-B-5). Difference between electron and neutral particle temperatures versus altitude for three solar zenith angles.

It can be shown that with increasing altitude a maximum and a minimum are introduced into the curve of cooling efficiency against temperature. Hence if Q is large enough at high altitudes, the electron temperature may run away from an equilibrium controlled by collisions with positive ions to one controlled by collisions with neutral particles. Thus, with our model, if at 650 km Q/n_e^2 were to increase through 6.8×10^{-9} eV cm³ sec⁻¹, $T_e - T_g$ would change from 1500°K to over 5000°K and if Q/n_e^2 were to decrease through 6.2×10^{-9} eV cm³ sec⁻¹, $T_e - T_g$ would change from 4000°K to 800°K. Such a heat source cannot be supplied by the local deposition of energy from solar ultraviolet radiation. However, Hanson and Mariani have pointed out that the faster photoelectrons escape and they must be a significant source of heat at great altitudes. According to our calculation of the production of fast electrons by solar ultraviolet radiation, the upward flux at dawn approaches 10^{10} cm⁻² sec⁻¹ which exceeds the critical value where n_e is less than about 10^5 cm⁻³. Cooling by thermal conduction prevents the electrons from attaining the very high temperatures that would otherwise result at great altitudes from the flux of fast photoelectrons, but the tendency of the electron temperature to run away should be observable at dawn. An estimate of the duration of the effect will require the solution of the time-dependent problem.

In this discussion it has been assumed that the positive ion temperature T_i is equal to the neutral particle temperature T_g . In fact, the heating effect of the escaping photoelectrons will cause T_i to exceed T_g .

6. Electron Temperatures in the D Region

- (a) GCA Technical Report No. 65-8-N.
- (b) To be published: Proc. Roy. Soc.

It is customary in analyzing radio wave measurements in the D region to assume that the electrons have a Maxwellian velocity distribution characterized by an electron temperature T_e equal to the temperature T_g of the ambient neutral particle atmosphere. Evidence has accumulated in recent years that equality of electron and neutral particle temperatures does not prevail in the upper ionospheric regions [22-26] and there have been suggestions that T_e exceeds T_g in the D region also. Thus from observations of cross-modulation, Rumi [27] has derived an electron temperature of 1200°K at an altitude of 40 km and Belrose and Hewitt [28] have suggested that the collision frequency in the D region is correlated with solar activity, the correlation arising through variations of T_e and not of T_g . A tentative theory has been advanced by Sears [29] which lends support to these observations, but the contrary view shall prevail in this discussion.

Fast electrons lose energy rapidly in the D region by exciting and ionizing the atmospheric constituents until their energy falls to about 5 eV. Below 5 eV energy is lost mainly in vibrational and rotational excitation of nitrogen and oxygen and in elastic collisions.

The cross section $\sigma(o, v|E)$ for vibrational excitation of nitrogen by electrons of energy E

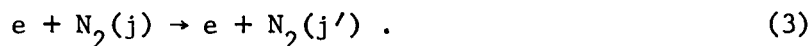


have been measured by Schulz [30]; Chen [31] has presented a theory which closely reproduces the measurements. The associated rate of energy loss for unit density of molecular nitrogen is

$$\frac{dE}{dt} = \left(\frac{2E}{m}\right)^{\frac{1}{2}} \sum_v \Delta(o,v) \sigma(o,v|E) \quad (2)$$

where $\Delta(o,v)$ is the internal energy change occurring in the process. The rate of energy loss through vibrational excitation of N_2 is shown in Figure 1 as a function of impact energy.

To calculate the rate of energy loss associated with rotational transitions in molecular nitrogen



The cross sections $\sigma(j,j'|E)$ of Dalgarno and Moffett [32] were used. The rate of energy loss for unit density of nitrogen at a temperature T_g is given by

$$\frac{dE}{dt} = \left(\frac{2E}{m}\right)^{\frac{1}{2}} \frac{\sum_j \sum_{j'} \Delta(j,j') \sigma(j,j'|E) (2j+1) \exp[-Bj(j+1)/kT_g]}{\sum_j (2j+1) \exp[-Bj(j+1)/kT_g]} \quad (4)$$

where B is the rotational constant. Values of (4) are given in Figure 2 for $T_g = 200^\circ K$.

Similar calculations have been carried out for molecular oxygen, using the quadrupole moment and polarization anisotropy measured by Bridge and Buckingham [33] and the values of dE/dt for electrons in molecular oxygen are also presented in Figure 2.

Energy can be lost in elastic collisions, the energy loss rate being

$$\frac{dE}{dt} = -2 \frac{m}{M} \left(\frac{2E}{m}\right)^{\frac{1}{2}} v Q_m \left(E - \frac{4}{3} E_g\right) \quad (5)$$

where E_g is the thermal energy of the gas, M is the mass of the molecule and Q_m is the momentum transfer cross section. It can be shown that energy loss in elastic collisions with molecules is negligible compared to loss through rotational transitions.

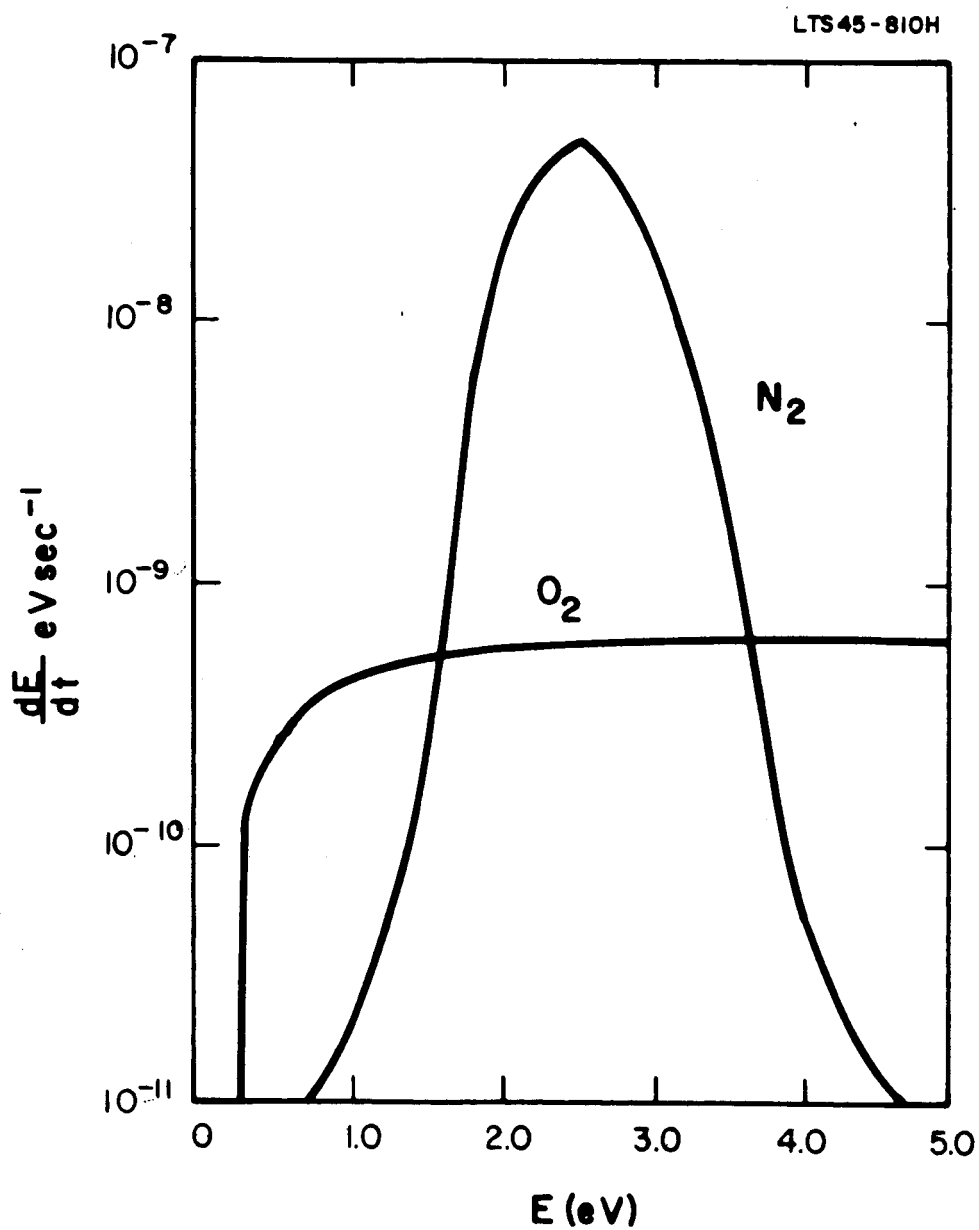


Figure 1 (II-B-6). Rates of energy loss through vibrational excitation of nitrogen and oxygen.

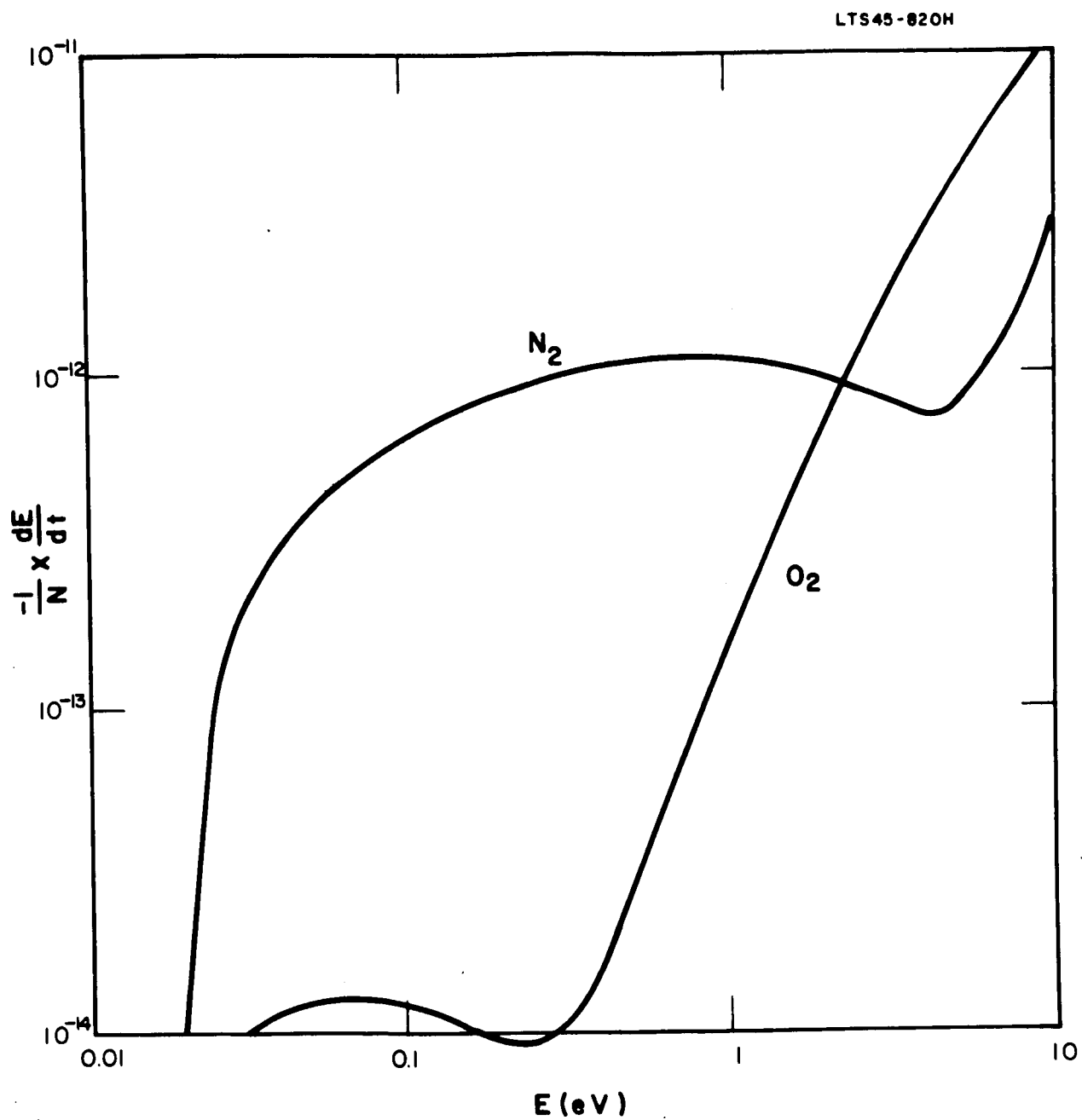


Figure 2 (II-B-6). Rates of energy loss through rotational excitation of nitrogen and oxygen.

In the upper ionospheric regions energy loss in elastic collisions with the ambient electrons is an important mechanism for preferentially heating the ambient electron gas and maintaining T_e above T_g [34,35]. If $n_e \text{ cm}^{-3}$ is the ambient electron density, the rate of energy loss by elastic electron-electron collisions is given approximately by

$$\frac{dE}{dt} = - \frac{7.7 \times 10^{-6}}{E^{\frac{1}{2}}} n_e \ln(\Lambda \text{ eV sec}^{-1}) , \quad (6)$$

where Λ depends upon n_e and T_e and E is measured in eV [35,36]. Values of $\ln \Lambda$ for various electron temperatures and densities are given in Table 1. The electron density in the D region rarely approaches 10^5 cm^{-3} even during periods of severe disturbance and an effective upper bound to (6) is accordingly

$$\left| \frac{dE}{dt} \right| < \frac{11}{E^{\frac{1}{2}}} \text{ eV sec}^{-1} . \quad (7)$$

A comparison of (7) with the rate of energy loss from vibrational and rotational excitation of nitrogen and oxygen is given in Figure 3 for electrons moving with energies of 1 eV, 0.1 eV and 0.03 eV in the D region. It is clear that electron-electron interactions are rarely of any importance in the D region. The main mechanisms tending to establish equilibrium consist of rotational transitions in molecular nitrogen so that if the electrons in the D region have a Maxwellian velocity distribution, it will be characterized by the neutral particle gas temperature T_g .

The velocity distribution of the D region electrons depends on the electron production and removal mechanisms. According to a recent review by Reid [37], the normal D region is produced by the absorption of Lyman- α by nitric oxide and by the absorption of X-rays and cosmic rays. During disturbed conditions at middle and low latitudes, the flux of incident X-rays is enhanced and at high latitudes an additional source of ionization is present, auroral absorption being due primarily to bombarding electrons and polar cap absorption by bombarding solar protons.

The fast electrons produced by the primary ionization processes lose energy rapidly. Some are removed by the two-body dissociative attachment process



which has a peak cross section of about $1.4 \times 10^{-18} \text{ cm}^2$ at an energy of about 6.5 eV [38-40], but most are removed by the three-body attachment process



the rate of which has been measured by Chanin, Phelps and Biondi [41].

TABLE 1 [II-B-6]
VALUES OF $\ln \Lambda$ (Eq. 6)

n_e (cm ⁻³)	10	10 ²	10 ³	10 ⁴	10 ⁵	10 ⁶	10 ⁷
T_e (°K)							
200	16.2	15.1	13.9	12.8	11.6	10.4	9.3
300	16.8	15.7	14.5	13.4	12.2	11.1	9.9
400	17.3	16.2	14.9	13.9	13.0	12.6	10.3
500	17.6	16.4	15.3	14.1	13.0	11.8	10.7
1000	18.6	17.5	16.3	15.2	14.0	12.9	11.7

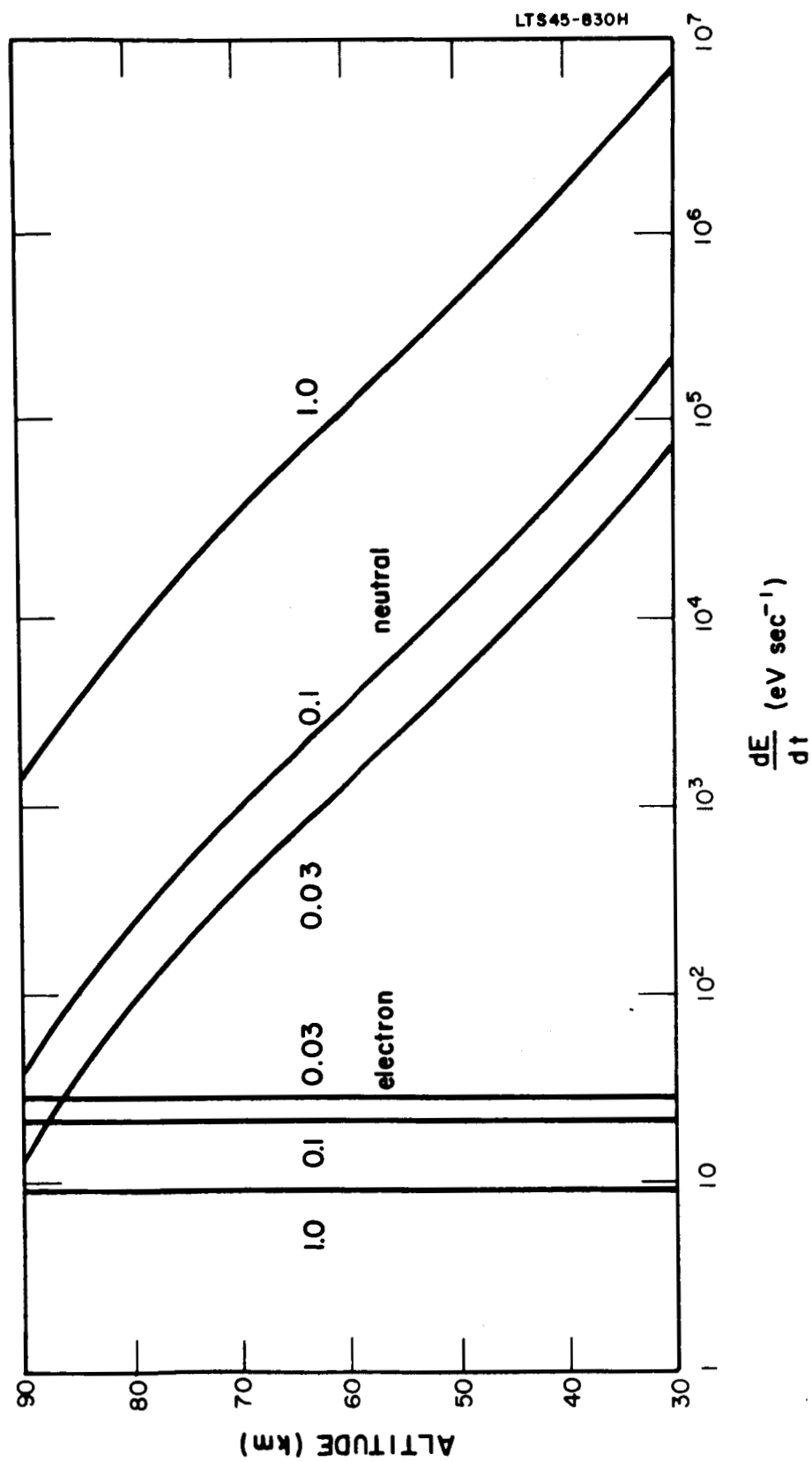


Figure 3 (II-B-6). Rates of energy loss in collisions with ambient electrons and with neutral particles for incident electrons with energies of 1 eV, 0.1 eV and 0.03 eV.

A comparison of the mean times for energy loss associated with vibrational and rotational transitions and elastic scattering with the mean times for attachment is given as a function of energy for a neutral particle density of 10^{15} cm^{-3} (appropriate to an altitude of 70 km) and as a function of altitude for energies of 1 eV, 0.1 eV and 0.03 eV, respectively. The energy loss times are in all cases much shorter than the attachment times. Thus nearly all the electrons are converted into thermal electrons before their removal by attachment and the removal mechanism has little effect on the electron velocity distribution. The thermal electrons will have a Maxwellian velocity distribution characterized by the gas temperature T_g . Superimposed upon the thermal distribution there will be a small high energy component, the magnitude of which is enhanced by photodetachment.

After an electron attaches to form a negative ion, it is soon detached by the absorption of solar radiation. If the major negative ion is O_2^- , the free electron has an initial energy peaking at about 2 eV. This supply of 2 eV electrons in the daytime D region is much larger than that provided by the primary ionization processes and it may give rise to a substantial nonthermal component in the velocity distribution [29].

An estimate was made of the nonthermal component of the velocity distribution by equating the number of electrons entering the energy interval dE in unit time to the number leaving it. Then if $f_a(E) dE$ is the number of electrons with energies lying between E and $E + dE$,

$$f_a(E) = - \sum_{E' > E} q(E') \bigg/ \frac{dE}{dt} \quad (10)$$

where $q(E')$ is the rate of production of electrons of energy E' . In general, the nonthermal component does not play a significant role.

Finally, if the electron gas in the D region is heated preferentially so that T_e exceeds T_g , it will cool mainly by rotational excitation of molecular nitrogen if T is less than 1300°K and by vibrational excitation of molecular nitrogen if T_e exceeds 1300°K . The rate of cooling through rotational excitation may be derived from calculations by Dalgarno and Moffett [42] and by Altshuler [43]. It is given approximately by

$$\frac{dT_e}{dt} = \frac{-3 \times 10^{-10} (T_e - T_g)}{T_e^{\frac{1}{2}}} N \text{ } ^\circ\text{K sec}^{-1} \quad (11)$$

where N is the air density. Values of the cooling rate for a gas temperature of 200°K are given in Table 2. The rate of cooling through vibrational excitation may be derived from calculations by Chen [44]. Values of it are given in Table 2.

TABLE 2 [II-B-6]

COOLING RATES - $\frac{1}{N} \frac{dT_e}{dt}$ °K/sec-cm³ FOR ROTATIONAL AND VIBRATIONAL EXCITATION

		Electron Temperature, T _e , °K					
		200	300	500	1000	1500	2000
Rotational (T _g = 200°K)	0		1x10 ⁻⁹	2x10 ⁻⁹	5x10 ⁻⁹	7x10 ⁻⁹	7x10 ⁻⁹
Vibrational	3x10 ⁻¹⁵		8x10 ⁻¹³	8x10 ⁻¹¹	2x10 ⁻⁹	9x10 ⁻⁹	2x10 ⁻⁸

The electron temperature of 1200°K derived by Rumi [6] at an altitude of 40 km implies, according to Table 2, an energy deposition into the electron gas of the order of $10^7 \text{ eV cm}^{-3} \text{ sec}^{-1}$ for an electron density of 10^2 cm^{-3} . Such an energy deposition rate seems unacceptably large and the interpretation of Rumi's observations through an enhanced electron temperature is implausible.

C. EXPERIMENTAL STUDIES IN THE VUV AND EUV SPECTRAL REGIONS: TECHNICAL SUMMARIES OF PUBLISHED REPORTS

The investigation of the experimental studies in the VUV and EUV spectral regions has resulted in the generation of nine technical papers, each of which has been accepted for publication in the open literature and/or has appeared as a GCA Technical Report. Comprehensive summaries of these reports are given below.

1. New Energy Levels in Xenon and Krypton

- (a) GCA Technical Report No. 64-3-N.
- (b) Presented (under the title "Photoionization of Rare Gases") at the APS Meeting, New York, New York, January 22-25, 1964.
- (c) Published: Phys. Letters 8, No. 2, 107 (15 January 1964).

In the development of the rare gas ionization chambers for absolute intensity measurements it was found necessary to avoid regions of discrete structure within the ionization continuum. Since no absorption studies had been made in the rare gases below 600Å, the position and existence of discrete structure was unknown. Possible structure could be expected from excitation of the inner s-electrons in transitions of the type $ms-np$ where $m = 3, 4$, and 5 for argon, krypton, and xenon, respectively, and $n = m + 1, m + 2, \dots$, etc. The position of these excited levels was predicted in an earlier work [45]. A search for these levels was carried out and found in Xe and Kr.

The absorption spectrum of Xe and Kr was obtained with a 2.217 M normal incidence vacuum spectrograph using a 1200 line/mm grating. This gave a plate factor of $3.76\text{\AA}/\text{mm}$. With a 30-micron slit width a wavelength separation of approximately 0.1Å could be resolved. The gas under investigation was introduced directly into the spectrograph at approximately 10^{-3} torr. Comparison spectra were then taken with and without the absorbing gas. Kodak SWR spectroscopic film was used for all exposures. The predicted wavelengths for these transitions in Xe and Kr are listed in Table 1. A search for these energy levels in absorption was carried out in the vicinity of the predicted values. The results obtained are also listed in Table 1.

The agreement between the observed and predicted values is remarkably good, especially for the highly-excited states. Complete agreement cannot be expected with this method, however, due to orbit penetration of the p-electron. The average cross section for the ionization continuum in the vicinity of the first auto-ionized line was found to be $30 \times 10^{-18} \text{ cm}^2$. Recently, we have measured the photoionization cross section in Xe at 600Å and obtained a value of $32 \times 10^{-18} \text{ cm}^2$.

TABLE 1 (II-C-1)

OBSERVED AND PREDICTED ABSORPTION SPECTRUM DUE TO EXCITATION
OF THE 4s- AND 5s-ELECTRONS IN Kr AND Xe, RESPECTIVELY
(Wavelengths are in Angstrom Units)

Krypton			Xenon		
Transition	λ pred. (a)	λ obs.	Transition	λ pred. (a)	λ obs.
$4(s^2 p^6)$			$5(s^2 p^6)$		
$-4(sp^6)5p$		501.11	$-5(sp^6)6p$		599.95
5p	498.0	497.46	6p	593.5	595.92
5p	497.4	496.87	6p	591.6	591.81
5p		496.04	6p		589.62
6p	471.8	471.54	x	--	579.25
7p	462.8	462.75	y	--	570.90
8p	458.6	457.85	7p	558.5	557.92
9p	456.2	456.14	z	--	552.07
			8p	546.5	546.16
			9p	540.7	540.71
			10p	537.6	537.40
			11p	535.6	535.62

(a) Energy levels used in the calculations were obtained from C. E. Moore, Atomic energy levels, Circ. Natl. Bur. Standards 467, Vol. II (1952); Vol. III (1958).

2. Experimental Photoionization Cross Sections in Argon from Threshold to 280Å

- (a) GCA Technical Report No. 64-3-N.
- (b) Presented (under the title "Photoionization of Rare Gases") at the APS Meeting, New York, New York, January 22-25, 1964.
- (c) Published: J. Opt. Soc. Am. 54, No. 3, 420 (March 1964).

Photoionization cross section measurements of the rare gases are important for many reasons. One major reason is that the experimental data provide a check for the validity of theoretical models. Another reason is that the rare gases are used as absolute standards in the determination of the intensity of vacuum ultraviolet radiation [46]. However, it is desirable to make absolute intensity measurements in regions free from structure. Until recently, the position - or even the existence - of discrete structure beyond the $2P_{1/2}$ threshold was unknown [47,48].

The data presented here were taken with a $\frac{1}{2}$ -m Seya-Namioka monochromator with a 1200 line/mm platinized grating providing a wavelength resolution of 1.3Å. The light source was a high voltage repetitive condensed spark discharge in argon which produced a densely populated line spectrum.

The absorption coefficients k were measured using the double ionization chamber technique in which k is proportional to $\ln(i_1/i_2)$, where i_1 and i_2 are the respective ion currents flowing in the two ion-chambers. A detailed account of this method is described in Reference [46]. The major advantages of this technique should be mentioned. One is that the measurement of i_1 and i_2 is simultaneous and therefore a measurement of k is independent of any fluctuations in light source intensity. The second advantage is that the ion-chambers are insensitive to scattered radiation longer than the ionization threshold.

Figure 1 presents the absorption cross sections of argon from threshold to 280Å. The vertical lines between the $2P_{3/2}$ and $2P_{1/2}$ levels simply indicate schematically the Beutler absorption lines which overlap the $2P_{3/2}$ continuum [49].

The theoretical value of k at the spectral head is in excellent agreement with the experimental value [50]. In the calculations no distinction was made between the two edges; thus, we have reproduced the point on the $2P_{1/2}$ edge for a clearer comparison [51]. Cooper's theoretical model [52] provides k -values of the correct order of magnitude; however, the spectral shape of the absorption curve shows an immediate decrease in the absorption coefficients to wavelengths shorter than the $2P_{1/2}$ edge in contradiction to the present experimental data. Recent experimental work by other groups [53,54] over the same spectral region confirm our spectral shape, and their k -values agree within a few percent of those reported here.

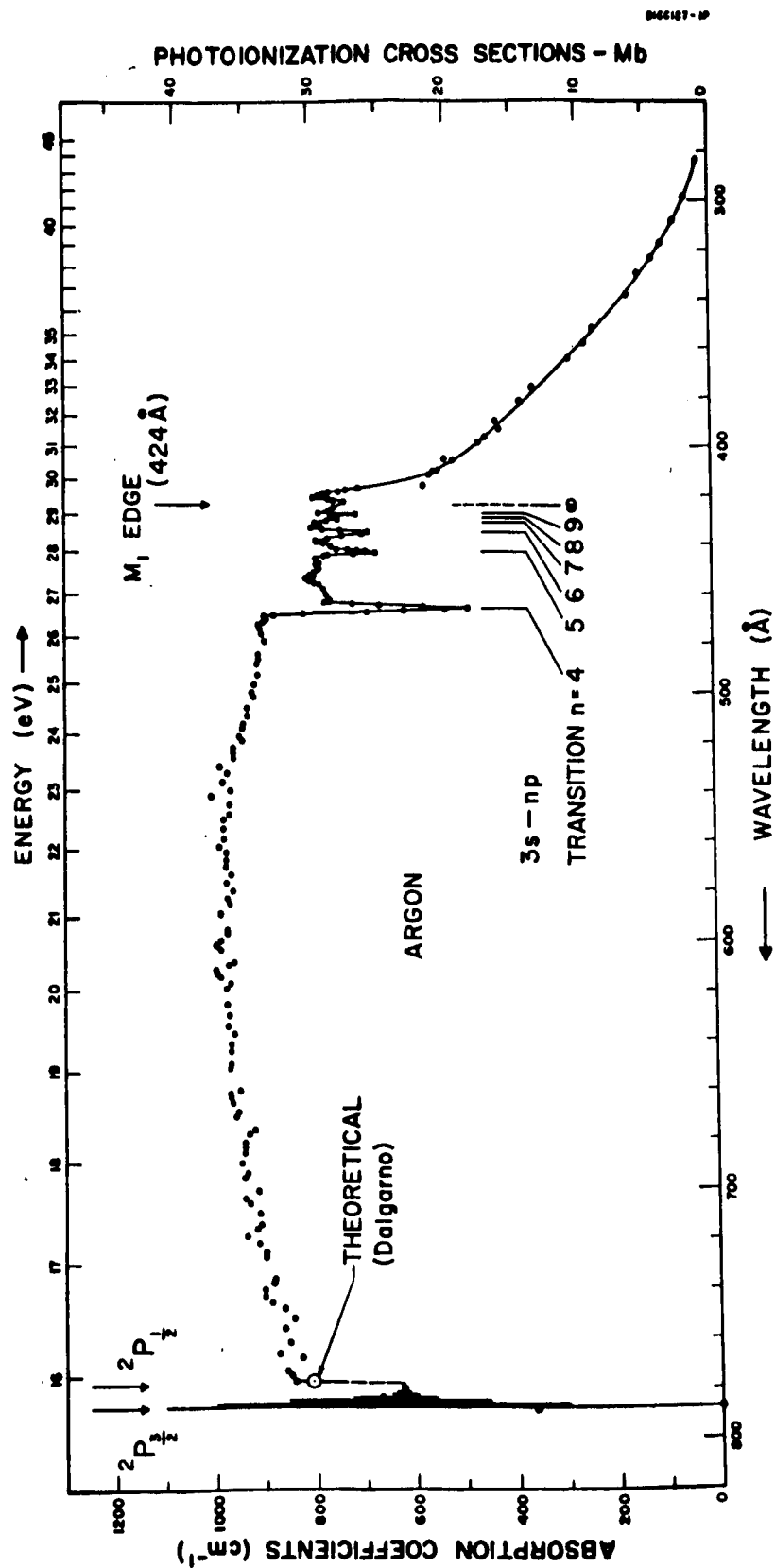


Figure 1 (II-C-2). Photoionization cross sections of argon. The vertical lines between the $2P_{3/2,1/2}$ edges indicate schematically the Beutler autoionization lines.

The complete spectral range of absorption cross sections shown in Figure 1 gave the oscillator strength in the ionization continuum as $f = 5.65$ for the contribution due to ionization of the 3s and 3p electrons.

The preliminary results presented here have provided absolute k -values and the spectral profile for the total photoionization absorption cross sections of argon from threshold to 50\AA where it is extended to 0.1\AA by the data of Allen [55]. Further, as can be seen from Figure 1, the spectral range from 780 to 470\AA is the most suitable when using argon as an absolute standard in the determination of the intensity of vacuum ultraviolet radiation.

3. Photoionization Cross Sections of Xenon from the $^2P_{1/2}$ Edge to 280\AA

- (a) GCA Technical Report No. 64-3-N.
- (b) Presented (under the title "Photoionization of Rare Gases") at the APS Meeting, New York, New York, January 22-25, 1964.
- (c) Published: J. Opt. Soc. Am. 54, No. 6, 842 (June 1964).

Until recently [56,57], no data on the photoionization cross sections of xenon existed and at present there are no published data to wavelengths shorter than 600\AA . Further, no theoretical treatment of the xenon cross sections is available.

The present data provide cross section measurements from the $^2P_{1/2}$ edge at 922.75\AA down to 280\AA and one point at the N_5 edge (190\AA) as measured by Ederer [58].

The data presented here were taken with a $\frac{1}{2}$ -m Seya-Namioka monochromator with a 1200 line/mm platinized grating providing a wavelength resolution of 1.3\AA . The light source was a high-voltage repetitive condensed-spark discharge in argon which produced a densely populated line spectrum.

The absorption coefficients k were measured using the double ionization chamber technique in which k is proportional to $\ln(i_1/i_2)$, where i_1 and i_2 are the respective ion currents flowing in the two ion chambers. A detailed account of this method was described previously.

The photoionization cross section at the $^2P_{1/2}$ spectral head is $61 \times 10^{-18} \text{ cm}^2$. Figure 1 shows the xenon cross sections as a function of wavelength. The large decrease in absorption at 595\AA is due to the excitation of the 5s electrons. The interaction between the discrete absorption lines and the underlying ionization continuum can produce a decrease or an increase in the absorption cross sections [59]. The solid vertical lines indicate the positions of absorption lines due to the 5s-np transitions while the dashed lines represent unidentified absorption structure [60,61].

The oscillator strength, f , for transitions into the ionization continuum has been measured and found to be 5.55. The contribution from the continuum and the Beutler lines between the $^2P_{3/2}$ and $^2P_{1/2}$ edges amounts to 0.43 [57].

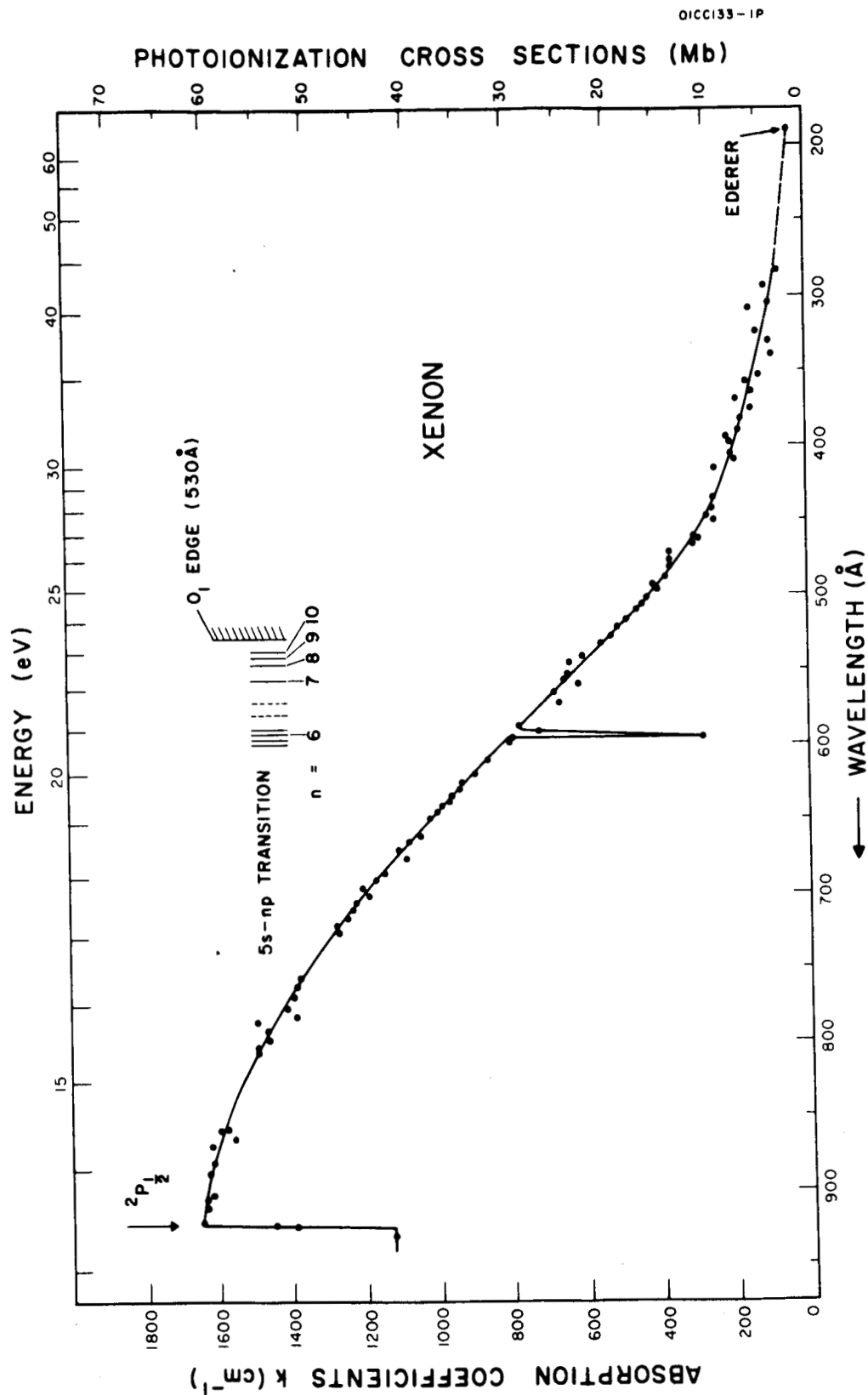


Figure 1 (II-C-3). Photoionization cross sections of xenon. The dashed line is an extrapolation of the present data to that of Ederer's at 190 Å.

Since no f -values are available for the discrete resonance lines preceding the ionization threshold, no precise total oscillator strength can be given. However, based on those calculated for argon an estimated value of 0.3 will be chosen [62]. This then gives the oscillator strength involving only the $5s^2p^6$ electrons down to the N_5 edge as $f = 6.28$. It is of interest to note, however, that the oscillator strength in argon involving the $3s^2p^6$ electrons down to the L-shell (a region similar to that discussed above) is found to be approximately the same as xenon; namely, 5.91 [63].

4. Photoionization Cross Sections of Helium

- (a) GCA Technical Report No. 64-3-N.
- (b) Presented (under the title "Photoionization of Rare Gases") at the APS Meeting, New York, New York, January 22-25, 1964.
- (c) Published: J. Opt. Soc. Am. 54, No. 7, 876 (July 1964).

All previous experimental cross section measurements for helium have been made using the photographic plate as a detector of radiation, and all depended on the incident radiation intensity remaining constant during the exposures taken with the absorption cell empty and then filled with helium. The difficulties and errors inherent in the above method were removed by using two ionization chambers in series [64]. This is the first time this method has been applied to helium. The cross sections shown in Figure 1 represent the average of four different determinations with the gas pressure varying from 0.5 to 1.0 torr.

The vertical lines in Figure 1 represent the positions of absorption lines discovered by Madden and Codling [65] using the continuum radiation from a 180 MeV synchrotron. They account for the series as being due to a double electron excitation process of the type $1s^2-2s,np$ and $1s^2-2p,ns$. The first member of the series, appearing at approximately 260\AA , is common to the two series and represents the transition $1s^2\ ^1S_0-2s,2p\ ^1P^0$. Only one series was observed.

The data were compared with the theoretical calculations of Cooper [66] and Stewart and Webb [67]. It can be seen in Figure 1 that the dipole length formulation is the best fit at the spectral head but at the shorter wavelengths, the velocity formulation appears superior. This is in agreement with the conclusion reached by Stewart and Webb.

The f -value integral was evaluated graphically from the ionization threshold to 0.01\AA using the k -values shown in Figure 1. A value of $f = 1.54$ was obtained. Since the contribution between 0.01 and 4.0\AA amounts to only 0.0001, the contribution below 0.01 is assumed to be negligible. The Thomas-Kuhn sum rule requires that the total oscillator strength be equal to the number of electrons in the atom; that is, equal to 2 for helium. Thus, the contribution to the oscillator strength due to discrete structure must be equal to 0.46. Theoretical values for the discrete transitions have been calculated by several investigators [68-77]. A value of 0.45 was obtained both by Dalgarno and Stewart [73] and by Salpeter and Zaidi [74]. The calculations included the

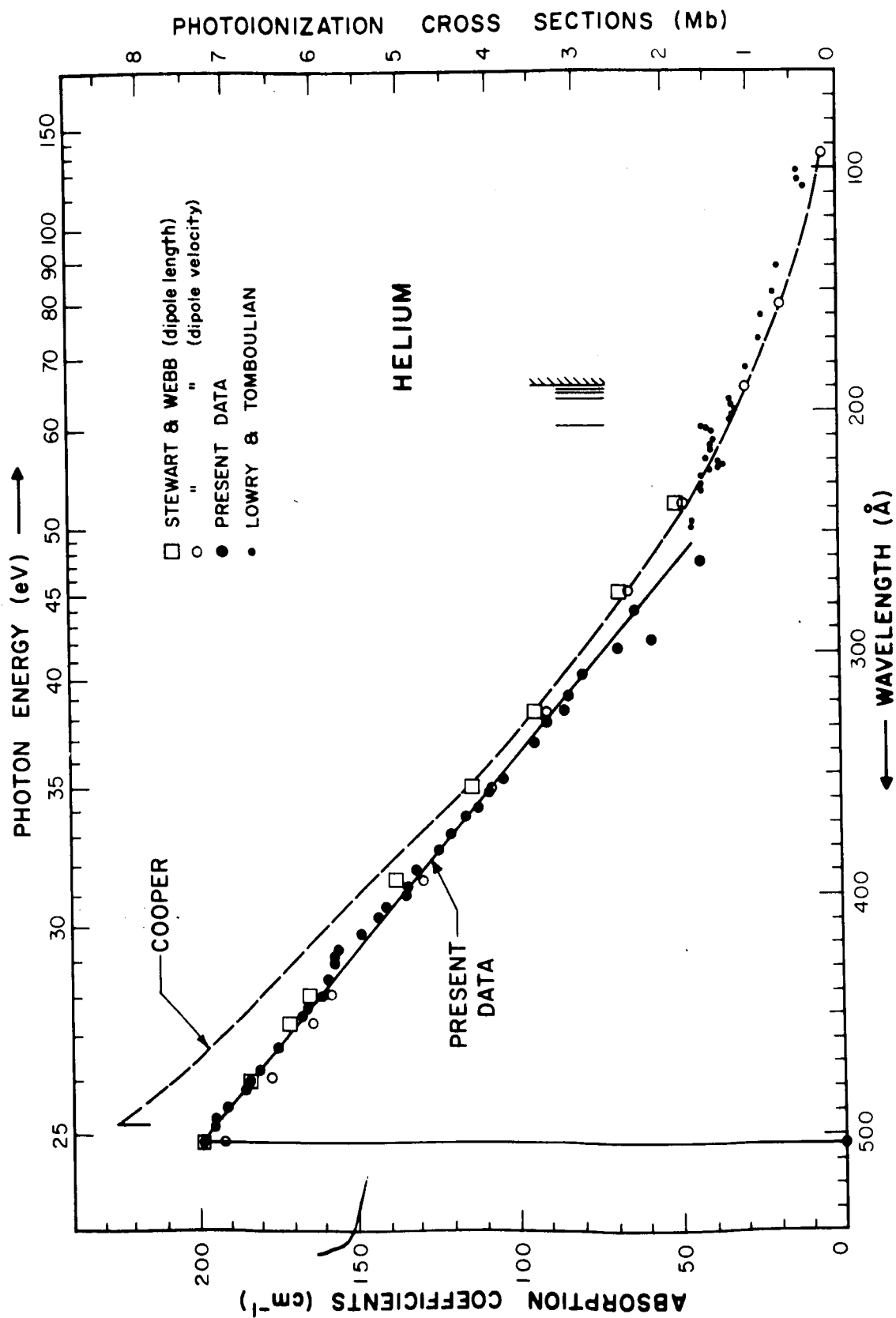


Figure 1 (II-C-4). Photoionization cross sections of helium compared to theoretical values. The vertical lines indicate the position of discrete absorption lines due to double electron excitations.

f-values for the doubly-excited transitions as well as those for the resonance series. Since Dalgarno and Stewart quote f-values for only $n = 2$ through 6, the remainder of the sum for $n = 7$ to ∞ was obtained from Dalgarno's earlier paper [72].

Discrete transitions for large n have f-values given [78], approximately, by $f = C/n^3$ where n is the principal quantum number and C is given by twice the value of $df/d\epsilon$ evaluated at the series limit ($k = 217 \text{ df/d}\epsilon \text{ cm}^{-1}$) and ϵ is the kinetic energy of the released photoelectron measured in rydbergs. Using the present experimental data, it is found that $C = 1.83$. Table 1 compares the results of Dalgarno and Stewart with the values obtained from the above relation. As n increases, it can be noted that the two results are in good agreement.

TABLE 1 (II-C-4)
HELIUM f-VALUES FOR THE TRANSITION 1^1S-n^1P AS OBTAINED
FROM THE RELATION $f = C/n^3$

n	Dalgarno and Stewart*	Present data $f = C/n^3$
2	0.270	0.229
3	0.0746	0.0679
4	0.0304	0.0286
5	0.01530	0.0147
6	0.00878	0.00848
7		0.00505
8		0.00359
9		0.00251
10		0.00183

* A. Dalgarno and A. L. Stewart, Proc. Phys. Soc. 76, 49 (1960)

5. Absorption and Photoionization Cross Sections of O_2 and N_2 at Intense Solar Emission Lines

(a) GCA Technical Report No. 64-13-N.

(b) Presented (under the title "Photoionization Cross Sections of O_2 and N_2 at Intense Solar Lines") at the Optical Society of America Meeting, Washington, D.C., April 1-3, 1964.

(c) Published: J. Geophys. Res. 69, No. 1, 4583 (November 1964).

The interaction of the solar extreme ultraviolet (EUV) and X radiation with atoms and molecules in the Earth's upper atmosphere is primarily responsible for the formation of the various ionospheric layers. To understand the details of the various processes leading to the formation of the different layers, it is necessary to know exactly where, in the atmosphere, the various solar wavelengths are absorbed. This in turn requires precise knowledge of the solar spectrum and of the absorption coefficients of O_2 and N_2 . Since absorption bands and narrow emission lines are involved, it is necessary to determine the absorption coefficients at the exact wavelengths in question if precise calculations are to be made.

In recent years, knowledge of the solar EUV has increased considerably owing mainly to the work of Tousey [79], Hinteregger and Watanabe [80], Hall et al. [81], Friedman [82], and Rense [83] and Violet and Rense [84]. The solar spectrum between 2000Å and the soft X-ray region is now known to be composed mainly of discrete emission lines. The interaction of each of these lines with each of the atmospheric gases can be described in terms of an absorption coefficient k and a photoionization yield γ .

During the past ten years photoionization cross sections in O_2 and N_2 , in the region between 200 and 2000Å, have been reported by various authors. With the exception of some early work by Weissler and Lee [85] and Weissler et al. [86], no cross sections have been measured at precisely the solar wavelengths with a resolution determined solely by the widths of the lines generated within the light source. For these reasons, the present investigation was performed.

The experimental techniques are not described here in any detail. However, a very brief description is included of the unique light sources employed.

Two light sources were used to reproduce the solar radiation. A dc glow capillary discharge produced radiation from excited neutral atoms. To produce the He I lines, pure helium was allowed to flow through the light source. For hydrogen, the molecular band emission was so profuse that it was impossible to produce the atomic lines isolated from neighboring lines. To produce radiation from ionized atoms, a high voltage low pressure spark discharge was used. The emission spectrum was characteristic of the gas used in the case of O_2 and N_2 . However, to reproduce the strong solar C III line at 977Å, a small amount of CO_2 was added to nitrogen.

The results are given in Table 1 and in each case represent the average of three or more measurements made at different pressures; they are believed to be accurate to within ± 5 percent, except where otherwise stated. No absorption coefficients are given for nitrogen for the 832 to 835 \AA group nor the 921 to 924 \AA group. Although most of these lines were clearly resolved by the monochromator, it was found that the measured coefficients did not obey Beer's law. As the pressure in the absorption cell increased, the apparent absorption coefficients decreased. This pressure effect can be explained by reference to high resolution absorption spectra [87-89].

TABLE 1 (II-C-5)

ABSORPTION COEFFICIENTS, CROSS SECTIONS AND
PHOTOIONIZATION YIELDS OF O₂ and N₂

Source Line $\lambda(\text{\AA})$	$k(\text{cm}^{-1})$	Oxygen $\sigma(\text{Mb})$	$\gamma(\%)$	$k(\text{cm}^{-1})$	Nitrogen $\sigma(\text{Mb})$	$\gamma(\%)$
303.781 He II	446*	16.6	100	326*	12.1	100
429.918 O II	480*	17.8	100	564*	21.0	100
430.041 O II						
430.177 O II						
434.975 O III	561	20.9	100	637	23.7	100
498.431 O VI	619	23.0	100	652	24.2	100
507.391 O III	622	23.1	97	654	24.3	100
507.683 O III						
508.182 O III	638	23.7	97	598	22.2	100
519.610 O IV	678	25.2	100	693	25.8	98
522.208 He I	561	20.9	99	635	23.6	97
525.795 O III	659	24.5	97	703	26.2	98
537.024 He I	571	21.2	98	678	25.2	97
553.328 O IV	705	26.2	93	669	24.9	96
554.074 O IV	685	25.2	97	680	25.3	93
554.514 O IV	709	26.4	97	660	24.6	93
555.262 O IV	698	26.0	97	666	24.8	95
584.331 He I	625	23.2	98	620	23.1	100
597.818 O III	774	28.8	92	629	23.4	97
599.598 O III	765	28.4	97	629	23.4	95
608.395 O IV	648	24.1	94	630	23.4	100
609.705 O III	714	26.6	94	636	23.7	100
609.829 O IV						
610.043 O III						
610.746 O III	764	28.4	96	626	23.3	99
610.850 O III						
616.933 O IV	655	24.4	97	637	23.7	98
617.033 O IV						
617.051 O II						
624.617 O IV	681	25.3	93	645	24.0	97
625.130 O IV	661	24.6	96	642	23.9	97
625.852 O IV	814	30.3	96	644	24.0	98
629.732 O V	801	30.0	97	652	24.2	97
684.996 N III	709	26.4	100	653	24.3	95
685.513 N III	496	18.4	100	670	24.9	95
685.816 N III						
686.335 N III	594	22.1	100	648	24.1	95

*Estimated error $\pm 10\%$

TABLE 1 (II-C-5) Continued

Source Line		Oxygen			Nitrogen				
$\lambda(\text{\AA})$		$k(\text{cm}^{-1})$	$\sigma(\text{Mb})$	$\gamma(\%)$	$k(\text{cm}^{-1})$	$\sigma(\text{Mb})$	$\gamma(\%)$		
758.677	O V	493	18.3	57	643	23.9	75		
759.440	O V	463	17.2	53	313	11.6	86		
760.229	O V	498	18.5	49	531	19.8	57		
760.445	O V								
761.130	O V	547	20.3	51	1077	40.1	55		
762.001	O V	545	20.3	50	747	27.8	46		
763.340	N III	604	22.5	58	734	27.3	80		
764.357	N III	479	17.8	60	364*	13.5	69		
765.140	N IV	615	22.9	54	2295	85.4	77		
774.522	O V	382	14.2	63	914	34.0	40		
779.821	O IV	733	27.3	33	344	12.8	65		
779.905	O IV								
787.710	O IV	644	24.0	54	226	8.41	89		
790.103	O IV	744	27.7	37	610	22.7	45		
790.203	O IV								
832.754	O II	707*	26.3	38	Variable See Text		0		
832.927	O III								
833.326	O II	-	-	-	Variable See Text		0		
833.742	O III	350*	13.0	39					
834.462	O II	285*	10.6	38			0		
835.096	O III	267	9.93	37					0
835.292	O III								
921.982	N IV	148	5.50	79			0		
922.507	N IV	171	6.36	84					0
923.045	N IV	272	10.1	88					
923.211	N IV								
923.669	N IV	246	9.15	90			0		
924.274	N IV	480	17.8	83					0
972.537	H I	860	32.0	83					
977.026	C III	107	3.98	62	2.2	0.082	0		
989.790	N III	37	1.38	69	4.5	0.167	0		
991.514	N III	47	1.75	69	2.0	0.074	0		
991.579	N III								
1025.722	H I	41	1.52	64	0.027	0.0010	0		
1031.912	O VI	28	1.04	1**	<0.02	0.00074	0		
1037.613	O VI	21	0.78	0.1**	<0.02	0.00074	0		

*Estimated error $\pm 10\%$ **Estimated error $\pm 50\%$

6. Absorption and Photoionization Cross Sections of CO₂, CO, A and He at Intense Solar Emission Lines

(a) GCA Technical Report No. 64-13-N.

(b) Published: J. Geophys. Res. 70, No. 1, 99 (January 1965).

The interaction of the solar extreme ultraviolet radiation with ambient atoms and molecules in the atmospheres of the planets partially controls the photochemistry and the degree of ionization of these regions. It is therefore important to know the composition of these atmospheres and the photoabsorption and photoionization cross sections of each constituent gas. Major constituents of the atmosphere of the Earth are N₂ and O₂ and of the atmospheres of Mars, Venus, and Jupiter are probably: Mars, N₂, CO₂, A^{*}; Venus, N₂, CO₂; and Jupiter, H₂, He^{*}. The substances marked with an asterisk have yet to be positively identified. Minor constituents can be important. For example, CO, a product of the photodissociation of CO₂, is thought to be more abundant than CO₂ in the atmospheres of Mars and Venus above the height of 150 km (Marmo and Schultz, private communication, 1964).

The photoionization and total absorption cross sections of N₂ and O₂ at wavelengths in the region 1040 to 3000 Å corresponding to solar emission lines were recently reported by Samson and Cairns [90]. Similar techniques have been used to obtain corresponding data for CO₂, CO, A, and He. Since this has been previously discussed, no experimental details are repeated here. The data obtained are shown in Tables 1, 2, and 3. Table 1 includes the pertinent data for CO₂ and CO whereas the data in Tables 2 and 3 are for argon and helium, respectively.

Carbon Dioxide: The data presented in this report have been compared with those previously published. Agreement, within the limits of the experimental accuracies claimed, is obtained with the early work of Sun and Weissler [91] at wavelengths shorter than 7000 Å. In this region the cross sections at all of the wavelengths considered are close to 33 Mb. At longer wavelengths where the cross sections are lower, the results are not in accord; those of Sun and Weissler [91] are lower sometimes by as much as a factor of 2. However, at wavelengths longer than 8400 Å the agreement with Watanabe's recent data [92] is good, with the exception of the cross section at 972.5 Å Lyman-γ.

At this wavelength, the apparent cross section depended upon the number of absorbing particles per cm²-column. The value of 55 Mb, obtained with 2×10^{16} molecules per cm²-column, is 65 percent higher than that reported by Watanabe. This difference could arise from the fact that Lyman-γ lies within a narrow absorption band. Thus a difference in wavelength resolution could affect the measurement, higher resolution giving a higher apparent cross section. The effective resolution in each of the two experiments could not be compared since it depends upon the half width and degree of self-reversal of the Lyman-γ line and its intensity relative to neighboring molecular hydrogen lines.

TABLE 1 (II-C-6)

ABSORPTION COEFFICIENTS, CROSS SECTIONS AND
PHOTOIONIZATION YIELDS OF CO₂ AND CO

Source Line $\lambda(\text{\AA})$	Carbon Dioxide			Carbon Monoxide		
	$k(\text{cm}^{-1})$	$\sigma(\text{Mb})$	$\gamma(\%)$	$k(\text{cm}^{-1})$	$\sigma(\text{Mb})$	$\gamma(\%)$
303.781 He II	630*	23.4*	100	307*	11.4*	93*
434.975 O III	743	27.6	100	519	19.3	100
507.391 O III	807	30.0	100	574	21.4	100
507.683 O III						
508.182 O III	778	28.9	100	568	21.1	98
522.208 He I	802	29.8	98	576	21.4	100
525.795 O III	838	31.2	100	580	21.6	97
537.024 He I	845	31.4	96	610	22.7	98
553.328 O IV	909	33.8	100	599	22.3	97
554.074 O IV	818	30.4	100	595	22.1	97
554.514 O IV	894	33.2	100	590	21.9	97
555.262 O IV	911	33.9	100	608	22.6	98
584.331 He I	919	34.2	99	609	22.6	97
597.818 O III	953	35.4	100	615	22.9	97
599.598 O III	952	35.4	100	616	22.9	97
608.395 O IV	951	35.4	100	611	22.7	98
609.705 O III	949	35.3	100	601	22.4	98
609.829 O IV						
610.043 O III	953	35.4	100	593	22.1	98
610.746 O III						
610.850 O III	947	35.2	100	607	22.6	97
616.933 O IV						
617.033 O IV	918	34.1	100	610	22.7	98
617.051 O II						
624.617 O IV	927	34.5	100	607	22.6	98
625.130 O IV	954	35.5	100	593	22.1	98
625.852 O IV	922	34.3	100	593	22.1	98
629.732 O V	968*	36.0*	96	596	22.2	100
684.996 N III	918	34.1	97	595	22.1	100
685.513 N III						
685.816 N III	948*	35.2*	93	590	21.9	100
686.335 N III						
758.677 O V	1009	37.5	86	616	22.9	57
759.440 O V	839	31.2	89	724	26.9	65
760.229 O V	1185	44.1	89	457	17.0	64
760.445 O V	1206	44.8	86	374	13.9	75
761.130 O V	1147	42.6	92	353	13.1	78

* Estimated error $\pm 10\%$

TABLE 1 (II-C-6) Continued

Source Line $\lambda(\text{\AA})$	Carbon Dioxide			Carbon Monoxide		
	$k(\text{cm}^{-1})$	$\sigma(\text{Mb})$	$\gamma(\%)$	$k(\text{cm}^{-1})$	$\sigma(\text{Mb})$	$\gamma(\%)$
763.340 N III	1238*	46.0*	90	628	23.4	68
764.357 N III	1635*	60.8	91	1011	37.6	46
765.140 N IV	2527	93.9	92	626	23.3	57
774.522 O V	996	37.0	77	678	25.2	56
779.821 O IV } 779.905 O IV }	1216	45.2	86	1049	39.0	67
787.710 O IV						
790.103 O IV } 790.203 O IV }	624	23.2	80	540	20.1	74
832.754 O II } 832.927 O III }						
833.742 O III	277**	10.3**	87	496**	18.1**	88
834.462 O II	341	12.7	88	510	19.0	92
835.096 O III } 835.292 O III }	385	14.3	87	474	17.6	94

At the following wavelengths, which are longer than the ionization threshold of both CO_2 and CO , the measured cross sections of CO were pressure dependent. In these cases three values of the cross section are given together with corresponding numbers (N) of absorbing particles per cm^2 -column. The symbol (***) has been used to indicate no pressure dependence.

Source Line $\lambda(\text{\AA})$	Carbon Dioxide			Carbon Monoxide		
	$k(\text{cm}^{-1})$	$\sigma(\text{Mb})$	$N(\text{cm}^{-3})$	$k(\text{cm}^{-1})$	$\sigma(\text{Mb})$	$N(\text{cm}^{-3}) \times 10^{-16}$
921.982 N IV	2695	100	***	239	8.88	2.60
				173	6.43	8.33
				166	6.17	15.6
922.507 N IV	1240	46.1	***	1214	45.1	2.60
				885	32.9	8.33
				733	27.3	15.6
923.045 N IV } 923.211 N IV }	See Text			896	33.3	2.60
				815	30.3	8.33
				669	24.9	15.6
923.669 N IV	1516	56.4	***	426	15.8	2.60
				389	14.5	8.33
				368	13.7	15.6
924.274 N IV	1526	56.7	***	406	15.1	2.60
				313	11.6	8.33
				253	9.40	15.6

* Estimated error $\pm 10\%$

** Estimated error $\pm 50\%$

TABLE 1 (II-C-6) Continued

Source Line $\lambda(\text{\AA})$	Carbon Dioxide			$k(\text{cm}^{-1})$	Carbon Monoxide	
	$k(\text{cm}^{-1})$	$\sigma(\text{Mb})$	$N(\text{cm}^{-3})$		$\sigma(\text{Mb})$	$N(\text{cm}^{-3}) \times 10^{-16}$
972.500 H I	See Text			{ 129	4.80	37.8
				{ 102	3.79	64.8
				{ 94.8	3.52	119.
977.000 C III	1154	42.9	***	{ 10.5	0.39	323.
				{ 9.5	0.35	604.
				{ 7.4	0.28	1630.
989.790 N III				{ 163	6.06	15.6
				{ 76	2.83	95.7
				{ 66.4	2.45	150.
991.514 N III	1603	59.6	***	{ 42.6	1.58	15.6
991.579 N III				{ 32.4	1.20	95.7
				{ 32.2	1.20	150.
1025.720 H I	407	15.1	***	< 0.4	<0.015	
1031.912 O IV	383	14.2	***	< 0.4	<0.015	
1037.613 O VI	367	13.6	***	< 0.4	<0.015	

TABLE 2 (II-C-6)

ABSORPTION COEFFICIENTS AND CROSS SECTIONS OF A

Source Line $\lambda(\text{\AA})$	$k(\text{cm}^{-1})$	$\sigma(\text{Mb})$	Source Line $\lambda(\text{\AA})$	$k(\text{cm}^{-1})$	$\sigma(\text{Mb})$
303.781 He II	60*	2.23*	617.033 O IV	982	36.5
434.975 O III	531	19.7	617.051 O II	982	36.5
507.391 O III	938	34.9	624.617 O IV	981	36.5
507.683 O III	938	34.9	625.130 O IV	980	36.4
508.182 O III	940	34.9	625.852 O IV	980	36.5
522.208 He I	953	35.4	629.732 O V	979	36.4
525.795 O III	957	35.6	684.996 N III	943	35.0
537.024 He I	963	35.8	685.513 N III	942	35.0
553.328 O IV	973	36.2	684.816 N III	942	35.0
554.074 O IV	974	36.2	686.335 N III	942	35.0
554.514 O IV	974	36.2	758.677 O V	864	32.1
555.262 O IV	975	36.2	759.440 O V	862	32.0
584.331 He I	983	36.5	760.229 O V	860	32.0
597.818 O III	985	36.6	760.445 O V	860	32.0
599.598 O III	985	36.6	761.130 O V	859	31.9
608.395 O IV	984	36.6	762.001 O V	857	31.9
609.705 O III	984	36.6	763.340 N III	854	31.7
609.829 O IV	984	36.6	764.357 N III	852	31.6
610.043 O III	984	36.6	765.140 N IV	850	31.6
610.746 O III	983	36.5	774.522 O V	836	31.0
610.850 O III	983	36.5	779.821 O IV	676	25.1
616.933 O IV	982	36.5	779.905 O IV	676	25.1

*Estimated error $\pm 10\%$

TABLE 3 (II-C-6)

ABSORPTION COEFFICIENTS AND CROSS SECTIONS OF He

Source Line $\lambda(\text{\AA})$	$k(\text{cm}^{-1})$	$\sigma(\text{Mb})$
303.781 He II	74*	2.75*
429.918 O II	154	5.73
430.041 O II	154	5.73
430.177 O II	154	5.73
434.975 O III	157	5.84
498.431 O VI	196	7.29
584.331 He I	See Text	

*Estimated error $\pm 10\%$

Cross sections were not obtained at the wavelengths 923.045 and 923.211 \AA since these two lines, which were not separately resolved, lie on the edge of an absorption band and their individual cross sections differ largely.

At certain wavelengths the absorption cross sections for CO_2 are considerably larger than for either O_2 or N_2 ; e.g., at Lyman- β , 1025.72 \AA . At this wavelength the cross sections are 1.52, 0.001 and 15.1 Mb for O_2 , N_2 and CO_2 , respectively. In the Earth's atmosphere above 95 km the number of CO_2 molecules per cm^2 -column is only about 1 percent of the number of O_2 molecules per cm^2 -column (1959 ARDC Model Atmosphere). However, the Lyman- β flux is significantly attenuated by CO_2 . At 99 km CO_2 will account for a 6 percent reduction in the intensity of the incident Lyman- β flux. At 97 km this reduction is 9 percent and at 95 km is 14 percent.

Carbon Monoxide: At the wavelengths where direct comparison is possible, the data presented in this paper have values most of which are about 20 percent greater than those given in the photographic work of Sun and Weissler but approximately 25 percent less than the recent work, using photoelectric detection but lower resolution, of Huffman *et al.* [93]. Huffman has reported that at a number of strong bands with wavelengths longer than the first ionization threshold — most of which are not classified — the absorption cross section was a function of the number of particles per cm^2 -column. This is due to rapid changes in cross section across the rotational lines of these bands. In the present work, even with a resolution of less than 0.1 \AA , the cross sections were pressure dependent. At each of these wavelengths, therefore, three 'apparent' cross sections are listed in the table with the corresponding numbers of particles per cm^2 -column.

Argon: For argon between 466 and 424 \AA , the cross section varies considerably due to the presence of a Rydberg series of autoionized lines [94,95]. The only solar line considered in this region, at 434.975 \AA , lies within the discrete absorption structure due to the third member of this Rydberg series corresponding to the transition $3s^23p^6 - 3s3p^66p$. Its absorption cross section is 19.7 Mb and its yield 100 percent.

Helium: In addition to absorption within the ionization continuum resonance line, absorption at 584 \AA is of importance. With no knowledge of the precise shape of the solar 584 \AA line, its apparent cross section cannot be determined. Po Lee and Weissler [96] gave a value of 2.7 Mb but did not specify the width of their source line. Apparent cross sections obtained under different experimental conditions illustrate the variation to be expected. For a self-reversed line of half width 0.14 \AA and 1.3×10^{17} absorbing particles per cm^2 -column, $\sigma(\text{apparent}) = 4.7 \text{ Mb}$. For a line of half width 0.05 \AA , also self-reversed and 1.6×10^{15} absorbing particles per cm^2 -column, $\sigma(\text{apparent}) = 225 \text{ Mb}$. These values can be compared with the maximum absorption cross section, $\sim 2 \times 10^5 \text{ Mb}$, calculated for the doppler broadened absorption line (temperature 20 $^\circ\text{C}$) using the theoretical f-value 0.275 [97].

7. Photoionization Cross Sections of Neon from Threshold to 200Å

(a) To be published: J. Opt. Soc. Am.

The early calculations on the photoionization cross sections of neon by Bates [98] gave the value of the photoionization cross section of neon at its spectral head as 5.8 Mb ($1 \text{ Mb} = 10^{-18} \text{ cm}^2$). Subsequent experimental values at the spectral head varied between 4 and 6.3 Mb providing substantial verification of the theoretical value. However, at shorter wavelengths the theoretical curve of Bates deviated considerably from the experimental curves.

Recently, Seaton [99,100], Cooper [101], and Sewell [102] have published theoretical treatments each using different assumptions and approximations. Unfortunately, the various theoretical curves deviate considerably from each other indicating the sensitivity of the calculations to the various approximate wavefunctions. These theoretical works have made it evident that reliable laboratory data will be especially useful at this stage. Since all of the necessary experimental techniques have been made available under the present contract requirements, it was decided to measure neon cross sections from threshold to 200Å.

The apparatus and procedure used have been described in detail previously. Briefly, the apparatus consisted of the following: a spark discharge light source which produced a line spectrum characteristic of the gas used, a $\frac{1}{2}$ -m Seya monochromator with a 1200 line/mm grating giving a bandpass of 1Å, and a double ion chamber to measure the photoionization cross sections. The absorption coefficient k is given by $k = (1/x) \times \ln(i_1/i_2)$, where x is the length, reduced to STP, of one of the identical pair of collector plates and i_1 and i_2 are the respective ion currents to the two collector plates.

Reagent grade neon was passed through a liquid nitrogen-cooled activated charcoal trap for further purification before it entered the absorption chamber. The neon pressure was varied from 0.1 to 0.8 Torr.

The experimental results are shown in Figure 1. The caption defines the various theoretical curves. Sewell's theoretical curves show the closest agreement with the experimental data, and were obtained using more accurate wavefunctions. The good agreement with the experimental data does favor Sewell's suggestion that the orbitals for the ionized atom should be used in computing the potential and exchange functions. No additional details are given here since they are available in an article accepted for publication.

Carrying this picture further into the subshells, we would expect the p-electrons to contribute 6 to the oscillator strength. If this is the case, more than half of their contribution must come from energies greater than the L_1 edge which implies that the major contribution to the photoionization cross section just below the L_1 edge is due to the ejection of a p-electron. This is the case according to Sewell's dipole velocity calculations [103].

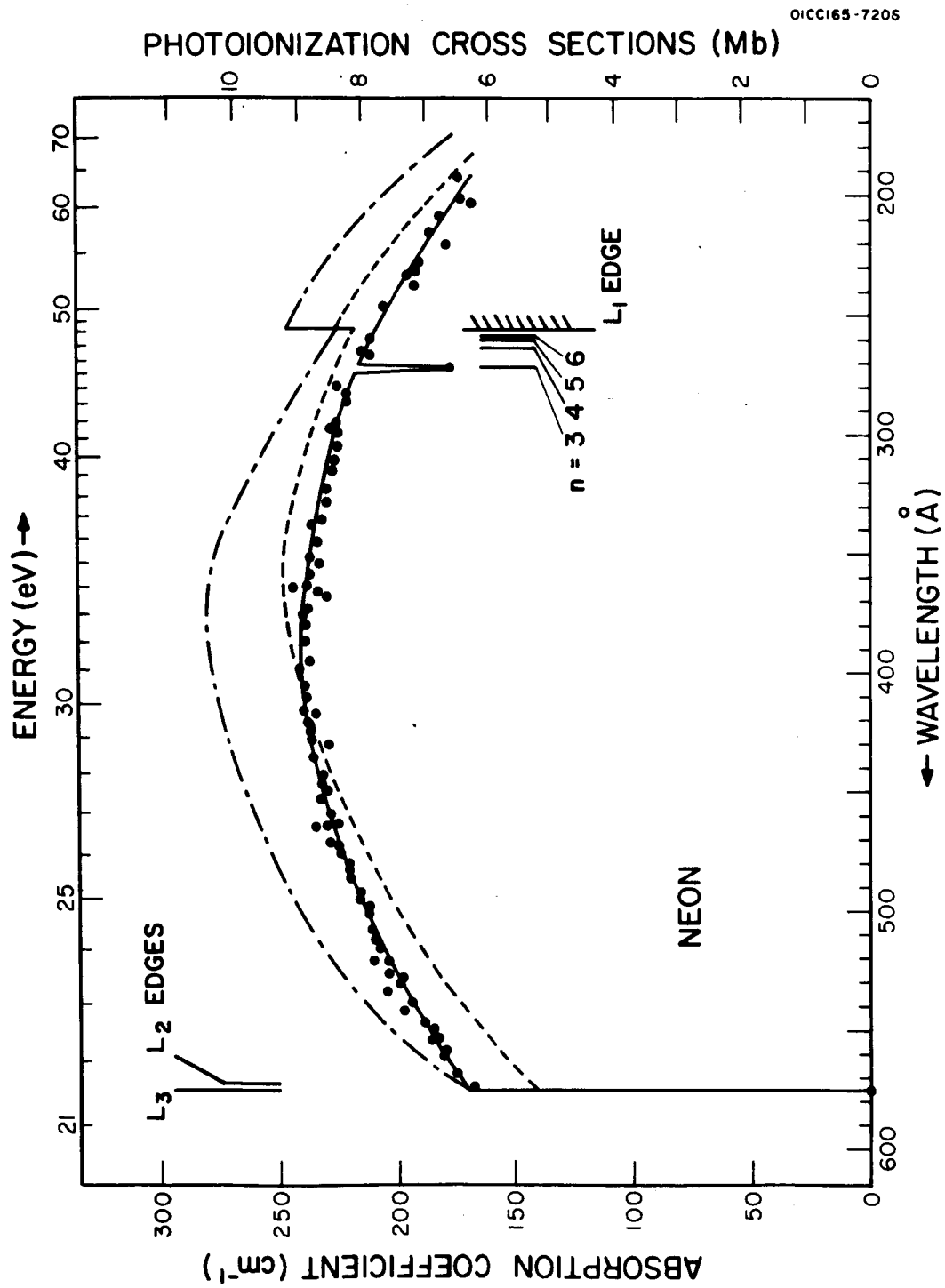


Figure 1 (II-C-7). Photoionization cross sections of neon compared to Sewell's theoretical values.
 --- dipole length approximation;
 - - - dipole velocity approximation.

It would be interesting to measure the individual cross sections for the ejection of s and p-electrons below the L_1 edge. This could be achieved by measuring the relative number of electrons ejected with energies $= h\nu - E(L_1\text{edge})$ and $= h\nu - E(L_{2,3}\text{edge})$, where $h\nu$ is the energy of the incident photon and E is the minimum energy necessary to eject the appropriate electron. A program of this nature is under way for the rare gases.

8. A Carbon Film-Scintillator Combination Suitable for the Selective Detection of Radiation in the Extreme Ultraviolet

(a) To be published: Applied Optics

No filters exist in the extreme ultraviolet at wavelengths shorter than the lithium fluoride cutoff with the exception of thin metallic films. The transmission characteristics of these films can be utilized to produce filters for narrow band detectors and also for the suppression of scattered light and light of unwanted orders in vacuum spectrographs. The data presented below show that thin carbon films are particularly suitable for transmitting the 304Å He II radiation while at the same time absorbing the 584Å He I resonance line. The thin films can be mounted on screens or evaporated directly on plastic scintillators. The scintillators provide an additional discrimination against the longer wavelengths.

A thin carbon film was evaporated on a clean microscope slide, floated off in water, and picked up on a 70 percent transparent screen. The thickness of the film was measured with a Tolansky interferometer [104] and found to be 270Å thick. The film had a transmittance of 47 percent for the visible light emitted from a tungsten lamp. The transmittance of the carbon film measured as a function of wavelength is shown in Figure 1. No discrete structure is observed in the vicinity of 1800Å where characteristic electron-energy losses have been reported [105-107]. The transmittance decreases continuously from 41 percent at 2000Å to 1 percent at 1000Å. Between 900 and 600Å carbon is very highly absorbing. In the vicinity of the free-electron plasma frequency (526Å) the transmittance again starts to increase reaching 56 percent at 209Å. Presumably, the transmittance will reach a maximum at shorter wavelengths and fall to zero at 43.6Å, the carbon K absorption edge. This is represented by the dashed curve in Figure 1. The transmittance at 304Å is 30 percent while at 584Å it is about 1 percent, a discrimination of 30:1. Increasing the thickness by a factor of 2 provides a discrimination of 900:1 with a transmittance of 9 percent at 304Å. The general characteristics of the transmittance curve are similar to previous preliminary results measured over a smaller wavelength range [108]. The estimate of the film thickness in those early results was in error. The estimate was made by determining the mass of the sample using a microbalance. However, the thickness and the transmittance measurements of the present sample suggest that the quoted value of 175Å for the previous method is in error and that the corrected thickness should be 470Å. Increased discrimination between the 304 and 584Å lines can be realized by using a plastic scintillator as a radiation converter. The characteristics of the scintillator are described below.

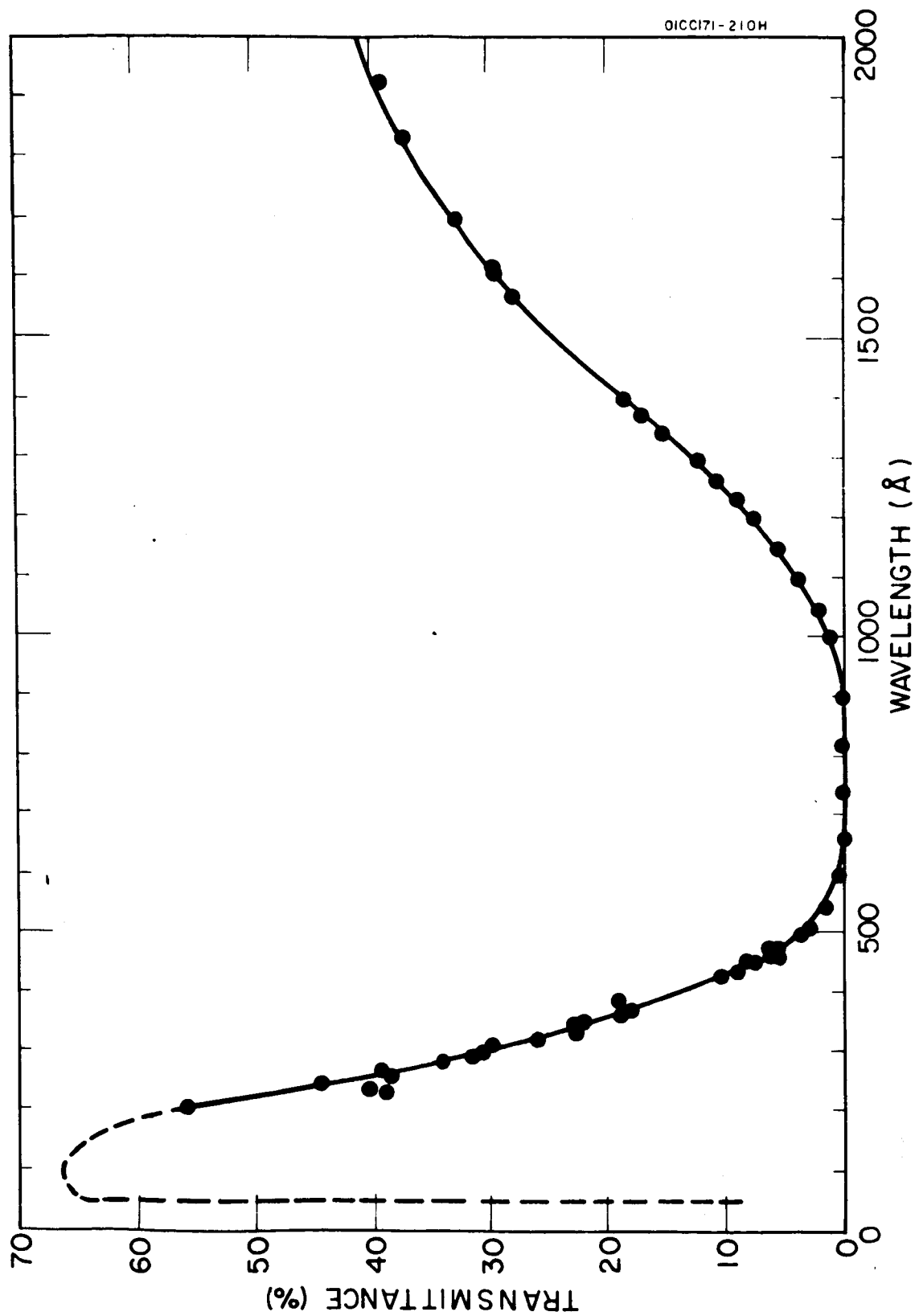


Figure 1 (II-C-8). Transmittance of carbon 270Å thick.

The plastic phosphor NE 102, manufactured by the Harshaw Chemical Co., was used in conjunction with an EMI 9514 B photomultiplier to detect the VUV radiation. From the manufacturer's specifications the NE 102 phosphor contains scintillation chemicals in polyvinyltoluene which have a peak fluorescence at 4300Å. The quoted fluorescence decay time is 3.5 nanoseconds. Figure 2 shows the relative fluorescence efficiency of the scintillator over the range 200 to 2000Å. The fluorescence efficiency is defined as the ratio of the photomultiplier output signal to the absolute intensity of the incident radiation measured in photons/sec. The absolute intensities were measured from 200 to 800Å using the rare gas ion chamber technique [109]. Relative intensities were measured from 800 to 2000Å with a fresh sodium-salicylate-coated photomultiplier and normalized to fit the short-wavelength data. If a thin film of aluminum 800 to 1000Å thick is evaporated onto the carbon-scintillator combination, the system will detect radiation only between 172 and 550Å. The aluminum film is highly absorbing from the visible down to 800Å at which point it starts to transmit. The transmittance increases to a maximum at the L edge, 172Å, and then suddenly drops to a very low value [110,111]. This provides another factor of 2 in discrimination between the 304 and 504Å lines, and, of course, the Lyman- α line is rendered opaque. The use of plastic scintillators should prove to be very useful in studies of the transmittance of thin films which cannot be removed from the substrate. The technique of overcoating a film with one of known transmittance should also provide information on films free from the interfering effects of surface oxide layers.

9. Total Absorption Cross Section of Atomic Oxygen below 910Å

- (a) GCA Technical Report No. 65-6-N.
- (b) Presented (under the title "The Measured Photoionization Cross Section of Atomic Oxygen") at the APS Meeting, New York, New York, January 28, 1965.
- (c) To be published: Phys. Rev.

For an improved understanding of the Earth's upper atmosphere it is necessary to know the photoionization cross section (σ_i) and the photoabsorption cross section (σ) of each of its component gases. Cross sections of the majority of the atmospheric gases have been measured; however, no experimental data exist for atomic oxygen which is a dominant constituent above 160 km. The photoionization cross section of atomic oxygen has been computed by Bates and Seaton [112], Dalgarno and Parkinson [113] and most recently by Dalgarno et al. [114]. This summary reports on an experimental determination of the total absorption cross section of atomic oxygen at wavelengths shorter than its ionization threshold, 910Å.

The overall experimental approach of obtaining reliable cross sections has been established in this laboratory. Thus, for the present task a major experimental difficulty was the quantitative production of oxygen in sufficient number, yet relatively free of excited atomic and/or molecular species to perturb the data. Basically, although atomic oxygen can be produced by passing an electrical discharge through molecular oxygen, the evidence in the literature concerning the state of the gas emerging is conflicting. Accordingly, minimum reliance was placed on previously-published reports in this regard.

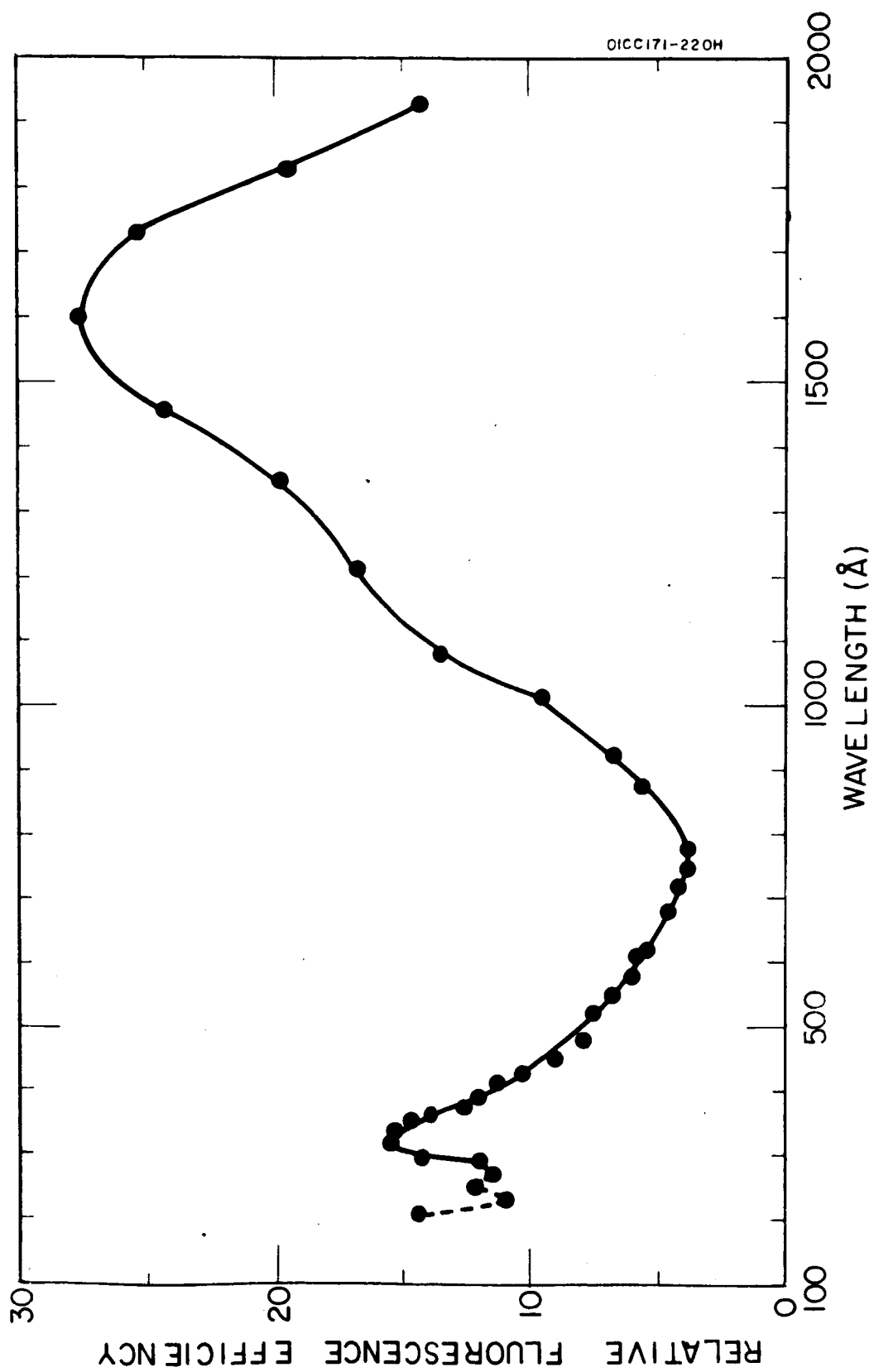


Figure 2 (II-C-8). Relative fluorescence efficiency of plastic scintillator.

The rather complex details of forming the required atomic oxygen are not repeated here. Rather, suffice it to note that the discharged gas did contain $O_2(^3\Sigma_g^-)$, $O_2(^1\Delta_g)$, $O(^3P)$, $He(1^1S)$, and $[He(2^1S) - (2^3S)]$. Helium 1^1S atoms do not absorb at wavelengths longer than 504\AA with the exception of the wavelengths corresponding to $1^1S - m^1P$ transitions. The 2^1S and 2^3S metastable helium atoms absorb continuously at wavelengths shorter than 3245\AA and 2610\AA , respectively. Their absorption was, however, sufficiently weak to be neglected. Therefore, a measurement of the oxygen atom photoabsorption cross section in the wavelength range 910\AA to 504\AA had to take account of only $O_2(^3\Sigma_g^-)$, $O_2(^1\Delta_g)$, and $O(^3P)$.

By proper application of analytical techniques it was possible to experimentally normalize the data in such a manner as to take account of any effect due to the $O_2(^3\Sigma_g^-)$, $O_2(^1\Delta_g)$, and $O(^3P)$. In any case, the details are given in the original paper with arguments to show that the data are good to ± 30 percent.

The measured total absorption cross section of atomic oxygen has been plotted in Figure 1 together with values of its ionization cross section obtained theoretically using both the dipole velocity and dipole length formulations [114].

The measured cross section at 902\AA , close to the photoionization threshold, is about 50 percent higher than that calculated. The increases in cross section obtained theoretically at 732\AA and 665\AA , due respectively to the added possibilities of ionization to the $2D$ and $2P$ states of O^+ , are not positively confirmed by experiment. At the 584\AA He I line, prominent in the solar spectrum, the measured cross section is $11.9 \times 10^{-18} \text{ cm}^2$. This is in good agreement with the value given by Dalgarno and Parkinson [113] and subsequently used in discussions of the formation of the Earth's ionosphere.

In the X-ray region the ionization cross section of atomic oxygen has been assumed to equal $1/2\sigma(O_2)$ [115]. This assumption cannot be arbitrarily extended to longer wavelengths. However, $1/2\sigma(O_2)$ measured over the wavelength range 300 to 200\AA shows close agreement with the dipole length calculation [114]. Measurements of $\sigma(O_2)$ in this region have been reported by several authors [116-118]. Excellent agreement was obtained with the work of Po Lee [118].

In addition to the absorption cross section of atomic oxygen, the experiment described gave both the product $n(O_2^*)\sigma(O_2^*)$ and information as to whether $\sigma(O_2^*)$ was greater or less than $\sigma(O_2)$. A technique for measuring $n(O_2^*)$ has been discussed by Elias *et al.* [119]. Thus, the absorption cross section of the $O_2(^1\Delta_g)$ molecule could be measured by these techniques.

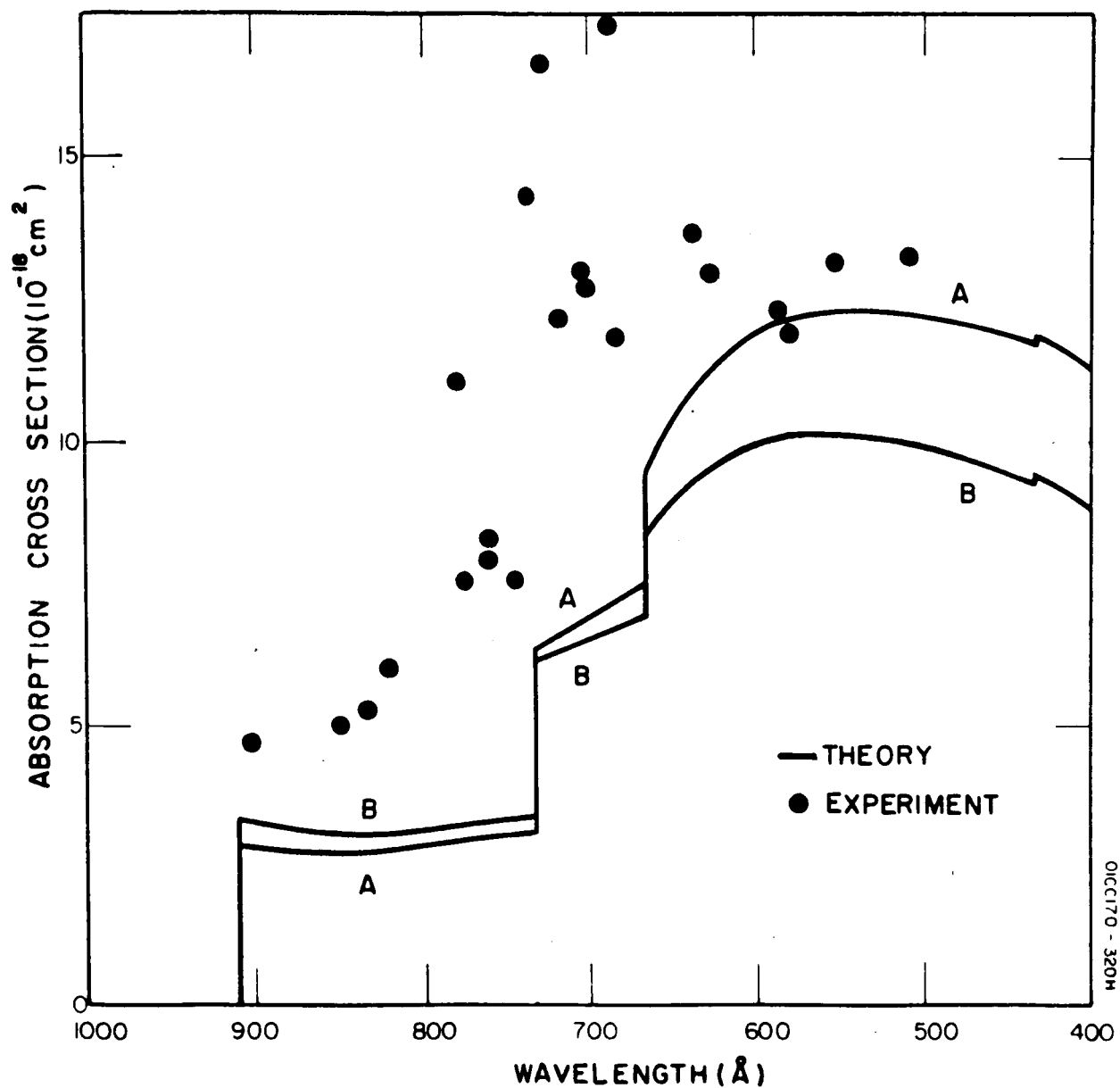


Figure 1 (II-C-9). The absorption cross section of atomic oxygen, λ 1000 – λ 400Å. Curves A and B were computed using the dipole length and dipole velocity formulations respectively. The experimental points have an estimated accuracy of ± 30 percent.

D. THEORETICAL AERONOMY: TECHNICAL SUMMARIES OF PUBLISHED REPORTS

The investigation of theoretical aeronomy has resulted in the generation of three technical papers, each of which has been submitted or accepted for publication in the open literature and/or has appeared as a GCA Technical Report. Comprehensive summaries of these reports are given below.

1. A Congeries of Absorption Cross Sections for Wavelengths Less Than 3000Å. II

(a) GCA Technical Report No. 64-20-N.

The importance and applicability of quantitative absorption cross section data to atmospheric physics studies is well known. For convenient and ready availability, a congeries of published absorption cross section data has been accomplished.

The cross section data were obtained from (1) literature searches, (2) studies recently completed in our laboratories, and (3) private communications from other investigators. The available data on each gas are given together with a historical sketch of the study of the gas and a list of the pertinent references. There has also been included an entirely new study on the absorption and photoionization coefficient of the major atmospheric gases at intense solar emission lines.

The principal sources of data are tables and graphs of absorption cross sections for various wavelengths in the ultraviolet region. These tables are, wherever possible, reproduced directly from the cited sources. In some cases, where the values of absorption cross sections were not reported in the literature, only plots of the absorption cross sections have been published. In these cases, the data were reproduced directly from the open literature if the investigator employed a continuum light source and a sufficiently high resolution. A convenient review of the data available and of the range of values of the absorption cross sections of each gas in the entire wavelength region and graphs of the cross sections vs wavelength are included, provided again that a continuum emission light source with a sufficiently high resolution was used. When additional data were available at solar lines (for O_2 , N_2 , CO , CO_2), these data were shown with vertical lines calling attention to the fact that they are taken with line emission light sources. With the exception of the data of Watanabe and co-workers, whose entire plots have been used, all other line emission measurements are presented in tabular form only. A summary of the gases included and the wavelength region covered by tables and/or graphs is given in Table 1.

2. Ozone Distribution in the Atmosphere of Mars

(a) Published: J. Geophys. Res. 70, 2270 (1965).

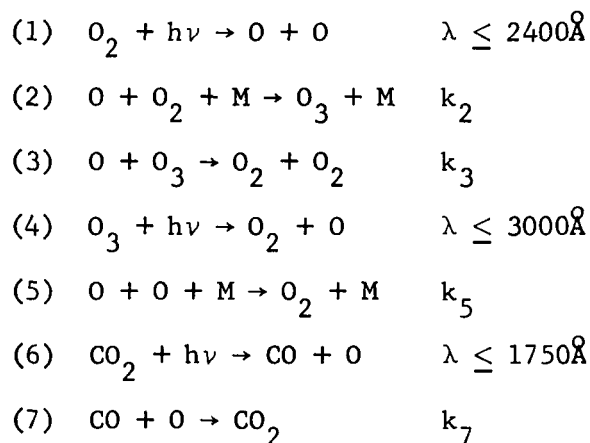
Ozone formation in the lower atmosphere of Mars via the solar photolysis of oxygen has been previously investigated by Marmo and Warneck [120] who found

TABLE 1 (II-D-1)
SUMMARY OF ABSORPTION CROSS SECTION STUDIES

Gas	Absorption Curves (Wavelength Region) (Å)	Tabulated Values (Wavelength Region) (Å)
Oxygen	600-1800 1850-2500	112-1751
Ozone	1050-3000	526-1305 2002-2992
Carbon Dioxide	840-1750	165-1752
Carbon Monoxide	600-1006 1050-1065	304-1306
Water Vapor	600-1850	195-1855
Nitrogen	600-1000	145-1306
Argon	283-788	283-788
Nitric Oxide	590-960 1065-2300	168-1450
Nitrous Oxide	600-950 1080-2160	163-981 1080-2160
Nitrogen Dioxide	1080-3000	2400-3000
Ammonia	560-1000 1080-2200	374-1306
Methane	170-1000 1065-1610	374-1306
Hydrogen Sulfide	1050-2720	--
Sulfur Dioxide	1065-3150	--

the resulting steady-state ozone concentration to increase monotonically with decreasing altitude with the maximum ozone concentration occurring at the surface of the planet. However, a more recent study by Paetzold [121] took exception to this view, since it suggested the existence of an ozone concentration peak at an altitude of around 40 km. From his results Paetzold derived conclusions concerning the stratospheric circulation and wind patterns, which can serve to demonstrate the importance of the Martian ozone distribution profile. The present note, accordingly, is concerned with the conflict between the previous notions about the ozone distribution profile and those advanced by Paetzold's paper.

There is agreement that the basic photochemical reactions involved in the atmosphere of Mars are:



At altitudes below about 80 km, a significant photodissociation of CO_2 can be precluded owing to the opacity of the Martian atmosphere for wavelengths below 1750\AA so that reactions (6) and (7) can be ignored [120-122]. Paetzold obtained the 40 km ozone concentration peak by applying only reactions (1) through (4); he also assumed a temperature distribution with a lapse rate of 2.5 degrees/km and a tropopause at 40 km. Marmo and Warneck, on the other hand, assumed an isothermal atmosphere but used reactions (1) through (5). The discrepancy between the two sets of results must obviously be attributed either to the difference in the temperature profiles or to the inclusion of reaction (5) in the set of reactions applied. The temperature variation mainly affects reaction (3), since the other reactions are roughly independent on temperature [123]. The influence of the temperature profile and that of reaction (5) were examined in the present calculations which make use of the previously-described iteration procedure to obtain self-consistent steady-state distributions of ozone [120]. The basic data summarized in Table 1 were employed.

In Figure 1 are shown the ozone distributions obtained (a) from an application of the four reaction systems used by Paetzold; and (b) when reaction (5) is included in the mechanism. It is evident that the use of reactions (1) through (4) produces an ozone peak at the tropopause level whereas if (5) is included, the set of reactions yields an ozone profile which is in essential

TABLE 1 (II-D-2)

PARAMETERS USED AND THEIR SOURCE

Surface temperature 250°K Lapse rate 2.9 degree/km Tropopause at 30 km altitude	Schilling (1962)
Surface pressure 25 mbar Constituents: 470 meters NTP N ₂ : 55 meters NTP CO ₂ ; 70 cm NTP O ₂ .	Kaplan, Münch and Spinrad (1964)
Solar flux on top of Earth atmosphere in 50Å intervals 1750-3000Å wavelength region	Detwiler, Garret, Purcell and Tousey (1961); Johnson (1954)
Average dilution factor to account for diminution of solar flux in the vicinity of Mars $\mu = 0.444$	
Absorption cross sections for oxygen and ozone 1750-3000Å wavelength region	Gast (1961) Inn and Tanaka (1959); Watanabe, Zelikoff and Inn (1953)
Photodissociation yield factors for oxygen and ozone: assumed to be unity.	
Rate constants: $k_2 = 2.2 \times 10^{-34} \text{ cc}^2/\text{molec}^2 \text{ sec}$ $k_3 = 5 \times 10^{-11} \exp(-6000/RT) \text{ cc/molec sec}$ $k_5 = 2.8 \times 10^{-33} \text{ cc}^2/\text{molec}^2 \text{ sec}$	Kaufman (1961)

REFERENCES TO TABLE I (II-D-2)

Schilling, G. F., Limiting Model Atmospheres of Mars, Rpt. R-402-JPL, Rand Corporation, Santa Monica, California (1962).

Kaplan, L. D., G. Münch and H. Spinrad, An Analysis of the Spectrum of Mars, *Astrophys. J.*, 139, 1-15 (January 1964).

Detwiler, C. R., D. L. Garrett, J. D. Purcell and R. Tousey, The Intensity Distribution in the Ultraviolet Solar Spectrum, *Ann. Geophys.*, 17, 263 (1961).

Johnson, F. S., The Solar Constant, *J. Meteorol.*, 11, 431-439 (1954).

Gast, P. R., in Handbook of Geophysics, revised edition, chapter 16, p. 25, The Macmillan Company, New York (1961).

Inn, E. C. Y. and Y. Tanaka, Ozone Absorption Coefficients in the Visible and Ultraviolet Regions, in Ozone Chemistry and Technology, Advances in Chemistry Series 21, p. 263, American Chemical Society, Washington, D. C. (1959).

Watanabe, K., M. Zelikoff and E. C. Y. Inn, Absorption Coefficients of Several Atmospheric Gases, AFCRL Tech. Rpt. 53-23, Geophysical Research Paper 21, Geophysics Research Directorate, Cambridge, Mass. (1953).

Kaufman, F., Reactions of Oxygen Atoms, in Progress in Reaction Kinetics, edited by G. Porter, Pergamon Press, New York (1961).

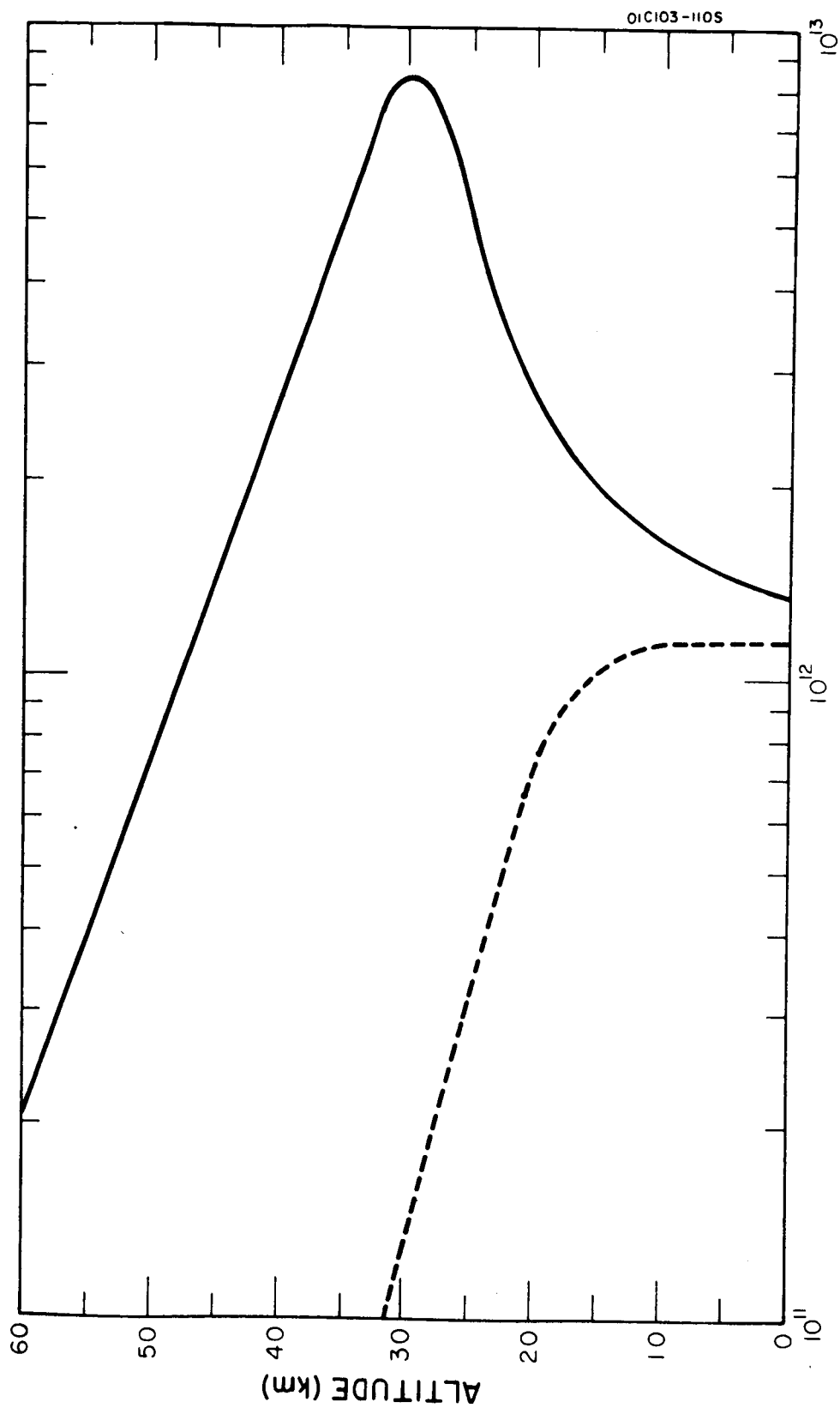


Figure 1 (II-D-2). Number density of O (cm^{-3}).

agreement with the results derived earlier by Marmo and Warneck [120]. This shows that reaction (5) is the overriding factor and that the temperature effect associated with (3) is negligible.

Some further calculations were performed in order that the influence of other parameters could be obtained. The effect of lowering the surface pressure to 10 mbar, keeping the oxygen content constant at the same time, was to decrease the ozone concentrations by a factor of about two, while the shape of the distribution remained essentially unaltered. When the nitrogen content was replaced by the same amount of argon, the change in the total ozone concentration was found to be negligible but the ozone concentration decreased more rapidly with altitude. This latter effect is mainly due to the difference in molecular weight of the bulk of the atmosphere which affects the scale height. None of these parameter variations, however, resulted in the development of an ozone layer.

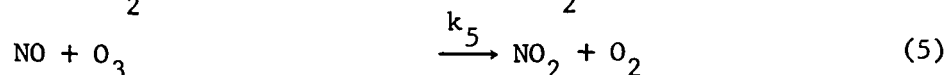
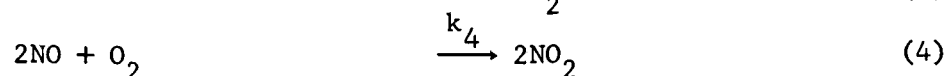
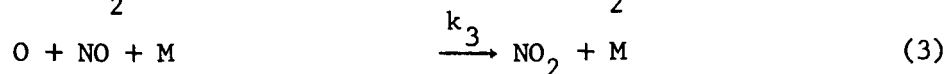
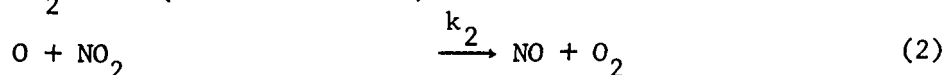
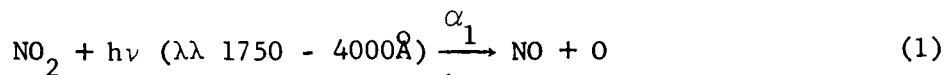
Finally, a lowering of the oxygen content decreased the total amount of ozone by approximately the same factor (this is in agreement with both Marmo and Warneck [120] and with Paetzold [121] without appreciably affecting the ozone distribution. Conversely, even for an oxygen abundance of 250 cm NTP which can be considered as a rather definite upper limit [124], no evidence could be obtained for the development of an ozone concentration peak at some altitude above the surface of Mars. On the basis of the present work, therefore, it appears that the existence of an ozone layer in the atmosphere of Mars can be denied.

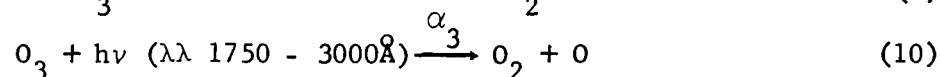
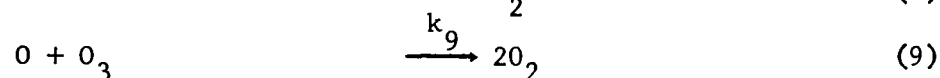
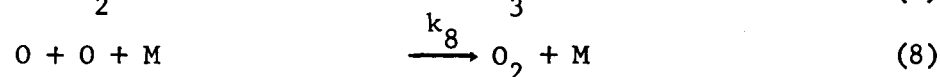
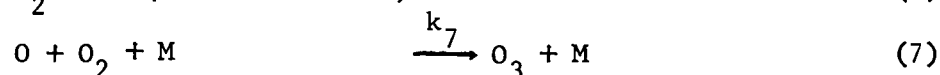
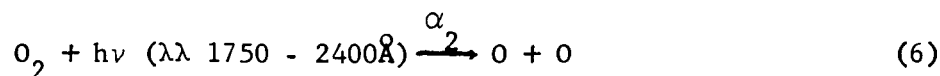
3. On the Presence of Ozone and Oxides of Nitrogen in the Martian Atmosphere

(a) Presented (under the title "The Solar Photodecomposition of NO₂ in the Martian Atmosphere") at the AGU Meeting, Washington, D. C., April 21-24, 1964.

(b) Submitted for Publication: J. Geophys. Res.

Considering all the photochemical reactions (see QPR No. 4) which are thought to occur in the photolysis of NO₂, it was found that for the present study only the following reactions are important.





It may be noted that the reactions (6) through (10) are responsible for the generation of ozone. This latter problem was studied separately (see previous summary paper, II-D-2) [125].

The above reactions were investigated in the steady-state conditions of solar illumination and it was found that for available limits ($\text{O}_2 = 70$ cm-atm [126], $\text{NO} = 87$ cm-atm [127], surface pressure [126] 25 Mb and surface temperature [128] 250°K), the amount of NO_2 is less than 0.1 mm-atm in agreement with the upper limit of 0.1 mm-atm reported by O'Leary [129]. This amount is insufficient to account for the "blue haze." It may be mentioned that for the limits cited above, only the reactions (1) through (4) are most important. At this stage, the other minor constituents such as NO_3 , N_2O_5 , O_3 , etc. were calculated and it was found that $\text{O}_3(10^4 \text{ cm}^{-3}$ at the surface) can only be a very minor constituent in the presence of the oxides of nitrogen as contrasted to $\text{O}_3(10^{12} \text{ cm}^{-3}$ at the surface) in the absence of the nitrogen oxides for the same amount of oxygen; namely, 70 cm-atm. Thus, it seems that there exists an important relationship between the concentrations of NO_2 and O_3 such that the permissible O_3 content decreases sensitively with increasing amounts of NO_2 . To investigate this interesting correlation between NO_2 and O_3 , a detailed study of the photochemistry of an oxygen-nitrogen system in the Martian atmosphere was undertaken. This study is essentially the combined study of the photochemistry of NO_2 and O_3 and is comprised of the above ten reactions. The variation of O_3 with NO_2 is shown in Figure 1. The scale heights for $\text{O}_3 \sim 8$ km and for $\text{NO}_2 \sim 5.5$ km were determined graphically. These scale heights correspond to one in the absence of the other.

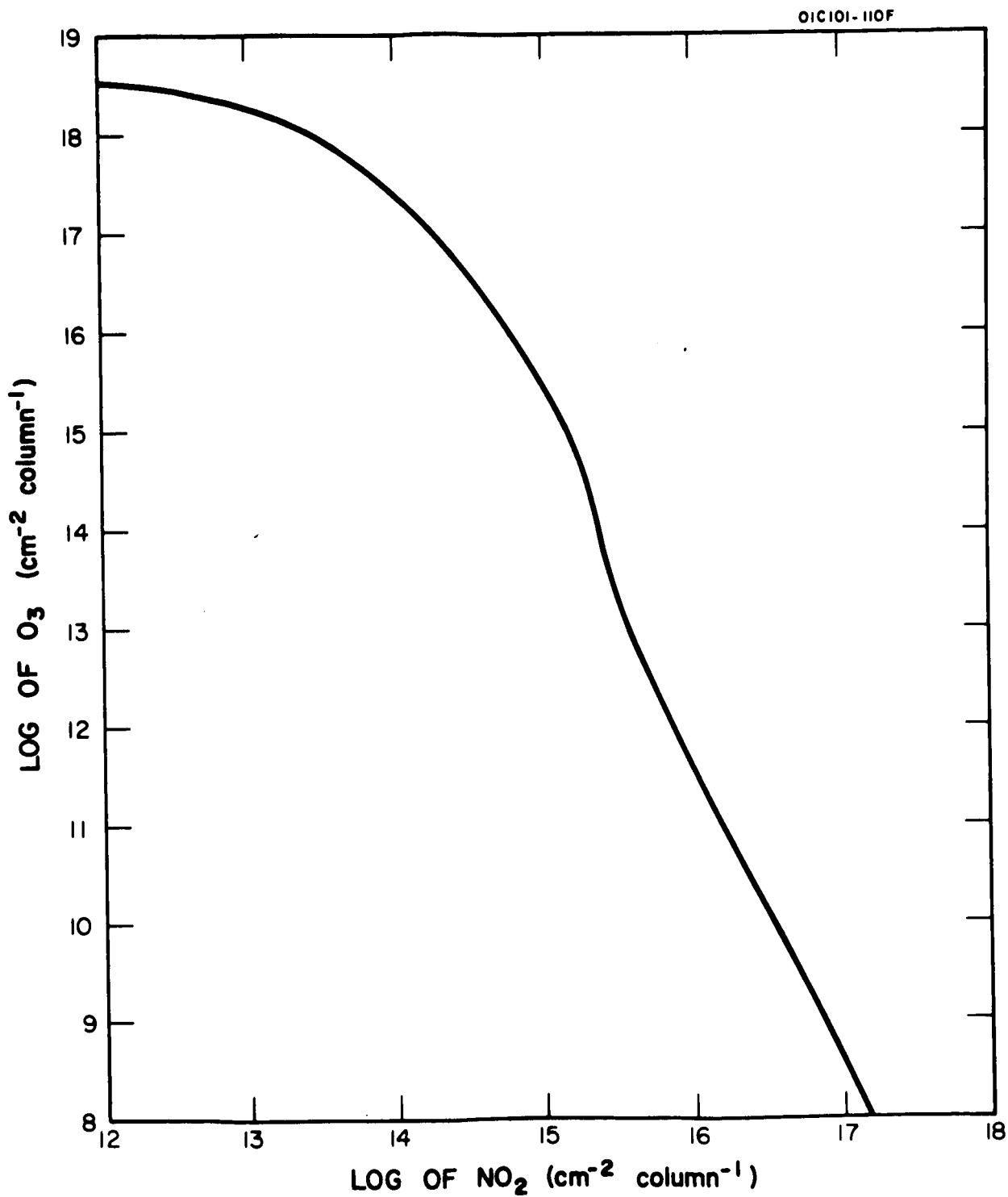


Figure 1 (II-D-3). O₃ contents as a function of NO₂ for O₂ = 70 cm-atm.

III. TECHNICAL SUMMARIES OF INCOMPLETE AND/OR UNPUBLISHED WORK GENERATED UNDER THE CURRENT CONTRACT

In the previous section, technical summaries were given of published reports generated under the present contract. In any continuing research effort of this nature, there is always some fraction of the data which is either not ready or not suitable for publication due to a variety of reasons. In this section, these data are summarized in order to: (a) demonstrate the level of effort, (b) illustrate the scope of the work involved, and (c) to indicate the scientific direction and approach of future investigations. For these purposes it is appropriate to give only very brief technical summaries since no definite conclusions or detailed analyses of these data can be offered at this time. In addition, more detailed accounts are available in the appropriate Quarterly Reports.

It is convenient to discuss this phase of the work in the same four categories as in Section II; namely,

- A. Photochemistry of Planetary Atmospheres
- B. Theoretical Studies
- C. Experimental Studies in the VUV and EUV Spectral Regions
- D. Theoretical Aeronomy.

A. PHOTOCHEMISTRY OF PLANETARY ATMOSPHERES: BRIEF TECHNICAL SUMMARIES OF UNPUBLISHED WORK

The investigation on the photochemistry of planetary atmospheres has resulted in the generation of one unpublished piece of work concerned with the photolysis of CO_2 at 1066\AA . This work was performed in order to complement the photolyses at 1215\AA and around 1700\AA (see Item II-A-1). It is anticipated that upon completion of this phase of the work and proper integration with the previous photolyses experiments, this material will also be submitted for publication in an accredited journal. A summary of the work thus far achieved is given below.

1. CO_2 Photolyses at 1066\AA

- (a) Principal Investigators: P. Warneck and J. O. Sullivan.

The experimental details closely follow those employed in the CO_2 photolyses at 1215 and around 1700\AA so that a detailed account is not required here. In this case, however, several additional difficulties are encountered (see Item II-A-5). In fact, this is the reason that this wavelength region was not included with the 1215 and 1700\AA regions. In any case, in this summary only the results and a brief analysis are given.

The CO_2 photolyses experiments at 1006\AA were carried out with CO_2 partial pressures varying from 1.6 to 1.4 mm Hg. At these pressures, the absorption of both argon lines is essentially complete. A small amount of helium was admixed in each experiment to provide a reference in the subsequent mass spectrometer analysis. Because of the transmittance decrease of the windows (see Item II-A-5), intensity determinations were made before and after each run. The exponential decrease of transmittance was taken into account. Carbon monoxide and oxygen were the only conspicuous products in the 1048 to 1066\AA photolysis of CO_2 . The final results are shown in Table 1. CO production occurred with a quantum yield of unity under all investigated conditions. The averaged determined CO quantum yield was $\Phi(\text{CO}) = 1.06 \pm 0.10$. The first two runs entered in Table 1 were performed with an indium filter which eliminated the effect of the Lyman-alpha line. No change in the CO quantum yield occurred in this case in comparison to the experiments employing no filter. However, in view of the comparatively small absorption cross section of CO_2 at 1216\AA , no effect of the Lyman-alpha line is expected. Runs 3 through 7 further show that the CO quantum yield is also independent of pressure. The finding that the CO quantum yield is unity indicates that dissociation or predissociation is the predominant primary process. The other primary product must then be atomic oxygen and we may inquire about the fate of this species.

The oxygen quantum yields expressed as the ratio $R = (\text{O}_2)/(\text{CO})$ exhibited a behavior very similar to that observed in the CO_2 photolysis at longer wavelengths; namely, in the 1200 - 1700\AA region. The $(\text{O}_2)/(\text{CO})$ ratios found in the present experiments were much smaller than the theoretical value $R = 0.5$ which should be expected if carbon monoxide and oxygen are the only products. In the 1200 to 1700\AA wavelength region, this behavior was shown to arise from the formation of CO_3 as the additional product and we may discuss the present results also under this aspect. One of the effects found previously is the increase of the $(\text{O}_2)/(\text{CO})$ ratio with time owing to the slow thermal decomposition of CO_3 . This effect is clearly indicated also by the present results in Table 1. Runs 1 and 2, in which the irradiation time was extended to several hours, exhibit an increase of R in comparison to runs 3 through 7. This is not caused by the lower intensity applied in the first two runs, since runs 8 and 9 show the same effect also when the time period between photolysis and analysis was increased to three-quarters of an hour.

It was also found previously that the ratio R decreases with decreasing intensity. At intensities around 10^{14} quanta/sec, $(\text{O}_2)/(\text{CO})$ ratios of $R \approx 0.1$ are expected if the derived relationship is applied. The R -values found in runs 3 through 7 are somewhat lower, but they are not in direct conflict with the previous data. Consideration must also be given to the fact that the amounts of oxygen observed were near the limit of mass spectrometric detectability. Accordingly, it appears that the photolytic mechanism of CO_3 formation and O_2 formation active in the 1200 to 1700\AA wavelength region can also describe the photolysis of CO_2 at 1048 to 1066\AA . If the observed oxygen deficiency is due to CO_3 formation,

TABLE 1 (III-A-1)

CO₂ PHOTOLYSIS RESULTS

Run No.	Irradiation Time Minutes	Irradiation Dose quanta x 10 ⁻¹⁷	Pressure mm Hg	He	CO ₂	Molecules Produced CO x 10 ⁻¹⁷	O ₂ x 10 ⁻¹⁶	R=O ₂ /CO	φ(CO)
1 ^a	210	0.864	1.50	1.85		0.864	2.0	0.232	1.00
2 ^a	120	3.40	6.50	2.0		1.15	2.13	0.185	1.05
3 ^b	16	1.28	1.65	1.35		1.21	0.45	0.037	0.95
4	10	1.52	2.75	1.00		1.45	1.15	0.080	1.06
5	15	2.6	10.0	2.00		3.0	1.2	0.042	1.15
6	21	4.75	11.5	2.00		5.18	0.95	0.018	1.00
7	15	3.1	14.0	2.00		3.3	0.92	0.028	1.06
8 ^c	16	1.1	4.0	2.00		1.15	2.13	0.185	1.05
9 ^c	10	1.45	12.0	2.00		1.43	3.0	0.210	0.98

^a indium filter^b no filter in all subsequent runs^c analysis done 45 minutes after termination of photolysis

it implies that the reacting oxygen atoms are in an excited metastable singlet state, since ground-state oxygen atoms are known to be unreactive with respect to carbon dioxide.

B. THEORETICAL STUDIES: BRIEF TECHNICAL SUMMARIES OF UNPUBLISHED WORK

Most of the material generated under Theoretical Studies has appeared in the form of journal articles as indicated in Section II-B. Specifically, only one theoretical effort was not in publication form at the close of the current contract. This work was concerned with the determination of the intensity of N_2^+ , O_2^+ and O^+ visible radiation arising from the fluorescence of the solar ultraviolet. This study is practically complete in that the only work remaining is the correlation of the new data with experimental results available in the open literature and the suggestion of meaningful experiments for the earth-bound monitoring of solar ultraviolet radiation. The current progress is briefly summarized below.

1. The Fluorescence of Solar Ionizing Radiation

(a) Principal Investigators: A. Dalgarno and M. B. McElroy

The mid-day dayglow intensities arising from the fluorescence of solar ionizing radiation were calculated. The predicted overhead intensities above 120 km of the $O^+(^2P-^2D)$ lines at $\lambda\lambda$ 7319-7330 Å, the Meinel band system of N_2^+ , the first negative system of N_2^+ , the first negative system of O_2^+ , the Hopfield emission of O_2^+ and the second negative system of O_2^+ are respectively 500 R - 1 kR, 9 kR, 600 R, 2 kR, 600 R and 400 R.

The mathematical details are not given in this summary; however, a more complete sample of some of the data obtained is given in Tables 1, 2 and 3 which show the column integrated rates ($\text{cm}^{-2} \text{sec}^{-1}$) for the production of the excited states of O^+ , N_2^+ and O_2^+ , respectively. The corresponding data concerned with volume rates is also given in the original report.

In any case, it has been demonstrated that the expected intensities can be detected by present-day optical techniques. Of special interest is the solar fluorescent line emission from O^+ since in this case, direct probing of the solar activity in the ultraviolet can be achieved by an earth-bound observer. The material discussed under Item II-D-1 (specifically, "The Photoionization of Atomic Oxygen") was directly employed in the calculations concerned with O^+ .

TABLE 1 (III-B-1)
COLUMN INTEGRATED RATES ($\text{cm}^{-2} \text{sec}^{-1}$) FOR THE PRODUCTION
OF EXCITED STATES OF O^+

Altitude	Solar Zenith Angle	Excited State Configuration				
		$(2p^3)^4S$	$(2p^3)^2D$	$(2p^3)^2P$	$(2s2p^4)^4P$	$(2s2p^4)^2P$
600	0°	8.71(5)	2.11(5)	7.18(4)	7.68(2)	4.19(2)
	90°	8.71(5)	2.11(5)	7.18(4)	7.67(2)	4.19(2)
500	0°	1.07(7)	2.58(6)	8.79(5)	9.40(3)	5.12(3)
	90°	1.07(7)	2.57(6)	8.76(5)	9.37(3)	5.11(3)
400	0°	9.78(7)	2.35(7)	8.00(6)	8.56(4)	4.67(4)
	90°	9.54(7)	2.27(7)	7.73(6)	8.34(4)	4.57(4)
300	0°	9.04(8)	2.18(8)	7.37(7)	7.92(5)	4.33(5)
	90°	7.15(8)	1.58(8)	5.35(7)	6.24(5)	3.51(5)
250	0°	2.60(9)	6.18(8)	2.10(8)	2.29(6)	1.26(6)
	90°	1.44(9)	2.84(8)	9.52(7)	1.24(6)	7.22(5)
200	0°	7.12(9)	1.63(9)	5.50(8)	6.33(6)	3.53(6)
	90°	1.89(9)	3.29(8)	1.10(8)	1.54(6)	9.30(5)
180	0°	1.00(10)	2.21(9)	7.45(8)	8.97(6)	5.05(6)
	90°	1.92(9)	3.31(8)	1.11(8)	1.56(6)	9.47(5)
160	0°	1.13(10)	2.74(9)	9.20(8)	1.18(7)	6.75(6)
	90°	1.94(9)	3.32(8)	1.11(8)	1.58(6)	9.59(5)
140	0°	1.56(10)	3.06(9)	1.02(9)	1.38(7)	8.06(6)
	90°	1.95(9)	3.33(8)	1.11(8)	1.58(6)	5.63(5)
120	0°	1.66(10)	3.14(9)	1.05(9)	1.45(7)	8.59(6)
	90°	1.96(9)	3.33(8)	1.12(8)	1.59(6)	9.67(5)

TABLE 2 (III-B-1)

COLUMN INTEGRATED RATES ($\text{cm}^{-2} \text{sec}^{-1}$) FOR THE PRODUCTION
OF EXCITED STATES OF N_2^+

Altitude	Solar Zenith Angle	Excited State Configuration			
		$(X^2\Sigma_g^+)$	$(^2\Pi_u)$	$(B^2\Sigma_u^+)$	$(^2\Sigma_g^+)$
600	0°	3.77 (2)	3.65 (2)	1.67 (2)	3.79 (1)
	90°	3.77 (2)	3.64 (2)	1.67 (2)	3.79 (1)
500	0°	1.87 (4)	1.78 (4)	8.18 (3)	1.85 (3)
	90°	1.86 (4)	1.77 (4)	8.14 (3)	1.85 (3)
400	0°	8.61 (5)	8.20 (5)	3.76 (5)	8.54 (4)
	90°	8.33 (5)	7.84 (5)	3.59 (5)	8.31 (4)
300	0°	4.32 (7)	4.11 (7)	1.88 (7)	4.33 (6)
	90°	3.09 (7)	2.62 (7)	1.19 (7)	3.32 (6)
250	0°	2.59 (8)	2.45 (8)	1.12 (8)	2.65 (7)
	90°	6.18 (7)	4.29 (7)	2.22 (7)	6.88 (6)
200	0°	1.58 (9)	1.41 (9)	6.39 (8)	1.72 (8)
	90°	2.00 (8)	1.11 (8)	4.92 (7)	2.29 (7)
180	0°	2.93 (9)	2.48 (9)	1.12 (9)	3.32 (8)
	90°	2.23 (8)	1.13 (8)	5.02 (7)	2.39 (7)
160	0°	4.89 (9)	3.77 (9)	1.68 (9)	5.83 (8)
	90°	2.51 (8)	1.15 (8)	5.11 (7)	2.48 (7)
140	0°	6.86 (9)	4.73 (9)	2.08 (9)	8.42 (8)
	90°	2.76 (8)	1.16 (8)	5.19 (7)	2.56 (7)
120	0°	8.27 (9)	5.05 (9)	2.22 (9)	9.61 (8)
	90°	2.85 (8)	1.17 (8)	5.22 (7)	2.59 (7)

TABLE 3 (III-B-1)

COLUMN INTEGRATED RATES ($\text{cm}^{-2} \text{sec}^{-1}$) FOR THE
PRODUCTION OF EXCITED STATES OF O_2^+

Altitude	Solar Zenith Angle	Excited State Configuration				
		($\text{X}^2\Pi_g$)	($\text{a}^4\Pi_u$)	($\text{A}^2\Pi_u$)	($\text{b}^4\Sigma_g^-$)	($\text{e}^4\Sigma_u^-$)
600	0°	3.13(0)	5.26(-1)	2.63(-1)	2.42(-1)	1.08(-1)
	90°	3.13(0)	5.25(-1)	2.63(-1)	2.42(-1)	1.08(-1)
500	0°	2.51(2)	4.20(1)	2.10(1)	1.94(1)	8.63(0)
	90°	2.50(2)	4.18(1)	2.09(1)	1.93(1)	8.59(0)
400	0°	2.00(4)	3.34(3)	1.67(3)	1.54(3)	6.86(2)
	90°	1.95(4)	3.19(3)	1.60(3)	1.47(3)	6.61(2)
300	0°	1.78(6)	2.95(5)	1.47(5)	1.36(5)	6.09(4)
	90°	1.42(6)	1.88(5)	9.41(4)	8.59(4)	4.25(4)
250	0°	1.39(7)	2.24(6)	1.12(6)	1.03(6)	4.70(5)
	90°	7.65(6)	7.12(5)	3.56(5)	3.22(5)	1.84(5)
200	0°	1.23(8)	1.75(7)	8.75(6)	8.01(6)	3.92(6)
	90°	2.35(7)	1.19(6)	5.95(5)	5.38(5)	3.58(5)
180	0°	2.69(8)	3.47(7)	1.74(7)	1.58(7)	8.19(6)
	90°	3.13(7)	1.27(6)	6.35(5)	5.79(5)	3.97(5)
160	0°	5.63(8)	6.02(7)	3.01(7)	2.73(7)	1.54(7)
	90°	4.44(7)	1.36(6)	6.81(5)	6.25(5)	4.43(5)
140	0°	1.04(9)	8.46(7)	4.23(7)	3.83(7)	2.36(7)
	90°	6.63(7)	1.45(6)	7.23(5)	6.67(5)	4.85(5)
120	0°	1.68(9)	9.79(7)	4.90(7)	4.47(7)	2.94(7)
	90°	1.08(8)	1.49(6)	7.43(5)	6.87(5)	5.05(5)

C. EXPERIMENTAL STUDIES IN THE VUV AND EUV SPECTRAL REGIONS: BRIEF TECHNICAL SUMMARIES OF UNPUBLISHED WORK

There are eight scientific areas to be discussed in this category. In some cases, the work is of a continuing nature and in others the work has been completed but has not been published in an accredited journal.

1. Laboratory Measurements of Cross Sections of Atomic Nitrogen and Atomic Hydrogen

(a) Principal Investigators: J. A. R. Samson and R. B. Cairns

Previous to the present investigations, quantitative absorption and/or photoionization cross sections for atomic species had not been achieved. The current program is involved in the determination of these cross sections for atomic oxygen, nitrogen and hydrogen. The case of atomic oxygen has been previously discussed under Section II-C-9 which reported the results of the first successful determination of quantitative absorption atomic cross sections. The cases of H and N are even more difficult since the generation of sufficient amounts and the required quantitative analysis of these species has not been achieved satisfactorily in any laboratory to date. An additional difficulty was made evident from previous experiments on atomic oxygen which emphasized the importance of identifying excited species in the discharge gas under investigation.

A major effort is currently under way to minimize these problems so that the required VUV and EUV measurements can be performed. Current thinking suggests that the Wrede-Hartek gauge may be employed in measuring the number density of atomic hydrogen which will be produced by a microwave-powered discharge similar to that employed for the production of atomic oxygen.

In the case of nitrogen, the tasks are even more difficult in that microwave-powered discharge through N_2 results in concentrations of atomic nitrogen which are too low to be useful for the present purpose. Accordingly, a new technique must be devised for the production of these atoms. Concerning the number density measurements, it may be mentioned that the Wrede-Hartek gauge has been employed for this purpose but does not appear too suitable so that titration techniques are also being considered.

In any case, a crude estimate of the expectation values for these two atomic cross sections has been obtained by utilizing the molecular cross sections of H_2 and N_2 ; these have been measured from 209Å to 500Å for this purpose. The values have been tabulated in Table 1 along with the measured cross sections for molecular oxygen for direct comparison.

The $\frac{1}{2}\sigma$ -values for H_2 have been compared to the theoretical values for H and found to be higher in all cases so that the need for quantitative laboratory data is evident. Once the described experimental difficulties are surmounted, quantitative absorption data should become available.

TABLE 1 (III-C-1)

ABSORPTION CROSS SECTIONS OF HYDROGEN, OXYGEN AND NITROGEN

$\lambda(\text{\AA})$	Cross Section in Mb		
	$\frac{1}{2}\sigma(\text{H}_2)$	$\frac{1}{2}\sigma(\text{O}_2)$	$\frac{1}{2}\sigma(\text{N}_2)$
209.3	0.133	4.52	3.23
225.2	--	5.30	--
234.2	0.201	5.30	--
239.6	0.220	5.95	--
247.2	0.247	6.15	4.88
260.5	0.289	--	--
266.3	0.319	7.00	5.25
283.5	0.395	7.60	5.45
297.6	0.475	--	5.75
303.1	0.510	8.65	5.80
314.9	0.560	8.20	6.20
323.6	0.610	8.35	6.55
335.1	0.680	8.40	7.00
345.1	0.755	8.50	7.40
358.5	0.875	--	7.85
362.9	0.920	8.75	8.05
374.4	1.02	8.95	8.65
387.4	1.13	9.25	9.30
428.2	1.44	9.70	11.0
434.3	1.51	9.80	11.2
452.2	1.68		11.3
463.7	--		11.3
508.2	--		11.4
512.1	--		11.6

2. Laboratory Measurements of the Kinetic Energies of Photoelectrons from N_2 and O_2

(a) Principal Investigators: R. B. Cairns and J. A. R. Samson

For proper understanding of the behavior of electron temperature in the earth's upper atmosphere, it is mandatory to have accurate values for the electron energies and geometric distributions produced by the solar photoionization of atmospheric species. This requirement has been thoroughly discussed by Geisler and Bowhill [130] in a very recent article concerned with the ionospheric temperature at sunspot minimum so that no further justification is given at this point. Theoretical investigations of these parameters are practically precluded due to the complex processes involved so that experimental measurements are indicated. In this regard, this problem has received considerable attention during the current contract period. Specifically, the energies of photoelectrons released in O_2 , N_2 and A have been studied at 584\AA (21.21 eV).

Experimentally, the setup employed a suitable electron analyzer coupled to a $\frac{1}{2}$ -m Seya monochromator. The electron energy analyzer consisted of three concentric cylindrical grids surrounded by a cylindrical collector plate (see Figure 3 of QPR No. 5). Ideally, with this setup if the photoelectrons are not scattered by the residual gas in the analyzer, the resulting electron current per photon versus retarding voltage would appear as the solid curve in Figure 1. Since this is not the case, a dotted line is shown in Figure 1 to indicate what might be expected for the more realistic case in which the scattering of electrons is real. This predicted behavior can now be compared with the data actually obtained for argon as shown in Figure 2. Since 584\AA photons were employed, only one electron is expected to be present, and that with an energy of 5.45 eV. The figure indicates that, indeed, all electrons have been retarded at the expected retarding voltage. However, on the other hand, the deviation of the curve from the ideal rectangular shape indicates a departure which is too far from ideality for application for quantitative work involving the expected fine structure for molecular ions such as N_2^+ and/or O_2^+ . Accordingly, it appears that further design refinements will be required.

In any case, the apparatus was employed to investigate the cases of oxygen and nitrogen; although it was found that the terminal energy of the electrons agreed with the expected values, the fine structure associated with vibrational transitions was not observed.

3. Photoionization Threshold for O_2

(a) Principal Investigators: J. A. R. Samson and R. B. Cairns

(b) Presented at Seventeenth Annual Gaseous Electronics Conference, Atlantic City, New Jersey, October 14-15, 1964.

Apparently, the ionization potential (IP) of O_2 is not precisely known since the work described in Section II-C-5 and the earlier work of Watanabe and Marmo show that ions are formed by radiation around 1030\AA in spite of the

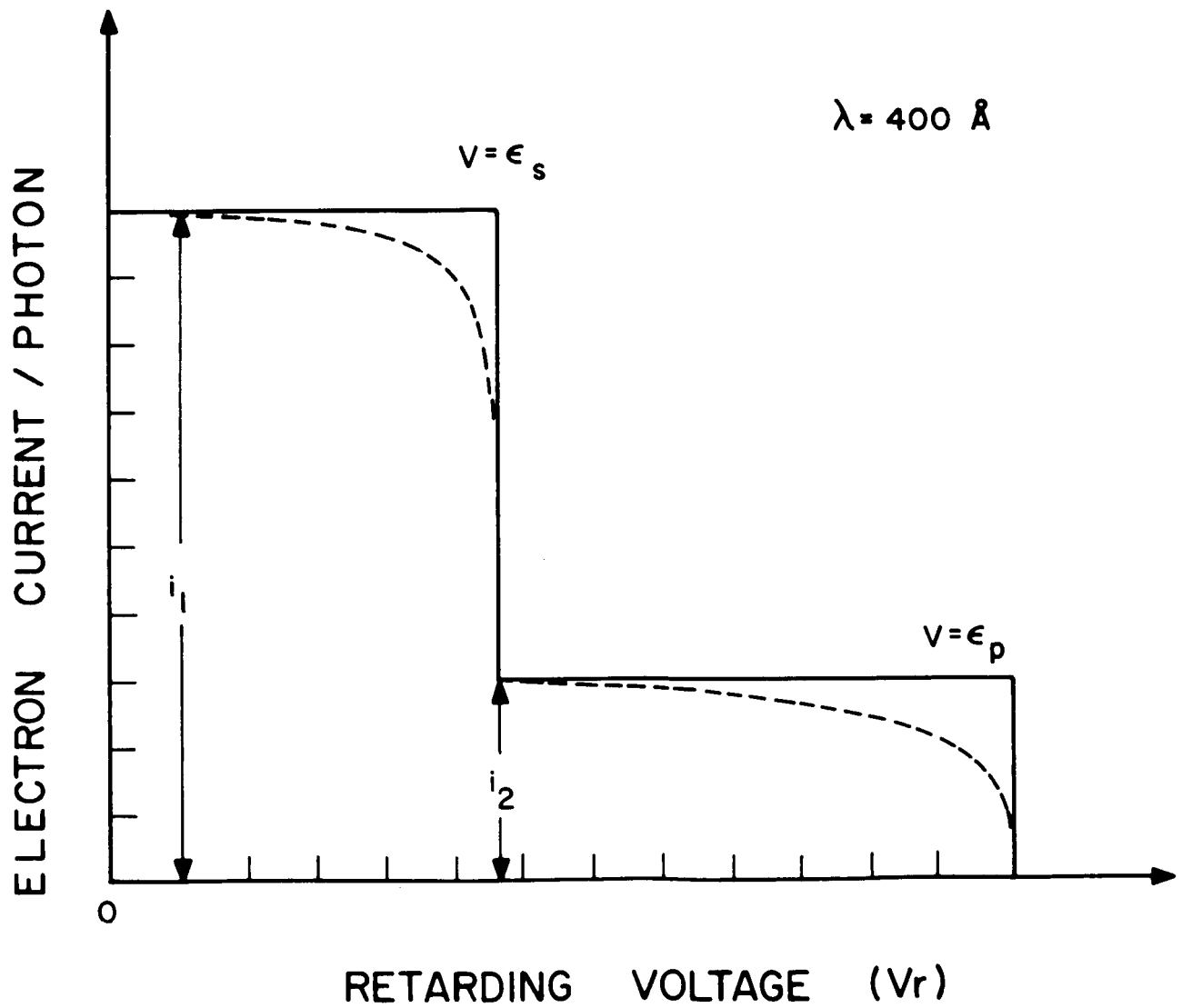


Figure 1 (III-C-2). Predicted electron current as a function of the retarding voltage. The discontinuity represents the suppression of the S-electron.

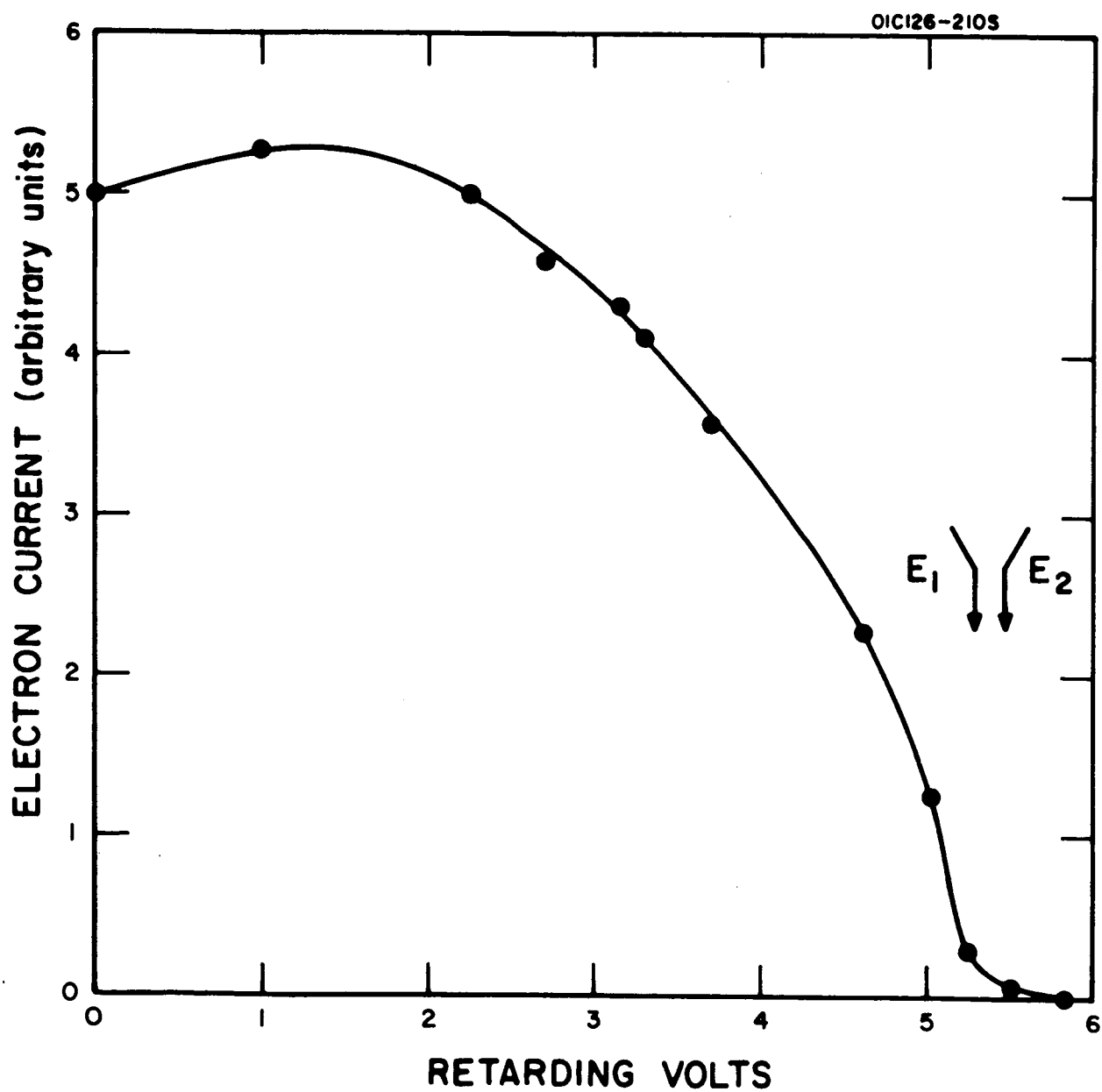


Figure 2 (III-C-2). Retardation of photoelectrons ejected from argon by 584.3\AA . The vertical arrows E_1 and E_2 represent the voltage necessary to retard electrons originating from the $2p_{3/2}$ and $2p_{1/2}$ thresholds.

fact that the presently-accepted value of the IP is at 1026.5\AA . It is clearly important to determine the true IP since the solar spectrum contains at least three lines of comparable intensity in the vicinity of the presently-accepted threshold value; namely, H I 1025.7\AA , O VI 1032\AA , and O VI 1038\AA . Some theories of the ionosphere have stressed the importance of the Lyman-beta line at 1025.7\AA as controlling the base of the E-region — but does this wavelength ionize O_2 ? Thus, what is the true IP of O_2 ?

For these experiments, the $\frac{1}{2}$ -meter Seya monochromator was employed with a 1\AA bandpass and a dc hydrogen discharge lamp; the threshold wavelength range from 1020\AA to 1050\AA was studied.

An ionization chamber was constructed which was surrounded by an outer jacket containing liquid oxygen. With this setup, the ionization yields of O_2 were measured first at room temperature and then at liquid oxygen temperature in the wavelength region 1020 to 1050\AA . Figure 1 is a plot of photo-ionization yield as a function of wavelength. The solid data points represent the results at room temperature which should be compared to the triangular data points of Watanabe and Marmo also obtained at room temperature. When their data are plotted on a semilog scale, an abrupt change in slope is apparent; Watanabe *et al.* ascribed this change to the (0-0) transition and hence to the true IP. If this were the case, however, those ions observed at the longer wavelengths would disappear at liquid O_2 temperatures. As can be seen, the ions do not disappear even out to the largest wavelengths. Thus, the true IP must be at least 1046\AA . Further, the energy difference between 1046\AA and 1026\AA (the break in the slope) corresponds almost exactly to the energy separation between the zero and first vibrational states of O_2^+ ; namely, 1843 cm^{-1} . Thus, in the present interpretation the 1026\AA break is considered to be due to the (1-0) transition. Subtracting the vibrational energy of 1843 cm^{-1} , one obtains the new IP at 1047.2\AA (11.84 eV).

The role of this new value on earth ionosphere studies is currently being evaluated.

4. EUV and VUV Fluorescence Radiation from Planetary Gases

(a) Principal Investigators: F. F. Marmo, Shardanand and
J. A. R. Samson

When solar ultraviolet radiation ionizes an atmospheric constituent, some of the radiation is absorbed into the excited electronic levels of the ion which may then radiate in the visible. For example, the first negative and the Meinel bands of nitrogen have been observed in the upper atmosphere. Emissions from O_2^+ and O^+ have also been associated with upper atmospheric phenomena as indicated in Section III-B-1. In spite of the importance of these areas of research, very little laboratory results have been obtained on the fluorescence radiation from planetary gases. The required quantitative data can only be obtained by means of a systematic laboratory study.

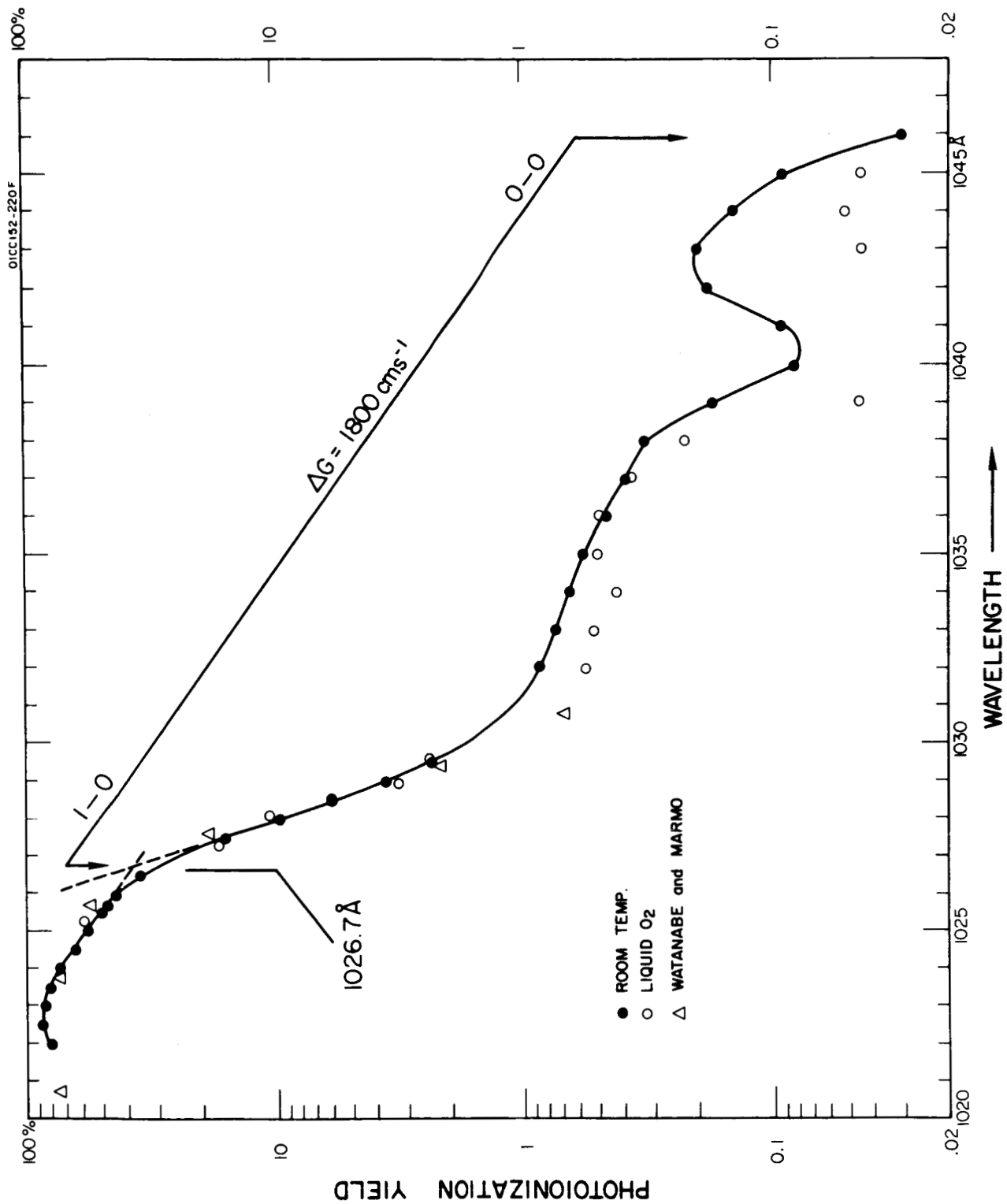


Figure 1 (III-C-3). Photoionization yield of O₂.

Some significant progress has been achieved in this area as follows. The photoelectron energies in helium have been measured and have shown a sudden loss of high energy electrons at wavelengths below 270\AA , indicating that their energies have been lost in excitational collisions with neutral helium. This is indirect evidence for the production of 584\AA fluorescence in helium at wavelengths below 270\AA . No experimental attempt has been accomplished as yet to observe this expected radiation.

Direct evidence for EUV fluorescence has also been achieved. For example, recent measurements have identified the onset of the first negative bands and the second negative bands at 683\AA and 734\AA , respectively. The results are quantitative and serve to verify the feasibility of such experiments. In a future investigation it is planned to use an experimental technique that has not as yet been employed in which it should be possible to obtain the discrete spectra associated with the first negative bands and the second negative bands.

5. The Mass Analysis of the Products of Photoionizing O₂, N₂ and CO₂ below 1000Å

(a) Principal Investigators: J. A. R. Samson, F. F. Marmo and P. Warneck

The main object of the present investigation is to obtain the photoionization cross sections as a function of wavelength for various planetary gases. Usually the total photoionization cross section is experimentally obtained with no specific identification of the actual species involved; i.e., atomic, excited molecular, or the state of ionization. For this information, then, it is required to obtain a mass analysis of the products of photoionization. A convenient method to achieve this is to couple a suitable mass spectrometer to an EUV monochromator and measure the mass spectrum as a function of wavelength.

The experimental setup which was designed, developed and constructed for the purpose is shown in Figure 1. The mass analyzer included a 180-degree magnetic mass spectrometer which employed wedge-shaped pole pieces (for high transmissivity) and a suitably-designed reactor housing. The complete analyzer was coupled to a vacuum monochromator; the associated electronic gear and gas-filling systems were attached as required. An appropriate light source was employed to produce the photoions which are then accelerated and focused onto the entrance aperture of the magnetic analyzer. The performance of these experiments for wavelengths below 1000Å necessitated the use of differential pumping. The overall performance of this instrumentation indicated that several instrumental bugs are still present but that for an initial model, the results obtained appear to be very encouraging as will become evident from the discussion below.

For the preliminary runs, ordinary air samples were used for which a dc-operated hydrogen light source was employed to obtain ionizing radiation (in the 950Å region). The radiation was chosen to ionize only O₂, so that the only observed ion was that of O₂⁺. For the 584Å experiments described later, a helium resonance light source was employed. Figure 2 shows the ion current observed at mass number 32 as a function of pressure in the ion source. The overall behavior can probably be described as follows. The initial linear rise of the ion current is a direct consequence of the increase of light absorption according to Beer's law where for sufficiently small pressures (weak absorption), the exponential function behaves linearly. In this manner, the linear increase up to about 70 microns can be explained. At higher pressures, the full exponential law must be applied. However, it can be shown that the behavior of the data does not follow the exponential absorption law. Accordingly, a different process must be responsible for the observed behavior. In this respect, it is of interest to note that the deviations from linearity become pronounced at that pressure at which the corresponding mean free path of the gas molecules is of the same order as the dimensions of the reaction chamber. This should result in excessive scattering which will tend to broaden the ion beam so that defocusing occurs at the mass analyzer entrance slit with a corresponding loss of ion intensity. This preliminary explanation is only one of other possible explanations and the true cause of this effect must

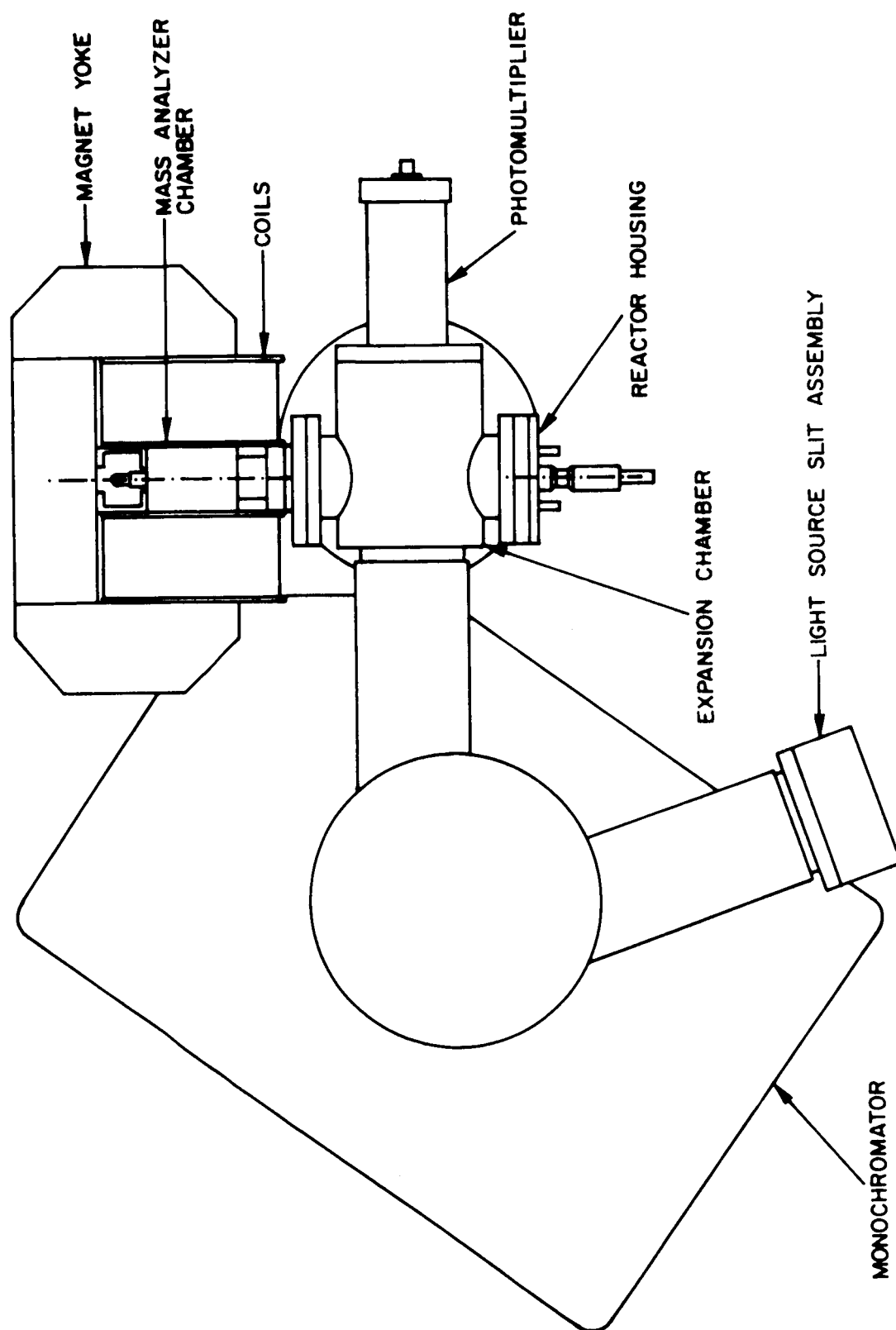


Figure 1 (III-C-5). Layout of proposed ion-molecule reaction experiment.

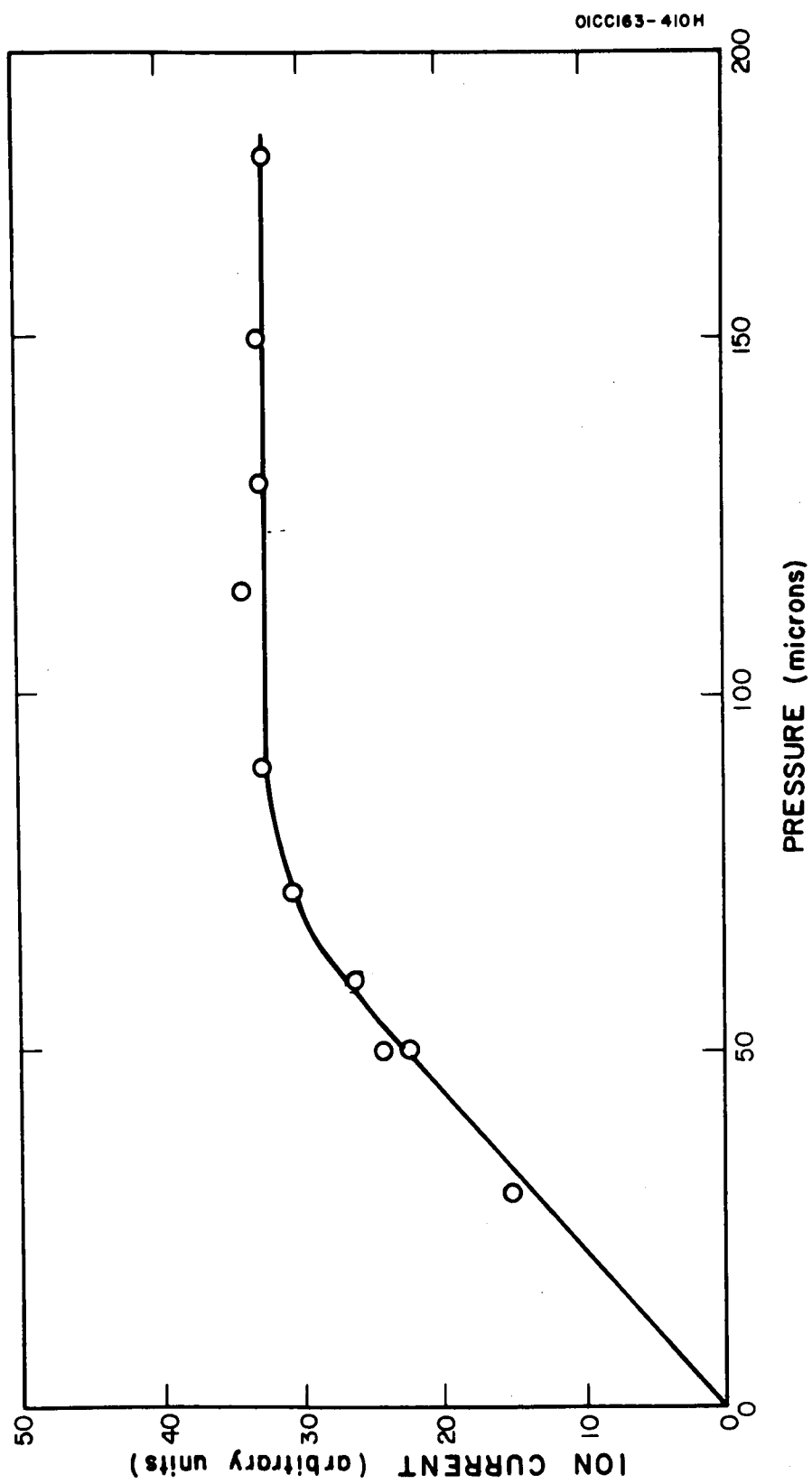


Figure 2 (III-C-5). Ion current observed at mass number 32.

await further investigation. In any case, it was encouraging to observe the actual generation of O_2^+ ions with 950Å radiation.

In order to check a region in which the ionization of other species occurs simultaneously, an air sample was tested at the 584Å He resonance line. In this case, the primary ionic species formed by photoionization were found to be N_2^+ , O_2^+ and O^+ . However, here again, the observed ion intensity-pressure relationships for these ions could not be easily explained; in fact, they behaved in a more complex manner than that for the 950Å radiation.

6. Absorption Coefficients of Acetaldehyde from 2000 to 3500Å

- (a) Principal Investigators: F. F. Marmo and J. O. Sullivan
- (b) Presented at Conference on Remote Investigations of Martian Biology, Cambridge, Mass., January 10-13, 1964.

Recent interpretations of the Martian Sinton IR bands pointed up the value of quantitative cross section data for acetaldehyde at the 2000 to 3500Å region. However, a literature search indicated that such data did not exist. Accordingly, these measurements were performed in the appropriate wavelength region by techniques already described in this report. The experimental data shown in Figure 1 indicate that even within the strongest absorption region, the coefficients are less than $4.5 \times 10^{-20} \text{ cm}^2$. Thus, for this molecule to play any significant role in scattering or absorption a total particle content of somewhat greater than 10^{19} cm^{-2} -column is required. It can be shown that this content is too large to sustain under conditions existing in the Martian atmosphere so on this basis, it can be concluded that the observed Sinton IR bands are not due to acetaldehyde.

7. The Scattering of Lyman-Alpha Radiation by Helium, Neon, Argon, Nitrogen and Hydrogen

- (a) Principal Investigators: F. F. Marmo and Y. Mikawa
- (b) Presented at the APS Meeting, Chicago, Illinois, October 23-24, 1964.

The experimental study of scattering of VUV radiation by molecules is a necessary input for investigations of the luminosity of solar-illuminated planetary atmospheres. Except for the most simple cases, the pertinent cross sections cannot be calculated on a theoretical basis. In spite of its importance, the only other experimental observations are those due to Gill and Heddle [131,132]. Undoubtedly, this is due to the fact that several experimental difficulties are encountered which are peculiar to VUV laboratory studies. In fact, it may be noted that even the investigations of Gill and Heddle were somewhat limited in that they were unable to obtain relative cross section data for helium and neon since their cross sections were too low. On the other hand, they did measure the relative cross sections for argon, hydrogen, nitrogen, krypton and xenon. In the present experimental study, a more sensitive technique was developed so that experimental cross section values

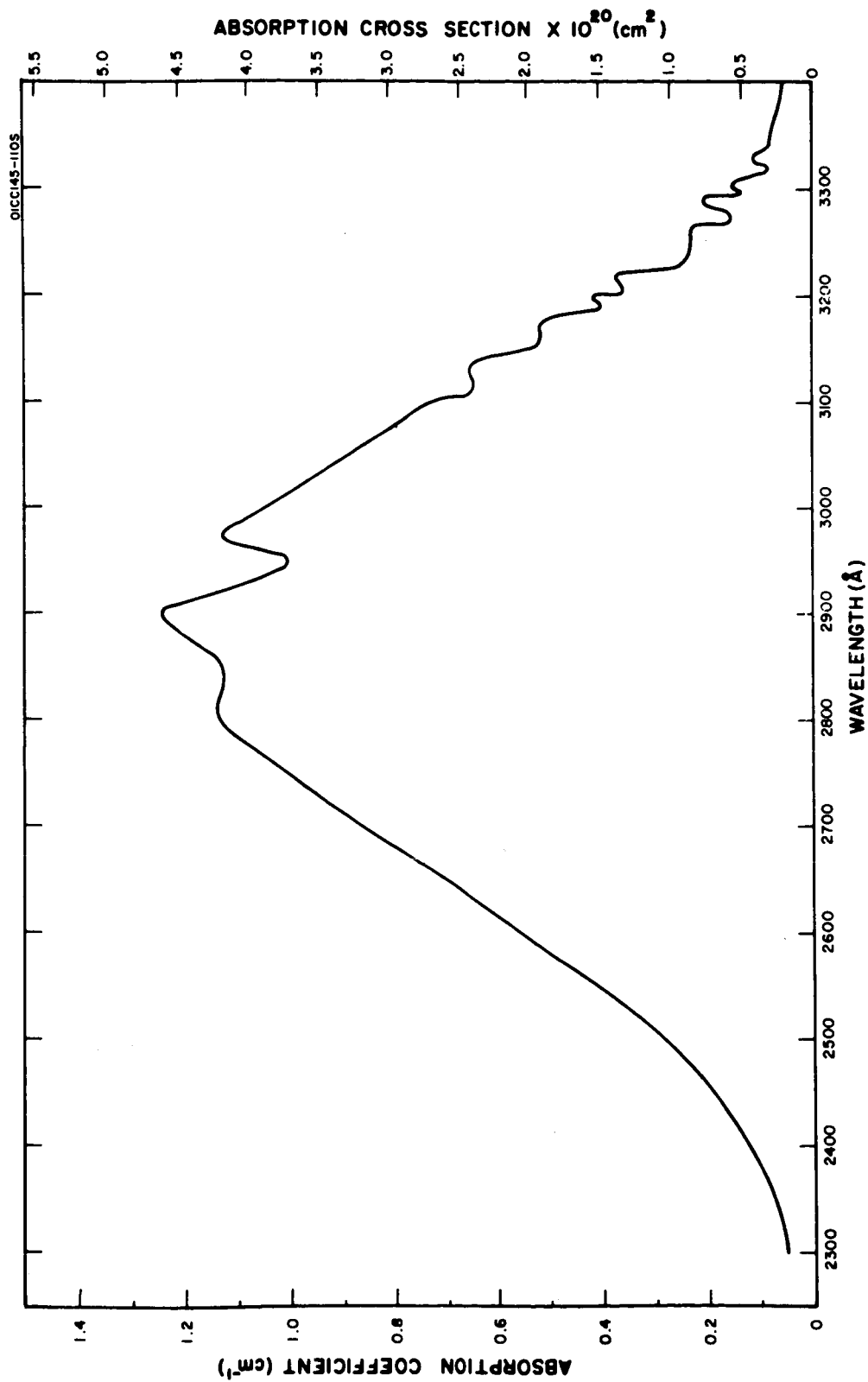


Figure 1 (III-C-6). Acetaldehyde vapor.

were obtained for neon and helium for the first time. It was particularly important to obtain a relative value for helium so that all the measured values could be placed on an absolute basis, due to the accurate calculations by Dalgarno [133] on the absolute scattering cross section of helium at Lyman-alpha.

The basic design of the apparatus was an improved modification of a system used by Gill and Heddle [131,132]. As shown in Figure 1, the incident light coming from the microwave-powered light source [134], S, was first passed through an oxygen filter and then collimated by collimating system C. The intensity of the incident light was measured by a nitric oxide-filled ionization chamber which received reflected light from a small mirror M. The scattered light at the observation area A is measured at right angles to the incident beam by a nitric oxide-filled Geiger counter.

According to the classical electromagnetic theory the reaction between the intensity Φ of the unpolarized incident light and the number of photons

$$\varphi \, d\omega = \Phi \frac{3n \sigma_s}{16\pi} V \frac{1}{1 + 1/2\rho_n} \left(1 + \cos^2 \theta + \rho_n \sin^2 \theta \right) d\omega \quad (1)$$

where n is the density of the gas at pressure p , V the scattering volume, σ_s the scattering cross section and ρ_n normal depolarization ratio which is a measure of anisotropy of the gas particle. Since the apparatus is designed to measure the scattered light at right angles to the incident beam, the above equation can be expressed as

$$\varphi_{90} / \Phi = \frac{3n_o \sigma_s V}{16\pi p_o} \cdot \frac{1 + \rho_n}{1 + 1/2\rho_n} \cdot p \quad (2)$$

where n_o is Loschmidt's number, p_o the normal pressure. If proper consideration is taken for the attenuation of the light in traversing the gaseous medium in the chamber, the ratio of the count rate of the Geiger counter C to the intensity I measured by the ion chamber can be expressed by

$$\frac{C}{I} = k \frac{\varphi_{90}}{\Phi} = k \frac{3n_o}{16\pi} \frac{V}{p_o} \frac{1 + \rho_n}{1 + 1/2\rho_n} \cdot \sigma_s p \exp(-\sigma_T n_o p/p_o) \quad (3)$$

or

$$\frac{C}{I} = \frac{3n_o}{16\pi p_o} V k \frac{1 + \rho_n}{1 + 1/2\rho_n} \sigma_s p \exp(-\sigma_T n_o p/p_o) \quad (4)$$

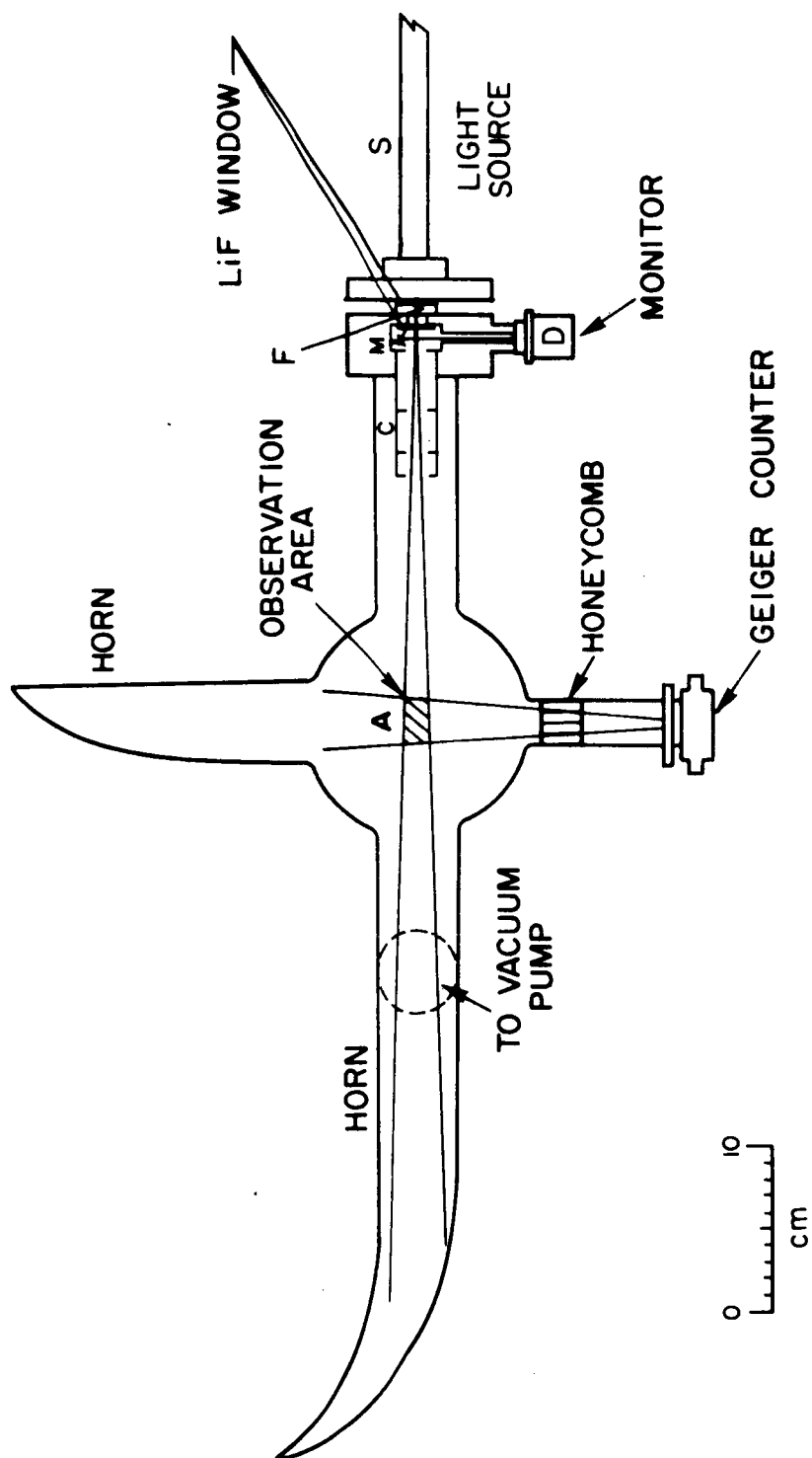


Figure 1 (III-C-7). Apparatus for measuring relative scattering cross sections.

If the exponential factor $\sigma_T n_O p/p_O$ is small compared to unity,

$$\frac{C}{I} = \frac{3n_O}{16\pi p_O} V k \frac{1 + \rho_n}{1 + 1/2\rho_n} \sigma_s p \quad (5)$$

Here k depends upon the sensitivity of the detectors and V upon the geometry of the apparatus. Thus, the value C/I is proportional to the pressure and the slope offers the relative value of the scattering cross section. For rare gases, ρ_n 's are zero and for hydrogen and nitrogen the values for ρ_n are 0.016 [135] and 0.036 [136], respectively.

The scattered light from the gases (A, N₂, H₂, He and Ne) were measured at several pressures up to one atmospheric pressure and the count rates were plotted against the pressure of the gas because the intensity of the incident radiation as measured by the ion chamber was kept constant. These plots of count rates versus pressure were straight lines, the slope of which are the measures of the relative cross sections. The relative cross sections for the gases are given in Table 1. The tabulated values were placed on an absolute basis by normalizing with the theoretical value of $3.5 \times 10^{-28} \text{ cm}^2$ derived by Dalgarno for the helium scattering cross section at 1215Å. This is the case for the values in Column 3 of Table 1.

TABLE 1(III-C-7)

The Relative Scattering Cross Sections

Gases	This Work	Gill and Heddle's Value[131]	Calculated Values by Dalgarno's Method[133]
Argon	1.0	1.0	6.3×10^{-24}
Helium	0.0052	-	3.5×10^{-26}
Neon	0.023	-	1.3×10^{-25}
Hydrogen	0.37	0.33	1.7×10^{-24}
Nitrogen	1.0	1.0	
Krypton	-	89.	
Xenon	-	930.	

8. Reflectance of Beryllium from 584 to 4030 \AA

(a) Principal Investigator: J. A. R. Samson

Project FIRE performed at Langley Research Center is involved in the studies of high-velocity entry into interplanetary atmospheres. For proper analysis of the radiometer and spectrometer field data, reliable laboratory data on the reflectivity of a specific sample of highly-polished beryllium was required. In this case, the NASA-supplied sample (Sample No. 6) was measured at 27°C between 1000 \AA and 4000 \AA with an additional measurement at 584 \AA . Data points were taken at approximately 50 \AA intervals with a wavelength resolution of 5 \AA . The angle of incidence for all measurements was 15°.

The reflectometer is shown in Figure 1. This was a specially-constructed instrument to mount onto the 2-m monochromator. By means of a rotary push-pull vacuum seal, the sample can be moved out of the light path without breaking the vacuum. The sample shaft is provided with a protractor for repositioning the sample at the proper angle of incidence. A protractor on the photomultiplier (PM) shaft also serves to determine the position of the PM. However, since the sensitivity of a PM cathode varies over its surface, as does the fluorescent coating on the PM glass envelope (sodium salicylate in this case), the photomultiplier was rotated until a maximum signal was observed. Since the cross section of the incident beam and reflected beam were the same when intercepted by the PM, it is assumed that by maximizing the signal the incident and reflected beams were positioned on the same area of the detector. The reflectance was defined as the ratio of the reflected energy (I) to that of the incident energy (I_0). The measurements were made as illustrated in Figure 2. The light source was a hydrogen glow discharge which produced useful radiation, after dispersion, from 1000 \AA to 4000 \AA . To eliminate the effects of higher order spectra, filters were used for different regions as follows:

1100 - 2000 \AA	no window
2000 - 2900 \AA	quartz window
2900 - 4000 \AA	pyrex window

The beryllium sample had some unidirectional polish marks. A drop in reflectance of approximately 20 percent was observed when these polish marks were vertical; i.e., parallel to the exit-slit. Thus, all measurements were made with the polish marks in the horizontal plane. No change in reflectance was observed when the sample was simply moved laterally. The observed percent reflectance of beryllium over the wavelength range 1000 to 4000 \AA is given in Table 1 for the wavelengths investigated.

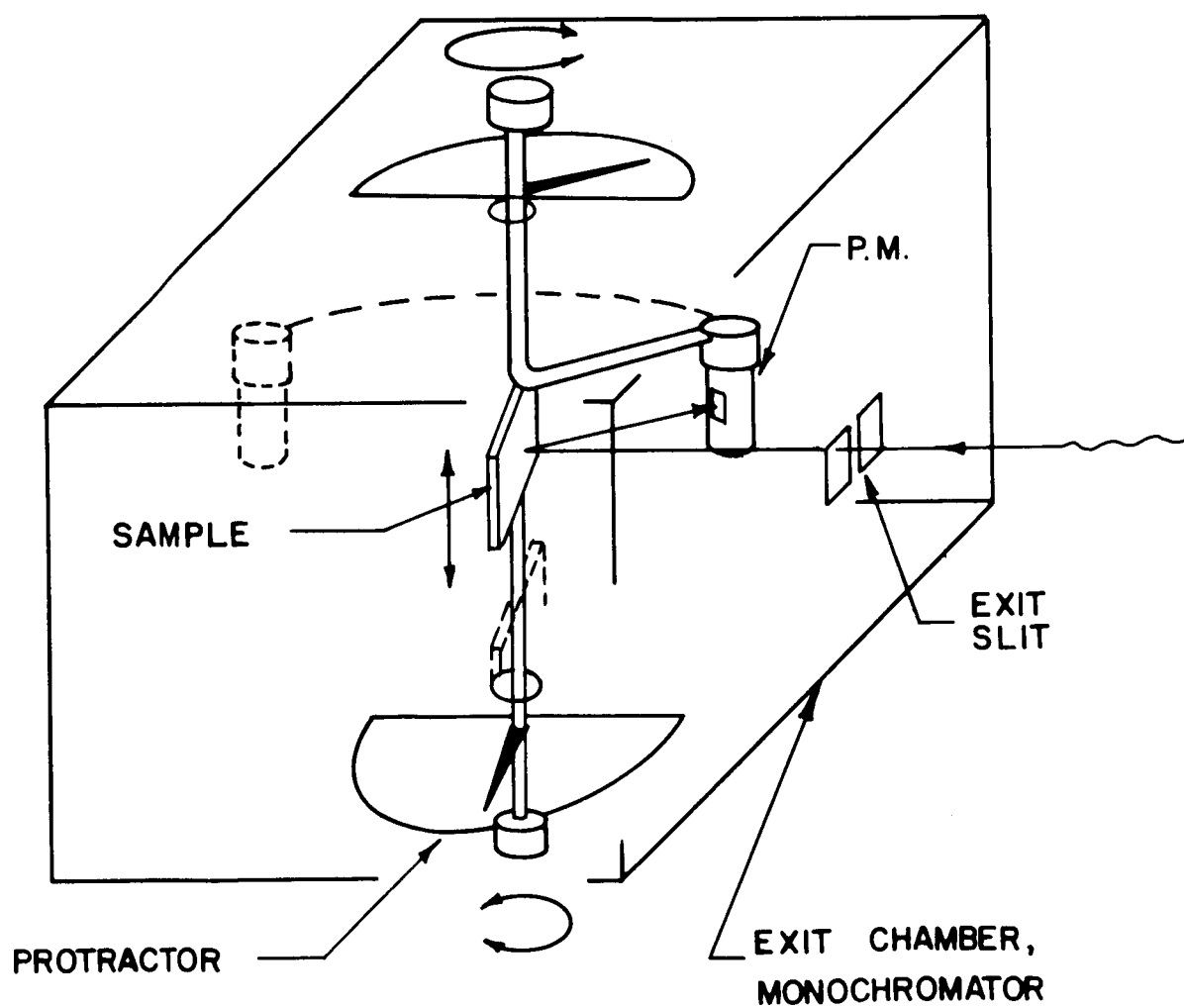
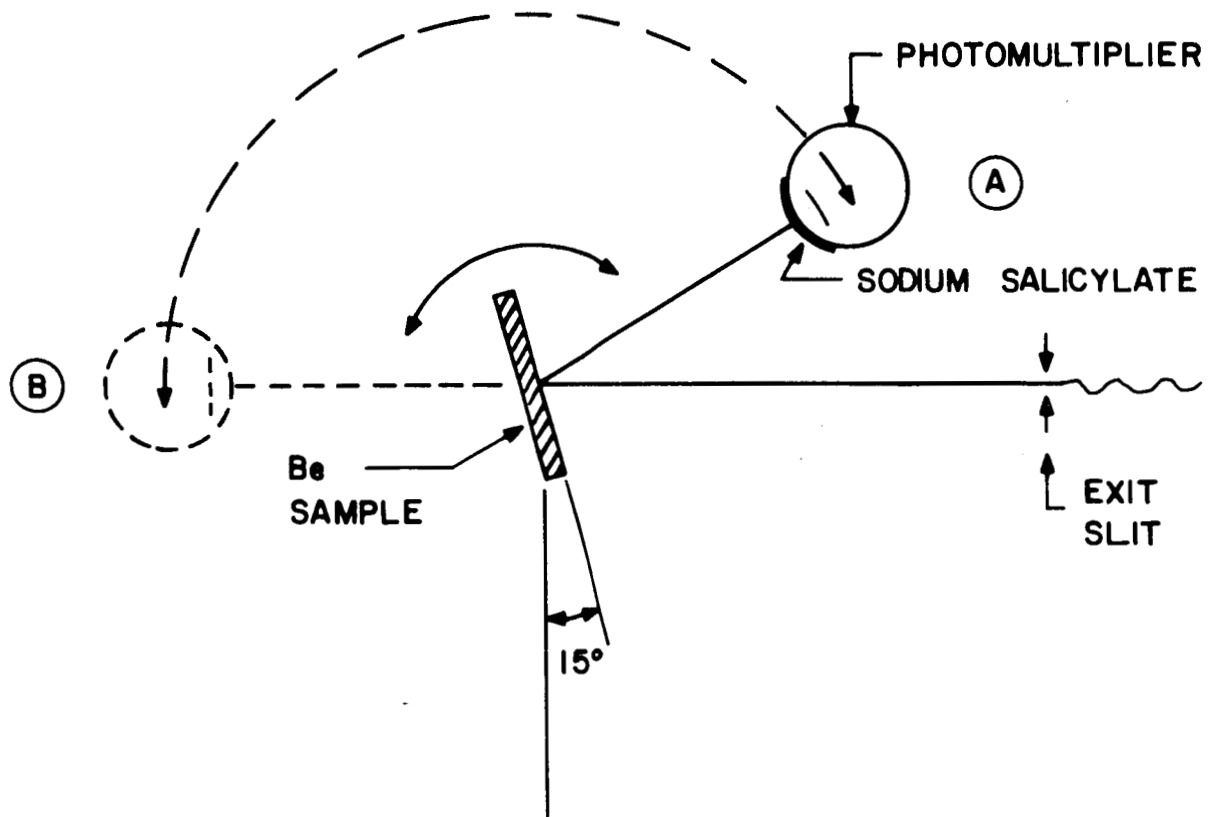


Figure 1 (III-C-8). Schematic diagram of reflectometer.



POSITION 'A' FOR MEASURING I
POSITION 'B' FOR MEASURING I_0

Figure 2 (III-C-8). Method used for measuring reflectance.

TABLE 1 (III-C-8)
REFLECTANCE OF BERYLLIUM

$\lambda(\text{\AA})$	Percent Reflectance	$\lambda(\text{\AA})$	Percent Reflectance	$\lambda(\text{\AA})$	Percent Reflectance
584	2.7	2070	33.5	3118	30.8
1113	3.7	2110	34.2	3168	30.8
1170	4.8	2180	34.8	3218	30.3
1213	5.5	2267	36.7	3268	30.3
1274	6.8	2318	37.2	3318	29.5
1313	7.7	2368	37.3	3368	29.5
1335	8.2	2418	37.0	3418	29.3
1372	9.3	2468	36.4	3468	29.0
1415	9.8	2518	36.1	3518	28.8
1480	11.8	2568	35.4	3568	28.8
1513	13.2	2618	34.8	3610	29.0
1620	17.0	2668	34.2	3660	29.1
1675	20.6	2718	33.8	3711	29.0
1713	22.4	2768	33.2	3771	29.5
1765	24.7	2818	32.8	3828	29.3
1816	27.0	2868	33.0	3873	32.4
1868	28.8	2918	33.2	2923	30.0
1920	30.0	2968	33.4	3980	29.8
1972	31.4	3018	32.6	4030	30.3
2020	32.2	3068	31.5		

D. THEORETICAL AERONOMY: BRIEF TECHNICAL SUMMARIES OF UNPUBLISHED WORK

There are three scientific areas to be discussed in this category. In each case, the investigations report a continuing effort and have not progressed to the point of final publication.

1. The Role of Interplanetary Debris in Planetary Atmospheres

- (a) Principal Investigators: F. F. Marmo and A. C. Holland
- (b) Presented at Conference on Remote Investigations of Martian Biology, Cambridge, Mass., January 10-13, 1964.

In an earlier report, Marmo and Brown [137] investigated the steady-state concentration of interplanetary debris atoms deposited in planetary atmospheres. In order for the model to take account of chemical consumption, eddy diffusion and molecular diffusion, considerable simplification was required. Later, numerical techniques were employed so that some of the simplifications could be removed. During the current contract period, the numerical integration methods were developed, tested and utilized to extend the previous studies in that more complex source functions could be employed. Specifically, a more realistic meteor vaporization source function was developed, a more realistic chemical consumption probability was employed and finally, the empirical diffusion coefficients were utilized. These improved source functions resulted in more accurate data which predicted the existence of certain specific metallic ions in the earth's upper atmosphere. In this regard, a recent rocket experimental study by R. S. Narcissi and A. D. Bailey verified the presence of these ions in the upper atmosphere. However, the altitude distribution did not coincide with the theoretical models; this was probably due to the fact that the chemical consumption probability employed is still not realistic in that the complete set of reactions has not been incorporated into the theory. This latter requirement is the subject of the current effort in this phase.

2. Spectral Reflectivity and Luminosity of the Earth's Atmosphere for 50Å Bandwidths for the Region Below 2000Å

- (a) Principal Investigators: F. F. Marmo and A. C. Holland

A determination of the luminosity of planetary atmospheres is an important input for estimating the background radiations one must encounter in performing optical experiments in planetary atmospheres. The determination of the luminosity of the earth atmosphere for $\lambda \lambda < 2000\text{\AA}$ has been performed under the current contract effort. Similar data for the cases of Mars and Venus can be performed in a strictly analogous manner but the data will be no more accurate than the atmospheric model employed. Accordingly, it was decided to perform a careful investigation of the earth atmosphere and to perform the required calculations for other planets when suitable models are available so that the effort can be justified.

The normal optical thickness of the model atmosphere - from both absorption and scattering - and the albedo for single scattering, ω_0 , were calculated for

all altitudes from 200 km to sea level in 2-km steps for each wavelength. The normal optical thickness due to absorption alone can be defined by:

$$\tau_a(\lambda, z) = \sum_{i=1}^k \sigma_{ai}(\lambda) N_i(z) \quad (1)$$

where $\sigma_{ai}(\lambda)$ is the absorption cross section of constituent i in $\text{cm}^{-2}/\text{molecule}$,
and
 $N_i(z)$ is the integrated number density of constituent i above altitude z in $\text{molecules}/\text{cm}^{-2}$.

$$N_i(z) \equiv \int_z^{\infty} \eta_i(z) dz \quad (2)$$

The normal optical thickness of the model atmosphere from scattering is defined in an analogous manner except that $\sigma_s(\lambda)$, the effective scattering cross section of the ambient atmospheric constituents for the wavelength λ in $\text{cm}^2/\text{molecule}$ is employed. The total normal optical thickness, τ , is then defined as the sum of the optical thickness due to absorption processes τ_a and that due to scattering:

$$\tau = \tau_a + \tau_s .$$

The albedo for single scattering - or more simply, the particle albedo ω_0 - is defined as

$$\omega_0(\lambda, z) = \frac{\sigma_s}{\hat{\sigma}_a + \sigma_s} \quad (3)$$

where

$$\hat{\sigma}_a \equiv \frac{\sum \sigma_{ai}(\lambda) N_i(z)}{\sum N_i(z)} \quad (4)$$

or

$$\omega_0(\lambda, z) = \frac{\tau_s}{\tau_a + \tau_s} = \frac{\tau_s}{\tau} . \quad (5)$$

According to Chandrasekhar, the intensity of light diffusely reflected from a semi-infinite, plane-parallel atmosphere that scatters light isotropically with an albedo ω_0 is:

$$I(o, \mu, \mu_o) = \frac{\omega_o I_o}{4\pi} \frac{\mu_o}{\mu + \mu_o} H(\mu) H(\mu_o) \quad (6)$$

where $I(o, \mu, \mu_o)$ is the intensity at the top of the atmosphere ($\tau = 0$) in the direction $\mu = \cos \theta$ in photons/cm²-sec-Å-ster.

I_o is the solar flux incident at the top of the atmosphere in the direction $\mu_o = \cos \theta_o$ in photons/cm²-sec-Å.

μ_o is the cosine of the zenith angle of the sun, measured from the outward normal to the atmosphere.

μ is the cosine of the zenith angle of the reflected intensity, again measured from the outward normal.

The H functions satisfy the equation,

$$H(\mu) = 1 + \mu H(\mu) \int_0^1 \frac{\psi(\mu')}{\mu + \mu'} H(\mu') d\mu' \quad (7)$$

where $\psi(\mu')$, the characteristic function, is equal to $\omega_o/2$ for isotropic scattering. Since for all calculations in the VUV the value of ω_o is small ($\omega_o < 0.13$), a method of successive approximations was used to solve the equation. Taking $H_o(\mu) = 1.00$ for the first approximation, for all values of ω_o :

$$\frac{1}{H_1(\mu)} = 1 - \frac{\omega_o}{2} + \frac{\omega_o}{2} \int_0^1 \frac{\mu' d\mu'}{\mu + \mu'} = 1 - \frac{\omega_o}{2} + \frac{\omega_o}{2} \left[1 + \mu \ln\left(\frac{\mu}{\mu+1}\right) \right] \quad (8)$$

With Equation (8) the diffusely-reflected intensity from a semi-infinite plane-parallel atmosphere was calculated for wavelengths between 1100 and 2000Å. The results are plotted in Figure 1 together with the incident flux at the top of the atmosphere. It is seen that while the incident solar flux varies smoothly from 10^8 to 10^{11} photons cm⁻² Å⁻¹ between 1100 and 2000Å, the diffusely-reflected light has a minimum near 1120Å, rises to a relative maximum at 1175Å, falls to a minimum near 1450Å, and then rises continuously with further increase in wavelength. The principal features of this graph have been discussed in QPR No. 6 and are not repeated in this brief summary.

3. CO₂ Photolyses and Photoionization Rates for Constituents of the Atmospheres of Mars and Venus

(a) Principal Investigators: F. F. Marmo and Shardanand

The object of this study phase was to obtain estimates for the solar photoionization rates for constituents in the atmospheres of Mars and Venus. To accomplish this, it is first necessary to generate suitable models of the

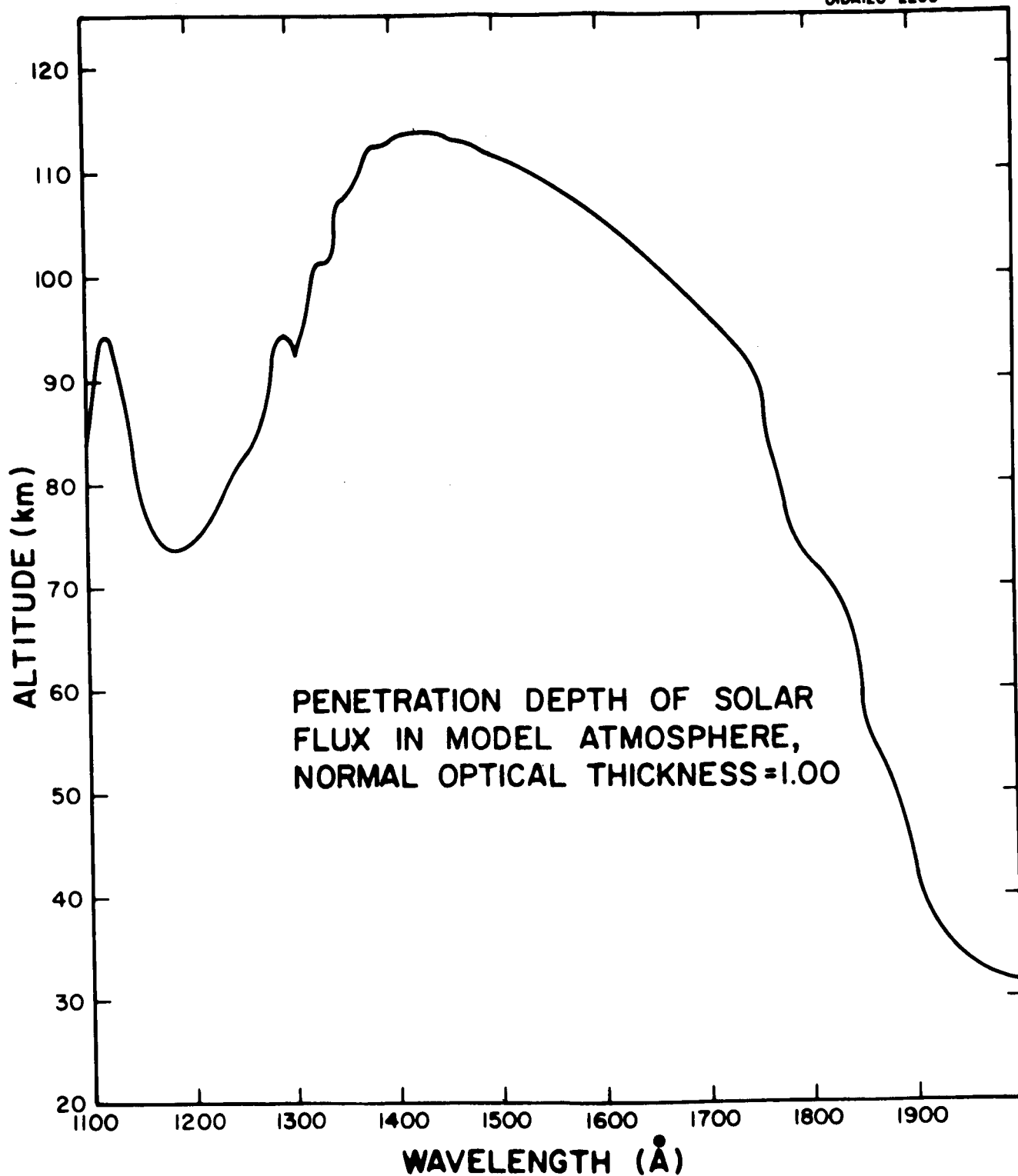
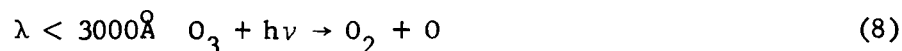
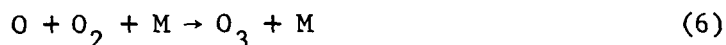
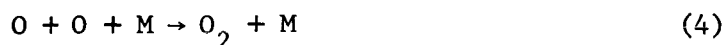
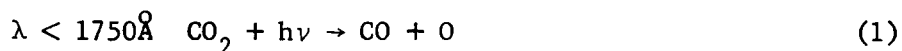


Figure 1 (III-D-2). Comparison of incident solar flux and maximum diffusely reflected flux in the vacuum ultraviolet.

neutral constituency and their altitude distributions. Thus, as an initial step the CO_2 photolysis was investigated in order to generate a model to employ. When this was accomplished, the appropriate calculations were performed to give estimates of the initial rates of ionization associated with the individual resident constituents as a function of altitude. A brief summary of this effort is given below.

Among the neighboring planets, Mars and Venus have been the principal target of investigation during the last few years; but no experimental data are available concerning the ionospheres since so little is known about the atmospheric constituents of these planets. For example, the only substance known to be present is carbon dioxide and even its abundance has been open to question. In addition, only upper limits for oxygen and water vapor have been reported. However, as sparse as these data are they can be utilized in conjunction with the solar energy distribution to construct the vertical distribution of density and composition by taking proper account of the solar photodissociation of the molecules and of mixing and diffusion. The generated model of neutral particles can then be employed producing an ionospheric model by considering the ionization processes and the processes such as recombination, ion-atom interchange, charge transfer, dissociative recombination, etc. This has been the approach adopted for the present study which is limited to the determination of the initial photoionization rates.

Concerning the initial photochemical phase, the following photochemical reactions were considered:



As the major constituent is not known, the following three cases were considered for the present study:

- (1) major constituent is only nitrogen
- (2) major constituent is only argon
- (3) nitrogen and argon are present in equal amounts.

For these cases, the appropriate photochemical equations were set up and solved on the 1620 IBM. To illustrate the data only Figure 1 is included here which is the representative case for the Martian atmosphere model in which CO_2 represents ten percent of the content whereas the remainder is nitrogen. The results for the other five cases are given in the original report in QPR No. 5. In any case, these then represent the initial models which were then employed to calculate the corresponding solar photoionization rates as a function of altitude for each individual constituent as well as the total rate.

For this part of the problem a numerical method of summation of various components was used. The photoionization rate p in the ion-pair $\text{cm}^{-3} \text{sec}^{-1}$ at a given altitude was computed according to the expression

$$p = \sum_{\lambda} I(\lambda, Z) [\sum \sigma_i(\lambda) n_i(Z)] \quad (9)$$

where $I(\lambda, Z)$ is the ionizing flux for a given wavelength at a given altitude, $\sigma_i(\lambda)$ is the average photoionization cross section for each constituent for a wavelength interval of 50\AA , and $n_i(Z)$ is the number density of each constituent at the given altitude. The parameters employed, the value employed and the source for these values are given in Tables 1 and 2 for the studies of Mars and Venus, respectively.

Representative results can be obtained from Figure 2 in which the calculated photoionization rates for various altitudes are given for the model illustrated in Figure 1. Again, the remaining five cases are not shown here since they are included in the detailed report (see QPR No. 5). A remaining task now, is to incorporate these values into a theory for estimating the corresponding steady-state electron number densities as a function of altitude. The more complex problem is currently under investigation.

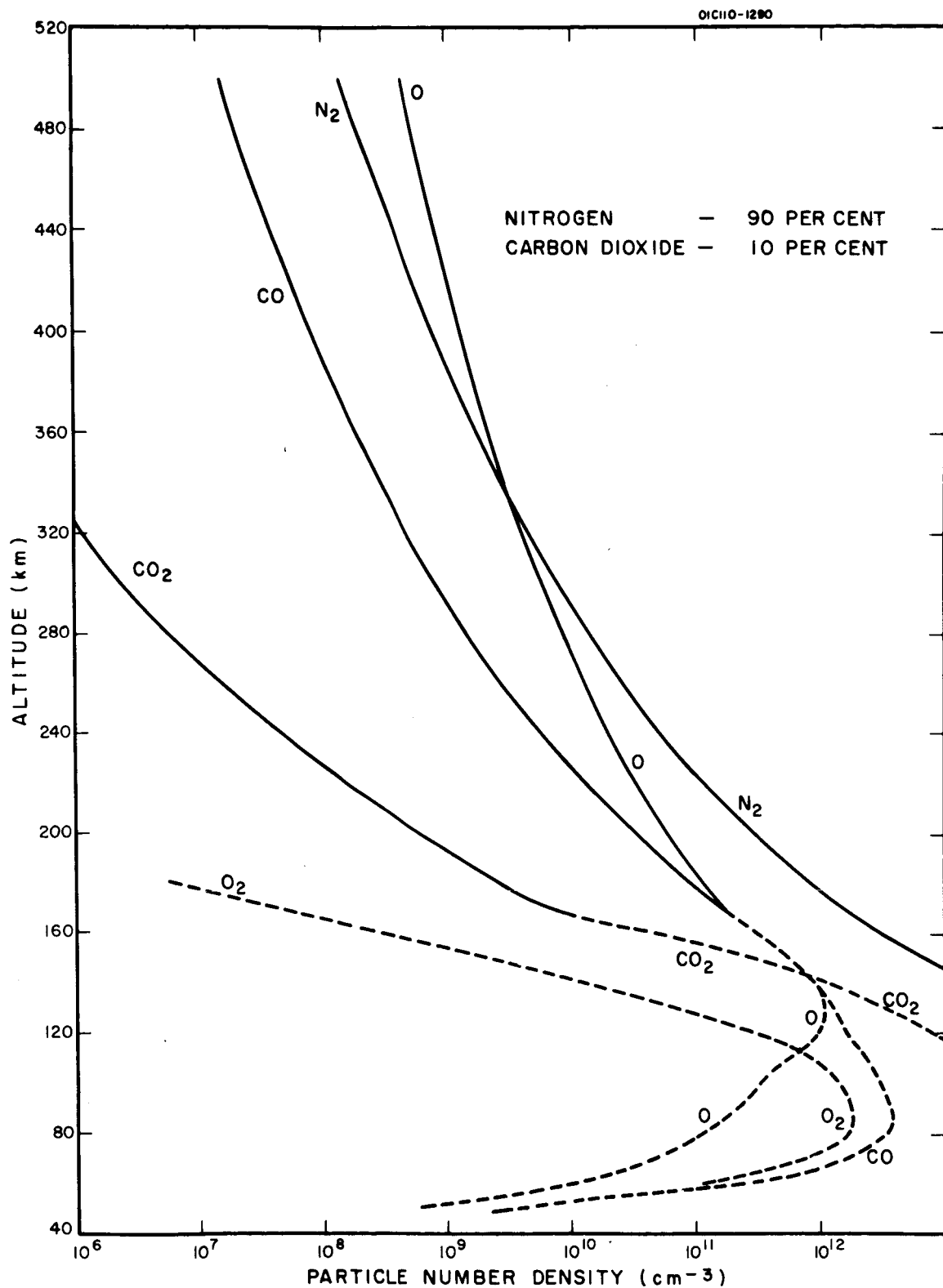


Figure 1 (III-D-3). Initial model atmosphere of Mars.

TABLE 1 (III-D-3)

PARAMETERS EMPLOYED FOR THE STUDY OF THE IONOSPHERE OF MARS

Surface Temperature 250°K	
lapse rate - 2.9 degrees/km	
tropopause at 30 km	Schilling (1962)
mesopause at 140 km above which	
lapse rate is +2.3 degrees/km	
Surface pressure 25 mbar	Kaplan, Münch & Spinrad (1964)
Carbon dioxides 55 meter NTP	
Solar flux on the top of the Earth's	Detwiler (1961)
atmosphere in 50Å intervals	Johnson (1954)
Wavelength regions 3000-2550Å	
2550-1000Å	
Average dilution factor to account for	
the diminution of solar flux in the	
vicinity of Mars, $\mu = 0.444$	
<u>Absorption Cross Sections</u>	
Carbon dioxide	Sullivan & Holland
Oxygen	(GCA TR No. 64-20-N, NASw-395)
Ozone	
<u>Photoionization Cross Sections</u>	
Carbon monoxide	Sun & Weissler (1955); Huffman, Larrabee and Tanaka (1964)
Atomic oxygen	Dalgarno, Henry & Stewart (1964)
Molecular nitrogen	
Argon	Samson (1964)
Photodissociation yield factors for	
oxygen, ozone and carbon dioxide and	
photoionization yield factors for carbon	
monoxide, atomic oxygen, nitrogen and	
argon: assumed to be unity.	

TABLE 1 (III-D-3) Continued

$k_2 = 1.6 \times 10^{-14} \exp \left(- \frac{4000}{RT} \right)$	Mahan and Solo (1962)
$k_3 = 0$	
$k_4 = 2.8 \times 10^{-33} \text{ cm}^6/\text{sec}$	Morgan & Schiff (1963)
$k_6 = 5.0 \times 10^{-34} \text{ cm}^6/\text{sec}$	Kaufman (1963)
$k_7 = 5 \times 10^{-11} \exp \left(- \frac{6000}{RT} \right) \text{ cm}^3/\text{sec}$	Benson and Axworthy (1957)

REFERENCES TO TABLE 1 (III-D-3)

Schilling, F. F., Limiting Model Atmospheres of Mars, Rpt. R-402-JPL, Rand Corporation, Santa Monica, California (1962).

Kaplan, L. D., G. Münch and H. Spinrad, An Analysis of the Spectrum of Mars, *Astrophys. J.*, 139, 1-15 (January 1964).

Detwiler, C. R., D. L. Garrett, J. D. Purcell and R. Tousey, The Intensity Distribution in the Ultraviolet Solar Spectrum, *Ann. Geophys.*, 17, 263 (1961).

Johnson, F. S., The Solar Constant, *J. Meteorol.*, 11, 431-439 (1954).

Sullivan, J. O. and A. Holland, Planetary Physics IX: A Congeries of Absorption Cross Sections for Wavelengths less than 3000Å. II, GCA Technical Report No. 64-20-N, NASw-840 (December 1964).

Sun, H. and G. L. Weissler, "Absorption Cross Sections of Carbon Dioxide and Carbon Monoxide in Vacuum Ultraviolet," *J. Chem. Phys.*, 23, 1625 (1955).

Huffman, R. E., J. C. Larrabee and Y. Tanaka, "Absorption Coefficients of Carbon Monoxide in the 1006-600Å Wavelength Region," *J. Chem. Phys.* 40, 2261 (1964).

Dalgarno, A., R. J. W. Henry and A. L. Stewart, "Photoionization of Atomic Oxygen," GCA Technical Report No. 64-1-N, Contract No. NASw-840 (1964).

Samson, J. A. R., "Experimental Photoionization Cross Sections in Argon from Threshold to 280Å," *J. Opt. Soc. Am.* 54, 420-421 (1964).

Mahan, B. H. and R. B. Solo, "Carbon Monoxide-Oxygen Atom Reactions," *J. Chem. Phys.* 37, 2669 (1962).

Morgan, J. E. and H. I. Schiff, "Recombination of Oxygen Atoms in the Presence of Inert Gases," *J. Chem. Phys.* 38, 1495 (1963).

Kaufman, F., Reactions of Oxygen Atoms in Progress in Reaction Kinetics, ed. G. Porter, Pergamon Press, New York (1961).

Benson, S. W. and A. E. Axworthy, "Mechanism of the Gas Phase, Thermal Decomposition of Ozone," *J. Chem. Phys.* 26, 1718 (1957).

TABLE 2 (III-D-3)

PARAMETERS EMPLOYED FOR THE STUDY OF THE IONOSPHERE OF VENUS

Case	Major Constituent	Pressure at the Top of the Cloud	Amount of CO ₂ above the cloud top	Estimated % Ratio	
				CO ₂	N ₂ or A
I	Nitrogen	1.036 atm	303 m-atm	3	97
II	Argon	1.725 atm	505 m-atm	4.5	95.5
III	Nitrogen [†]	1.339 atm	392 m-atm	4	N ₂ -48
	Argon				A -48

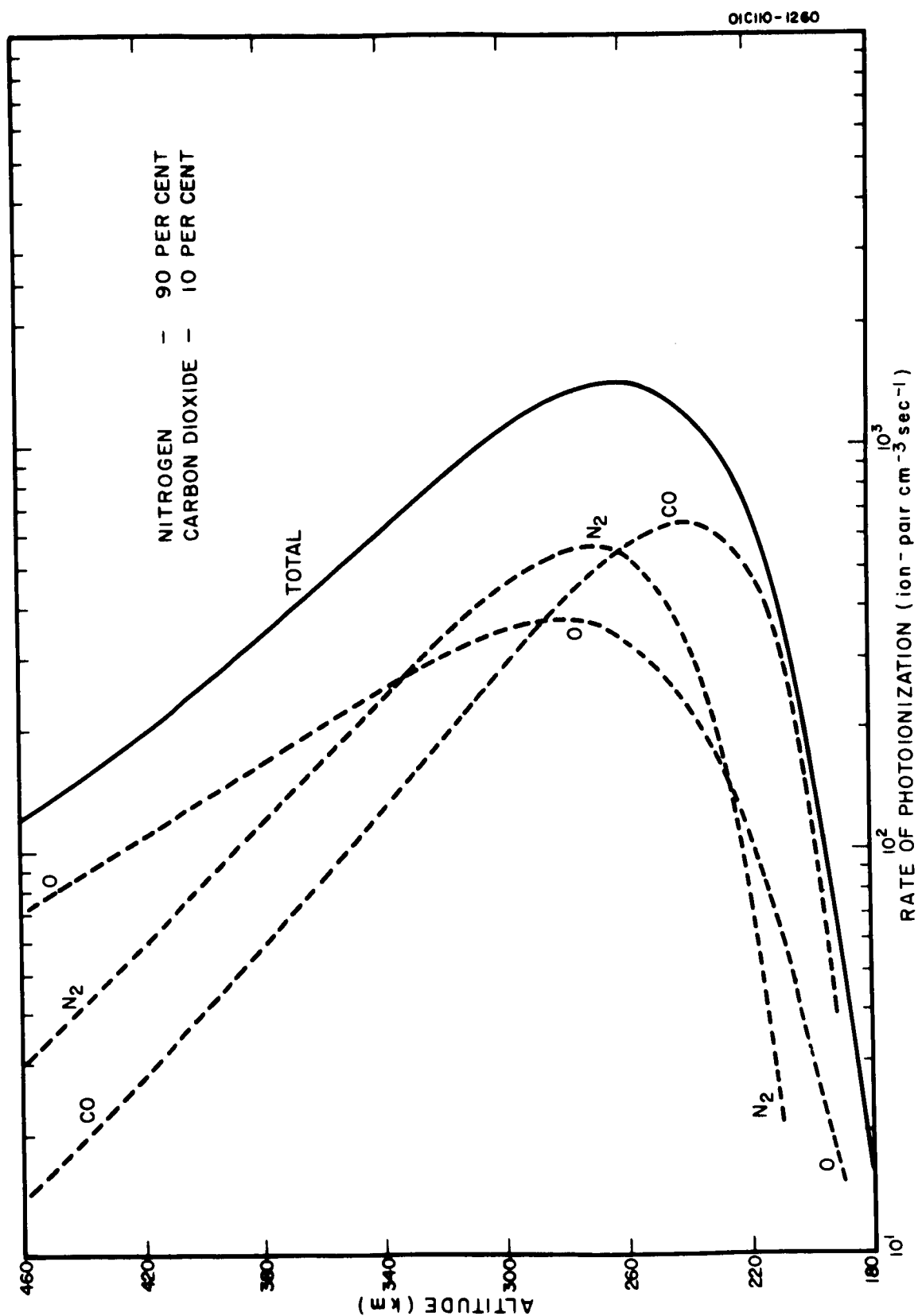


Figure 2 (III-D-3). Photoionization rates for the atmosphere of Mars.

REFERENCES

1. Barth, C. A., J. Geophys. Res. 69, No. 15, 3301 (1964).
2. Yamazaki, H. and R. J. Cvetanovic, J. Chem. Phys. 39, 1902 (1963).
3. Yamazaki, H. and R. J. Cvetanovic, J. Chem. Phys. 40, 582 (1964).
4. Yamazaki and R. J. Cvetanovic, J. Chem. Phys. 41, 3703 (1964).
5. Warneck, P., Discussions Faraday Soc. 37, 57 (1964).
6. Warneck, P., J. Chem. Phys. 41, 3435 (1964).
7. GCA Corporation, Quarterly Progress Report Nos. 3 and 4, Contract No. NASw-840 (July and October 1964).
8. Zelikoff, M. and L. M. Aschenbrand, J. Chem. Phys. 22, 1680 (1954).
9. Kaufman, F. and Clarke, J. Chem. Phys. 38, 1388 (1963).
10. Bates, D. R. and M. J. Seaton, Mon. Not. Roy. Astr. Soc. 109, 698 (1949).
11. Dalgarno, A. and D. Parkinson, J. Atmos. Terr. Phys. 18, 335 (1960).
12. Dalgarno, A., M. B. McElroy, and R. J. Moffett, Planet. Space Sci. 11, 463 (1963).
13. Dalgarno, A. and M. B. McElroy, Planet. Space Sci. 11, 727 (1963).
14. Seaton, M. J., Proc. Phys. Soc. A67, 927 (1954).
15. Ditchburn, R. W., Proc. Phys. Soc. 75, 461 (1960).
16. Dalgarno, A. and J. T. Lewis, Proc. Phys. Soc. A69, 285 (1956).
17. Hall, L. A., K. R. Damon, and H. E. Hinteregger, Space Research 3, 745 (1963).
18. Dalgarno, A., J. Atmos. Terrest. Phys. 12, 219 (1958).
19. Dalgarno, A., Phil Trans. Roy. Soc. 250, 426 (1958).
20. Stebbings, R. F., A. C. H. Smith, and H. Ehrhardt, Third International Conference on Electronic and Atomic Collisions, London, 1963.
21. Dalgarno, A., Annales de Geophys. 17, 16 (1961).

REFERENCES (continued)

22. Boggess, R. L., L. H. Brace, and N. W. Spencer, J. Geophys. Res. 64, 1627 (1959).
23. Spencer, N. W., L. H. Brace, and G. R. Carignan, J. Geophys. Res. 67, 157 (1962).
24. Brace, L. H., N. W. Spencer, and G. R. Carignan, J. Geophys. Res. 68, 5397 (1963).
25. Bowen, P. J., R. L. F. Boyd, C. L. Henderson, and A. P. Willmore, Proc. Roy. Soc. A281, 514 (1964).
26. Brace, L. H., N. W. Spencer, and A. Dalgarno, Planet. Space Sci. (in press).
27. Rumi, G. C., IRE Trans. Antennas Propagation 10, 594 (1962).
28. Belrose, J. S. and L. N. Hewitt, Nature 202, 267 (1964).
29. Sears, R. D., J. Geophys. Res. 68, 5135 (1963).
30. Schulz, G. J., Phys. Res. 135, A 988 (1964).
31. Chen, J. C. Y., J. Chem. Phys. 40, 3507; 3513 (1964); also private communication.
32. Dalgarno, A. and R. J. Moffett, Proc. Nat. Acad. Sci. India A33, pt. IV, 511 (1963).
33. Bridge, N. J. and A. D. Buckingham, J. Chem. Phys. 40, 2733 (1964).
34. Hanson, W. B. and F. S. Johnson, Mem. Soc. Sci. Liege, Series 5, 4, 390 (1961).
35. Dalgarno, A., M. B. McElroy, and R. J. Moffett, Planet. Space Sci. 11, 463 (1963).
36. Butler, S. T. and A. D. Buckingham, Phys. Rev. 126, 1 (1962).
37. Reid, G. C., J. Geophys. Res. 69, 3296 (1964).
38. Buchelnikova, I. S., Soviet Phys. (JETP) 35, 783 (1959).
39. Schulz, G. J., Phys. Rev. 128, 178 (1962).
40. Asundi, R. K., J. D. Craggs, and M. V. Kurepa, Proc. Phys. Soc. 82, 967 (1963).

REFERENCES (continued)

41. Chanin, L. M., A. V. Phelps, and M. A. Biondi, Phys. Rev. Letters 2, No.8, 344 (1959).
42. Dalgarno, A. and R. J. Moffett, Planet. Space Sci. 9, 439 (1962).
43. Altshuler, S., J. Geophys. Res. 68, 4707 (1963).
44. Chen, J. C. Y., J. Chem. Phys. 49, 3513 (1964).
45. Samson, J. A. R., Phys. Rev. 132, 2122 (1963).
46. Samson, J. A. R., J. Opt. Soc. Am. (January 1964).
47. Samson, J. A. R., Phys. Rev. (December 1963).
48. Madden, R. and K. Codling, Phys. Rev. Letters 10, 516 (1963).
49. Beutler, H., Z. Physik 93, 177 (1935).
50. Dalgarno, A., Proc. Phys. Soc. (London) 65, 663 (1952).
51. Dalgarno, A., Queen's University, Belfast (private communication).
52. Cooper, J. W., Phys. Rev. 128, 681 (1962).
53. Rustgi, O. P., Northrop, Hawthorne, California (private communication).
54. Wheaton, J. and W. R. S. Garton, Imperial College, London (private communication).
55. Compton, A. H. and S. K. Allison, X-Rays in Theory and Experiment, (D. Van Nostrand Company, Inc., New York, 1935), 2nd edit., p.799.
56. Huffman, R. E., Y. Tanaka, and J. C. Larrabee, J. Chem. Phys. 39, 902 (1963).
57. Metzger, P. H. and G. R. Cook, (to be published).
58. Ederer, D., Physics Department, Cornell University, Ithaca, New York (private communication).
59. Fano, U., Phys. Rev. 124, 1866 (1961).
60. Madden, R. and K. Codling, J. Opt. Soc. Am. (February 1964).
61. Samson, J. A. R., Physics Letters 8, 107 (January 1964).

REFERENCES (continued)

62. Knox, R. S., Phys. Rev. 110, 375 (1958).
63. Samson, J. A. R., J. Opt. Soc. Am. 54, 842 (June 1964).
64. Samson, J. A. R., J. Opt. Soc. Am. 54, 6 (1964).
65. Madden, R. P. and K. Codling, Phys. Rev. Letters 10, 516 (1963).
66. Cooper, J. W., Phys. Rev. 128, 681 (1962).
67. Stewart, A. L. and T. G. Webb, Proc. Phys. Soc. 82, 532 (1963).
68. Vinti, J. P., Phys. Rev. 44, 524 (1933).
69. Wheeler, J. A., Phys. Rev. 43, 258 (1933).
70. K  wien, H., Z. Physik 91, 1 (1934).
71. Huang, S., Astrophys. J. 108, 354 (1948).
72. Dalgarno, A. and N. Lynn, Proc. Phys. Soc. 70, 802 (1957).
73. Dalgarno, A. and A. L. Stewart, Proc. Phys. Soc. 76, 49 (1960).
74. Salpeter, E. E. and M. H. Zaidi, Phys. Rev. 125, 248 (1962).
75. Vinti, J. P., Phys. Rev. 42, 632 (1932).
76. Hylleraas, E. A., Z. Physik 106, 395 (1937).
77. Trefftz, E., A. Schulter, K. H. Dettmar, and K. Jorgens, Z. Astrophysik 44, 1 (1957).
78. Hargreaves, J., Proc. Camb. Phil. Soc. 25, 91 (1928-29).
79. Tousey, R., "Solar Spectroscopy in the Far Ultraviolet," J. Opt. Soc. Am. 51, 384 (1961).
80. Hinteregger, H. E. and K. Watanabe, "Photoionization Rates in the E and F Regions, 2," J. Geophys. Res. 67, 3373 (1962).
81. Hall, L. A., K. R. Damon, and H. E. Hinteregger, Space Res. 3, 745 (1963).
82. Friedman, H., Physics of the Upper Atmosphere, ed. J. A. Ratcliffe, Academic Press, New York, 1960, p. 133.

REFERENCES (continued)

99. Seaton, M. J., Proc. Roy. Soc. 208, 408 (1951).
100. Seaton, M. J., Proc. Phys. Soc. 67, 927 (1954).
101. Cooper, J. W., Phys. Rev. 128, 681 (1962).
102. Sewell, K. G., Phys. Rev. (to be published).
103. Sewell, K. G. (private communication. For tabulated data see Samson, J. A. R., Atomic and Molecular Processes, D. R. Bates, ed. (Academic Press, New York, in press) Vol. 2.
104. Tolansky, S., Multiple Beam Interferometry of Films and Surfaces, (Oxford University Press, London and New York, 1948).
105. Marton, L., Rev. Mod. Phys. 28, 172 (1956).
106. Klein, W., Optik 11, 226 (1954).
107. Garbor, D. and G. W. Jull, Nature 175, 718 (1955).
108. Samson, J. A. R., J. Opt. Soc. Am. 54, 1491 (1964).
109. Samson, J. A. R., J. Opt. Soc. Am. 54, 6 (1964).
110. Hunter, W. R. and R. Tousey, J. de Physique 25, 148 (1964).
111. Rustgi, O. P., J. Opt. Soc. Am. (to be published, 1965).
112. Bates, D. R. and M. J. Seaton, Mon. No. Roy. Astron. Soc. 109, 698 (1949).
113. Dalgarno, A. and D. Parkinson, J. Atmos. Terrest. Phys. 18, 335 (1960).
114. Dalgarno, A., R. J. W. Henry, and A. L. Stewart, Planet. Space Sci. 12, 235 (1964).
115. Compton, A. H. and S. K. Allison, X-rays in Theory and Experiment, (D. Van Nostrand Co., New York, 1935).
116. Aboud, A. A., J. P. Curtis, R. Mercure, and W. A. Rense, J. Opt. Soc. Am. 45, 767 (1955).
117. DeReilhac, L. and N. Damany-Astoin, C. R. Acad. Sci. (Paris) 258, 519 (1964).
118. Lee, Po, J. Opt. Soc. Am. 45, 703 (1955).

REFERENCES (continued)

119. Elias, L., E. A. Ogryzlo, and H. I. Schiff, Can. J. Chem. 37, 1680 (1959).
120. Marmo, F. F. and P. Warneck, "Photochemical Processes in the Atmosphere of Mars," Final Report, Contract No. NASw-124, GCA Corporation Tech. Rpt. No. 61-20-N (1961).
121. Paetzold, H. K., "On the Problems of Martian Ozonosphere," Mem. Soc. Roy. Sci. Liege 7, 452-459 (1963).
122. Shimizu, M., "Vertical Distribution of Neutral Gases on Mars," Rpt. Ionosphere Space Res. Japan 16, 425 (1963).
123. Kaufman, F., "Reactions of Oxygen Atoms," in Progress in Reaction Kinetics, ed. G. Porter (Pergamon Press, New York, 1961).
124. Dunham, T., "Spectroscopic Observations of the Planets at Mount Wilson," in The Atmospheres of the Earth and Planets, ed. G. P. Kuiper (Univ. of Chicago Press, Chicago, Illinois, 1952) p. 296.
125. Marmo, F. F., Sharda Nand, and P. Warneck, J. Geophys. Res. 70, No. 9, 2270 (1965).
126. Kaplan, L. D., G. Münch, and H. Spinrad, Astrophys. J. 139, No. 1, 1-15 (1964).
127. Sagan, C., P. L. Hanst and A. T. Yound, Planet. Space Sci. 13, 73-88 (1965).
128. Schilling, G. F., Report No. R-402-JPL, The Rand Corporation, Santa Monica, California, 1962.
129. O'Leary, B. T. (private communication).
130. Geisler, J. E. and S. A. Bowhill, "Ionosphere Temperature at Sunspot Minimum," J. Atmos. Terrest. Phys. 27, No. 4, 457-474 (April 1965).
131. Gill, P. and D. W. O. Heddle, J. Opt. Soc. Am. 53, 847 (1963).
132. Heddle, D. W. O., Quant. Spectroscopy Radiative Transfer 2, 349 (1962).
133. Dalgarno, A. and A. E. Kingston, Proc. Roy. Soc. A259, 424 (1960).
134. Warneck, P., Appl. Optics 1, 721 (1962).
135. Yoshino, T. and H. J. Bernstein, J. Molec. Spectros. 2, 213 (1958).

REFERENCES (continued)

136. Bhagavantum, S., Light Scattering and the Raman Effect, (Chemical Publishing Company, Inc., New York, 1942).
137. Marmo, F. F. and H. K. Brown, GCA Tech. Rpt. No. 63-4-N, Contract No. NASw-395 (March 1963).